

COMBUSTION PERFORMANCE OF OIL SHALE AND BIOMASS FUELS
AND THEIR BLENDS

A THESIS SUBMITTED TO
THE GRADUATE SCHOOL OF NATURAL AND APPLIED SCIENCES
OF
MIDDLE EAST TECHNICAL UNIVERSITY

BY

EMRE ÖZGÜR

IN PARTIAL FULFILLMENT OF THE REQUIREMENTS
FOR
THE DEGREE OF DOCTOR OF PHILOSOPHY
IN
PETROLEUM AND NATURAL GAS ENGINEERING

FEBRUARY 2014

Approval of the thesis:

**COMBUSTION PERFORMANCE OF OIL SHALE AND BIOMASS FUELS AND
THEIR BLENDS**

submitted by **EMRE ÖZGÜR** in partial fulfillment of the requirements for the degree of
**Doctor of Philosophy in Petroleum and Natural Gas Engineering Department, Middle
East Technical University** by,

Prof. Dr. Canan Özgen _____
Dean, Graduate School of **Natural and Applied Sciences**

Prof. Dr. Mahmut Parlaktuna _____
Head of Department, **Petroleum & Natural Gas Engineering**

Prof. Dr. Mustafa Verşan Kök _____
Supervisor, **Petroleum & Natural Gas Engineering Dept., METU**

Examining Committee Members:

Prof. Dr. Mahmut Parlaktuna _____
Petroleum & Natural Gas Engineering Dept., METU

Prof. Dr. Mustafa Verşan Kök _____
Petroleum & Natural Gas Engineering Dept., METU

Prof. Dr. Serhat Akın _____
Petroleum & Natural Gas Engineering Dept., METU

Prof. Dr. Mustafa Ümit Atalay _____
Mining Engineering Dept., METU

Prof. Dr. Tülay Durusoy _____
Chemical Engineering Dept., Hacettepe Univ.

Date: 04/02/2014

I hereby declare that all information in this document has been obtained and presented in accordance with academic rules and ethical conduct. I also declare that, as required by these rules and conduct, I have fully cited and referenced all material and results that are not original to this work.

Name, Last name : EMRE ÖZGÜR

Signature:

ABSTRACT

COMBUSTION PERFORMANCE OF OIL SHALE AND BIOMASS FUELS AND THEIR BLENDS

Özgür, Emre

Ph.D., Department of Petroleum and Natural Gas Engineering

Supervisor: Prof. Dr. Mustafa Verşan Kök

February 2014, 161 pages

The aim of this thesis was to evaluate the co-combustion performance of different origins of oil shales (Ulukışla and Himmetoğlu regions of Turkey) and various biomass samples (hazelnut shell, wheat bran, poplar, and miscanthus) at different biomass proportions (10, 20, and 50% by weight) using thermogravimetric analyzer (TGA), differential scanning calorimeter (DSC), and thermogravimetric analyzer-mass spectrometer (TGA-MS) at different heating rates (10, 30, 50 °C/minute). The ignition temperatures of the parent fuels and blended fuels as indicators of the level of improvement in combustion performance were investigated with the addition of biomass. The effect of biomass model compounds (cellulose, hemicellulose, and lignin) on the combustion performance were also investigated to identify the components that have the most influence in a combustion system.

It is noticed that the ignition temperature of Ulukışla and Himmetoğlu oil shale is 244, 296, and 302 °C and 197, 224, and 231 °C, respectively; whereas the ignition temperature of biomass fuels are in the range of 219-233, 240-255, 250-260 °C, at the same experimental conditions (at heating rates of 10, 30, 50 °C/minute, respectively).

Biomass fuels were characterized as low ash content fuels in the range of 0.1-2.9% by weight. Himmetoğlu oil shale and Ulukışla oil shale were observed to have ash contents of 18.5 and 84.5% by weight, respectively.

The activation energies of all oil shale and biomass samples were determined using Arrhenius, Coats-Redfern Kissenger, Ozawa-Flynn-Wall, and ASTM kinetic methods. The results of the values for oil shale combustion are in the range of 99-107 kJ/mol and 66-76 kJ/mol, respectively for Arrhenius and Coats-Redfern kinetic methods. The results for the combustion of biomass fuels are in the range of 72-85 kJ/mol for Arrhenius and Coats-Redfern kinetic methods. The results of isoconversional kinetic methods are in the range of

101-284 kJ/mol by Kissinger method, 113-184 kJ/mol for ASTM method and in the range of 176-302 kJ/mol by Ozawa-Flynn-Wall method for oil shale; and in the range of 129-222 kJ/mol by Kissinger method, 139-151 kJ/mol for ASTM method and 184-198 kJ/mol by Ozawa-Flynn-Wall method for biomass fuels. It was observed that activation energies were in direct relation with the ignition temperatures.

It was observed that the addition of biomass improved the combustion performance of high-ash oil shale by lowering the ignition temperature of the blends in a synergistic manner.

Cellulose was the most difficult one to combust among biomass model compounds (cellulose, hemicellulose, and lignin) because of its strong structure.

All results were evaluated statistically to identify possible relationships between the physical properties of the fuels and the combustion performance. It was observed that carbon content and volatile matter content are the most deterministic parameters for the ignition temperature of fuels. Carbon content and volatile matter content has a reducing effect on ignition temperature. It was also observed that as the heating rate increases, the dependence of ignition temperature on carbon content and volatile matter content increases. This is due to the better ignition conditions at higher heating rates by decreasing the loss of volatile matters in the devolatilization stage before combustion. The R^2 values of 94.0, 84.1, and 76.7 were obtained between sample and combustion properties for the heating rates of 50, 30, and 10 °C/minute, respectively.

Keywords: Combustion, oil shale, biomass, thermogravimetric analyzer, differential scanning calorimeter, mass spectrometry, energy

ÖZ

PETROL ŞEYLİ VE BİYOKÜTLE YAKITLARININ VE KARIŞIMLARININ YANMA PERFORMANSININ İNCELENMESİ

Özgür, Emre

Doktora, Petrol ve Doğal Gaz Mühendisliği Bölümü

Tez Yöneticisi: Prof. Dr. Mustafa Verşan Kök

Şubat 2014, 161 sayfa

Bu çalışmada, iki farklı petrol şeyli (Ulukışla ve Himmetoğlu) ve dört farklı biyokütle numunelerinin (fındık kabuğu, buğday kepeği, kavak odunu ve fil otu) türünün birlikte yanması, farklı biyokütle oranlarında (ağırlıkça %10, 20 ve 50) ve farklı ısıtma hızlarında (10, 30, ve 50 °C/dakika) türevsel taramalı kalorimetri (DSC), termal gravimetri (TGA) ve termal gravimetri – kütle spektrometresi (TGA-MS) yöntemleri kullanılarak incelendi. Ana numunelerin ve karışımların tutuşma sıcaklıkları, yanma performansı göstergesi olarak, biyokütle artışı doğrultusunda incelendi. Biyokütle temel bileşenlerinin de (selüloz, hemiselüloz ve lignin) yanmaya etkileri incelendi.

Ulukışla ve Himmetoğlu petrol şeyllerinin tutuşma sıcaklıkları sırasıyla 244, 296, 302 °C and 197, 224, 231 °C olarak ve de aynı deney koşullarında (10, 30, 50 °C/dakika) biyokütlelerin tutuşma sıcaklıkları 219-233, 240-255, 250-260 °C arasında ölçüldü.

Biyokütlelerin kütlece %0.1-2.9 arasında düşük kül miktarlarına sahip olduğu gözlemlendi. Himmetoğlu ve Ulukışla petrol şeyllerinin de kül miktarlarının sırasıyla kütlece %18.5 ve %84.5 olduğu gözlemlendi.

Tüm petrol şeyllerinin ve biyokütlelerin aktivasyon enerjileri Arrhenius, Coats-Redfern, Kissenger, Ozawa-Flynn-Wall, ve ASTM kinetik yöntemleri kullanılarak tespit edildi. Arrhenius ve Coats-Redfern kinetik metodları için petrol şeyllerinin yanma aktivasyon enerjilerinin sırasıyla 99-107 kJ/mol ve 66-76 kJ/mol aralığında olduğu; biyokütlelerin yanma aktivasyon enerjilerinin aynı kinetik metodlar için ise 72-85 kJ/mol aralığında olduğu tespit edildi. Petrol şeyllerinin yanma aktivasyon enerjilerinin Kissenger metodu için 101-284 kJ/mol, ASTM metodu için 113-184 kJ/mol, Ozawa-Flynn-Wall metodu içinse 176-302 kJ/mol aralığında olduğu tespit edildi. Biyokütlelerin yanma aktivasyon enerjilerinin Kissenger metodu için 129-222 kJ/mol, ASTM metodu için 139-151

kJ/mol, Ozawa-Flynn-Wall metodu içinse 184-198 kJ/mol aralığında olduğu tespit edildi. Tutuşma sıcaklıklarıyla aktivasyon enerjilerinin doğrudan ilişkili olduğu gözlemlendi.

Biyokütle eklenmesinin yüksek küllü petrol şeylinin yanmasını etkileşim ile tutuşma sıcaklığını düşürerek kolaylaştırdığı gözlemlendi.

Selülozun güçlü yapısından dolayı biyokütle model bileşenleri (selüloz, hemiselüloz, lignin) arasında en zor yanan bileşen olduğu tespit edildi.

Tüm elde edilen sonuçlar istatistiksel olarak incelenip, numunelerin fiziksel özellikleri arasında bağlantılar bulunmaya çalışıldı. Karbon ve uçucu bileşen miktarının numunenin tutuşma sıcaklığında en belirleyici özellikler olduğu tespit edildi. Karbon ve uçucu bileşen miktarının numunenin tutuşma sıcaklığını düşürücü bir etkisi olduğu tespit edildi. Isıtma hızı arttıkça, tutuşma sıcaklığı ve karbon ve uçucu bileşen miktarları arasındaki ilişkinin arttığı gözlemlendi. Bunun muhtemel sebebinin yüksek ısıtma hızlarında tutuşma öncesi buharlaşmadan dolayı kaçan uçucu bileşenin azalmasından kaynaklı olduğu düşünüldü ve numune ve yanma özellikleri arasındaki ilişkiyi belirleyen R^2 değerlerinin 50, 30, 10 °C/dakika ısıtma hızları için sırasıyla %94.0, 84.1, 76.7 olduğu tespit edildi.

Anahtar Kelimeler: Yanma, petrol şeyli, biyokütle, termal gravimetri, türevsel taramalı kalorimetri, kütle spektrometresi, enerji

ACKNOWLEDGEMENTS

First of all, invaluable guidance, continuous encouragement and supervision of Prof. Dr. Mustafa Verşan Kk in completing this study are to be mentioned.

Thanks to Middle East Technical University for the financial support.

I would like to express my special appreciation to Dr. zgen Karacan for his confidence to be a reference for my one year thesis research in USA.

I am very grateful to Bruce G. Miller and Dr. Sharon Falcone Miller under whose advisorship at Pennsylvania State University – EMS Energy Institute, I think I was able to broaden my technical and scientific horizons.

I would like to thank TBİTAK and Pisa University for their supports during the research. I also would like to thank my friends research assistant Marco Simone in Pisa University for providing certain samples, and research assistant Cemil Acar in METU for his cooperation in sample preparation.

Thanks are extended to my colleagues; Sevtaç Blbl, Aslı Gndoęar and Őkr Meray for their helps while studying my thesis.

Finally I also would like to express my biggest thanks to my family and my aunts for their endless supports during my thesis study.

TABLE OF CONTENTS

ABSTRACT.....	v
ÖZ.....	vii
ACKNOWLEDGEMENTS.....	ix
TABLE OF CONTENTS.....	x
LIST OF FIGURES.....	xiii
LIST OF TABLES.....	xvii
NOMENCLATURE.....	xix
CHAPTERS	
1. INTRODUCTION.....	1
2. BIOMASS AND OIL SHALE RESOURCES.....	3
2.1 Biomass.....	3
2.1.1 Thermal Conversion of Biomass.....	3
2.1.1.1 Pyrolysis.....	3
2.1.1.2 Gasification.....	4
2.1.1.3 Liquefaction.....	4
2.1.1.1 Combustion.....	4
2.1.2 Biomass Model Compounds.....	4
2.1.2.1 Cellulose.....	5
2.1.2.2 Hemicellulose.....	5
2.1.2.3 Lignin.....	5
2.1.3 Biomass Usage.....	5
2.1.4 Biomass Potential of Turkey.....	6
2.2 Oil Shale.....	8
2.2.1 Oil Shale Potential of Turkey.....	10
2.3 Fuel Blending.....	11
3. LITERATURE SURVEY.....	13
3.1 Biomass Combustion.....	13
3.2 Oil Shale Combustion.....	14
3.3 Co-combustion.....	16
3.4 Co-combustion of Oil Shale and Biomass.....	17
4. STATEMENT OF THE PROBLEM.....	19
5. SAMPLES, EXPERIMENTAL EQUIPMENT & PROCEDURES.....	21
5.1 Equipment.....	21
5.2 Samples.....	21
5.2.1 Sample Preparation.....	22

5.3 Experimental Conditions & Procedures.....	22
6. SAMPLE ANALYSES.....	25
6.1 Ignition Temperature.....	25
6.2 Proximate and Ultimate Analysis.....	25
6.2.1 Proximate Analysis.....	25
6.2.2 Ultimate Analysis.....	26
6.3 Activation Energy.....	26
6.3.1 Kinetic Analysis.....	27
6.3.1.1 Coats&Redfern Method.....	27
6.3.1.2 Arrhenius Method.....	28
6.3.1.3 Ozawa-Flynn-Wall Method.....	28
6.3.1.4 Kissenger Method.....	29
6.3.1.5 ASTM Method.....	30
7. RESULTS AND DISCUSSION.....	31
7.1 Proximate Analysis.....	31
7.2 Ultimate Analysis.....	32
7.3 Heat Content.....	33
7.4 DSC Analysis.....	34
7.4.1 DSC Curves of Parent Fuels.....	34
7.4.1.1 Oil Shale.....	34
7.4.1.2 Biomass.....	37
7.4.2 DSC Curves of Blended Fuels.....	43
7.4.3 Comparison of DSC Curves.....	44
7.5 Ignition Temperature.....	45
7.6 Biomass Model Compounds.....	50
7.6.1 DSC curves of Biomass Model Compounds.....	51
7.7 TGA Analysis.....	53
7.7.1 TGA Curves of Parent Fuels.....	53
7.7.2 TGA Curves of Blended Fuels.....	63
7.7.3 Comparison of TGA Curves.....	64
7.7.4 TGA curves of biomass model compounds curves.....	67
7.8 Additive or Interactive Effect.....	69
7.9 TGA-MS Curves.....	73
7.10 SEM Images.....	77
7.11 Kinetic Analysis.....	81
7.12 Statistical Analysis.....	87
8. CONCLUSIONS.....	91
9. RECOMMENDATIONS.....	93
REFERENCES.....	95

APPENDICES	
A. EQUIPMENT.....	107
A.1 Differential Scanning Calorimetry.....	107
A.2 Thermogravimetry.....	109
A.3 Thermogravimetric Analyzer coupled to Mass Spectrometer.....	111
A.4 Scanning Electron Microscopy.....	112
A.5 Carbon-Hydrogen- Nitrogen (CHN) Analyzer.....	112
B. DERIVATION OF DAEM EQUATION.....	113
C. DSC&TGA CURVES OF SAMPLES.....	115
C1. DSC Curves.....	115
C2. TGA Curves.....	133
D. REPEATABILITY TESTS.....	151
E. OTHER RESULTS.....	155
CIRCULUM VITAE.....	159

LIST OF FIGURES

FIGURES

Figure 7.1 Reaction regions in DSC curve of Ulukışla oil shale at 50 °C/min.....	35
Figure 7.2 Reaction regions in DSC curve of Himmetoğlu oil shale at 50 °C/min	36
Figure 7.3 DSC curve of hazelnut shell at 50 °C/min	38
Figure 7.4 DSC curve of miscanthus at 50 °C/min.....	39
Figure 7.5 DSC curve of poplar at 50 °C/min.....	39
Figure 7.6 DSC curve of wheat bran at 50 °C/min.....	40
Figure 7.7 Reaction regions in DSC curve of biomass fuels at 50 °C/min	43
Figure 7.8 Comparison of DSC curves for miscanthus- Ulukışla at 50 °C/min.....	44
Figure 7.9 Comparison of DSC curves for miscanthus- Himmetoğlu at 50 °C/min.....	45
Figure 7.10 Change of ignition temperature of Ulukışla oil shale-biomass blend with biomass ratio (10, 20, 50%) at 50 °C/min	48
Figure 7.11 Change of ignition temperature of Ulukışla oil shale-biomass blend with biomass ratio (10, 20, 50%) at 30 °C/min	48
Figure 7.12 Change of ignition temperature of Ulukışla oil shale-biomass blend with biomass ratio (10, 20, 50%) at 10 °C/min	49
Figure 7.13 Variation of ignition temperature with volatile matter content.....	50
Figure 7.14 DSC curve of cellulose	52
Figure 7.15 DSC curve of hemicellulose.....	52
Figure 7.16 DSC curve of lignin.....	53
Figure 7.17 Reaction regions in TGA curve of Ulukışla oil shale at 50 °C/min.....	55
Figure 7.18 Reaction regions TGA curve of Himmetoğlu oil shale at 50 °C/min.....	55
Figure 7.19 TGA curve of hazelnut shell at 50 °C/min.....	58
Figure 7.20 TGA curve of miscanthus at 50 °C/min.....	58
Figure 7.21 TGA curve of poplar at 50 °C/min.....	59
Figure 7.22 TGA curve of wheat bran at 50 °C/min.....	59
Figure 7.23 Reaction regions in TGA curve of biomass fuels at 50 °C/min.....	60
Figure 7.24 Comparison of TGA curves for miscanthus- Ulukışla at 50 °C/min	65
Figure 7.25 Comparison of TGA curves for miscanthus- Himmetoğlu at 50 °C/min.....	65
Figure 7.26 TGA curve of cellulose.....	67
Figure 7.27 TGA curve of hemicellulose.....	68
Figure 7.28 TGA curve of lignin.....	68
Figure 7.29 TGA-MS curve of hydrogen.....	74
Figure 7.30 TGA-MS curve of methane.....	75

Figure 7.31 TGA-MS curve of water.....	76
Figure 7.32 TGA-MS curve of carbondioxide.....	77
Figure 7.33 SEM picture of Ulukışla oil shale (x270).....	78
Figure 7.34 SEM picture of Ulukışla oil shale (x250).....	78
Figure 7.35 SEM picture of miscanthus (x750).....	79
Figure 7.36 SEM picture of miscanthus (x300).....	79
Figure 7.37 SEM picture of poplar (x300).....	80
Figure 7.38 SEM picture of poplar (x600).....	80
Figure A.1 DSC sensor assembly.....	109
Figure A.2 Typical DSC power compensation sample holder with twin furnaces and sensors.....	109
Figure A.3 Mechanism of a typical TGA.....	111
Figure C.1 DSC curve of Ulukışla oil shale at different HR.....	115
Figure C.2 DSC curve of Himmetoğlu oil shale at different HR.....	115
Figure C.3 DSC curve of hazelnut shell at different HR	116
Figure C.4 DSC curve of miscanthus at different HR	116
Figure C.5 DSC curve of poplar at different HR.....	117
Figure C.6 DSC curve of wheat bran at different HR	117
Figure C.7 DSC curve of hazelnut shell – oil shale blend (10-90) at different HR	118
Figure C.8 DSC curve of hazelnut shell – oil shale blend (20-80) at different HR	118
Figure C.9 DSC curve of hazelnut shell – oil shale blend (50-50) at different HR.....	119
Figure C.10 DSC curve of miscanthus – oil shale blend (90-10) at different HR.....	119
Figure C.11 DSC curve of miscanthus – oil shale blend (80-20) at different HR.....	120
Figure C.12 DSC curve of miscanthus – oil shale blend (50-50) at different HR.....	120
Figure C.13 DSC curve of poplar – oil shale blend (10-90) at different HR.....	121
Figure C.14 DSC curve of poplar – oil shale blend (20-80) at different HR.....	121
Figure C.15 DSC curve of poplar – oil shale blend (50-50) at different HR.....	122
Figure C.16 DSC curve of wheat bran – oil shale blend (10-90) at different HR.....	122
Figure C.17 DSC curve of wheat bran – oil shale blend (20-80) at different HR.....	123
Figure C.18 DSC curve of wheat bran – oil shale blend (50-50) at different HR.....	123
Figure C.19 DSC curve of hazelnut shell – oil shale blend (10-90) at different HR.....	124
Figure C.20 DSC curve of hazelnut shell – oil shale blend (20-80) at different HR.....	124
Figure C.21 DSC curve of hazelnut shell – oil shale blend (50-50) at different HR.....	125
Figure C.22 DSC curve of miscanthus – oil shale blend (90-10) at different HR.....	125
Figure C.23 DSC curve of miscanthus – oil shale blend (80-20) at different HR.....	126
Figure C.24 DSC curve of miscanthus – oil shale blend (50-50) at different HR.....	126
Figure C.25 DSC curve of poplar – oil shale blend (10-90) at different HR.....	127
Figure C.26 DSC curve of poplar – oil shale blend (20-80) at different HR.....	127
Figure C.27 DSC curve of poplar – oil shale blend (50-50) at different HR.....	128

Figure C.28 DSC curve of wheat bran – oil shale blend (10-90) at different HR.....	128
Figure C.29 DSC curve of wheat bran – oil shale blend (20-80) at different HR.....	129
Figure C.30 DSC curve of wheat bran – oil shale blend (50-50) at different HR.....	129
Figure C.31 Comparison of DSC curves for hazelnut shell- Ulukışla at 50 °C/min.....	130
Figure C.32 Comparison of DSC curves for poplar-Ulukışla at 50 °C/min.....	130
Figure C.33 Comparison of DSC curves for wheat bran-Ulukışla at 50 °C/min.....	131
Figure C.34 Comparison of DSC curves for hazelnut shell-Himmetoğlu at 50 °C/min.....	131
Figure C.35 Comparison of DSC curves for poplar- Himmetoğlu at 50 °C/min.....	132
Figure C.36 Comparison of DSC curves for wheat bran- Himmetoğlu at 50 °C/min.....	132
Figure C.37 TGA curve of Ulukışla oil shale at different HR	133
Figure C.38 TGA curve of Himmetoğlu oil shale at different HR	133
Figure C.39 TGA curve of hazelnut shell at different HR	134
Figure C.40 TGA curve of miscanthus at different HR	134
Figure C.41 TGA curve of poplar at different HR	135
Figure C.42 TGA curve of wheat bran at different HR	135
Figure C.43 TGA curve of hazelnut shell – oil shale blend (10-90) at different HR.....	136
Figure C.44 TGA curve of hazelnut shell – oil shale blend (20-80) at different HR.....	136
Figure C.45 TGA curve of hazelnut shell – oil shale blend (50-50) at different HR.....	137
Figure C.46 TGA curve of miscanthus – oil shale blend (90-10) at different HR	137
Figure C.47 TGA curve of miscanthus – oil shale blend (80-20) at different HR	138
Figure C.48 TGA curve of miscanthus – oil shale blend (50-50) at different HR	138
Figure C.49 TGA curve of poplar – oil shale blend (10-90) at different HR	139
Figure C.50 TGA curve of poplar – oil shale blend (20-80) at different HR	139
Figure C.51 TGA curve of poplar – oil shale blend (50-50) at different HR	140
Figure C.52 TGA curve of wheat bran – oil shale blend (10-90) at different HR	140
Figure C.53 TGA curve of wheat bran – oil shale blend (20-80) at different HR	141
Figure C.54 TGA curve of wheat bran – oil shale blend (50-50) at different HR	141
Figure C.55 TGA curve of hazelnut shell – oil shale blend (10-90) at different HR	142
Figure C.56 TGA curve of hazelnut shell – oil shale blend (20-80) at different HR	142
Figure C.57 TGA curve of hazelnut shell – oil shale blend (50-50) at different HR	143
Figure C.58 TGA curve of miscanthus – oil shale blend (90-10) at different HR	143
Figure C.59 TGA curve of miscanthus – oil shale blend (80-20) at different HR.....	144
Figure C.60 TGA curve of miscanthus – oil shale blend (50-50) at different HR	144
Figure C.61 TGA curve of poplar – oil shale blend (10-90) at different HR	145
Figure C.62 TGA curve of poplar – oil shale blend (20-80) at different HR	145
Figure C.63 TGA curve of poplar – oil shale blend (50-50) at different HR	146
Figure C.64 TGA curve of wheat bran – oil shale blend (10-90) at different HR.....	146
Figure C.65 TGA curve of wheat bran – oil shale blend (20-80) at different HR.....	147
Figure C.66 TGA curve of wheat bran – oil shale blend (50-50) at different HR.....	147

Figure C.67 Comparison of TGA curves for hazelnut shell- Ulukışla at 50 °C/min.....	148
Figure C.68 Comparison of TGA curves for poplar-Ulukışla at 50 °C/min	148
Figure C.69 Comparison of TGA curves for wheat bran-Ulukışla at 50 °C/min	149
Figure C.70 Comparison of TGA curves for hazelnut shell-Himmetoğlu at 50 °C/min.....	149
Figure C.71 Comparison of TGA curves for poplar- Himmetoğlu at 50 °C/min	150
Figure C.72 Comparison of TGA curves for wheat bran- Himmetoğlu at 50 °C/min.....	150
Figure D.1. Repeatability Test for DSC Curve at HR 10.....	152
Figure D.2. Repeatability Test for DSC Curve at HR 50.....	152
Figure D.3. Repeatability Test for DSC Curve at HR 50.....	153
Figure D.4. Repeatability Test for TGA Curve at HR 10.....	153
Figure D.5. Repeatability Test for TGA Curve at HR 30.....	154
Figure D.6. Repeatability Test for TGA Curve at HR 50.....	154

LIST OF TABLES

TABLES

Table 1.1 Share of energy sources.....	1
Table 2.1 Biomass Utilization for Energy in Various Countries.....	6
Table 2.2 Amounts of Agricultural Residues in Turkey.....	7
Table 2.3 World Oil Shale Reserves.....	10
Table 2.4 World Oil Shale Reserves.....	10
Table 2.5 Oil Shale Reserves of Turkey.....	11
Table 5.1 Information about samples.....	22
Table 7.1a Proximate analysis of fuels.....	32
Table 7.1b Ultimate analysis of fuels.....	32
Table 7.2 Heat contents of fuels.....	33
Table 7.3 Samples studied by others.....	33
Table 7.4 Reaction regions of oil shale samples.....	36
Table 7.5 Reaction regions of biomass samples.....	41
Table 7.6 Peak temperatures and heat values obtained from DSC curves.....	42
Table 7.7 Ignition temperatures of the parent fuels at different heating rates.....	46
Table 7.8 Ignition temperatures of the blend of Ulukışla oil shale and other biomass fuels at different heating rates.....	47
Table 7.9 Ignition temperatures of the blend of Himmetoğlu oil shale and other biomass fuels at different heating rates.....	47
Table 7.10 Ignition temperatures of biomass model compounds.....	50
Table 7.11 Lignocellulosic contents of biomass fuels.....	51
Table 7.12 Reaction regions of oil shale samples.....	56
Table 7.13 Weight loss of oil shales in the reaction regions.....	57
Table 7.14 Reaction regions of biomass samples.....	61
Table 7.15 Weight loss of biomass fuels in the reaction regions.....	62
Table 7.16 Peak temperatures in TGA curves.....	63
Table 7.17 Weight loss of blends in the reaction regions.....	66
Table 7.18 Difference between experimental and calculated values of ignition temperatures for each fuel blend at 50 °C/min heating rate.....	70
Table 7.19 Difference between experimental and calculated values of ignition temperatures for each fuel blend at 30 °C/min heating rate.....	71
Table 7.20 Difference between experimental and calculated values of ignition temperatures for each fuel blend at 10 °C/min heating rate.....	71

Table 7.21 Difference between experimental and calculated values of ignition temperatures for each fuel blend at 50 °C/min heating rate.....	72
Table 7.22 Difference between experimental and calculated values of ignition temperatures for each fuel blend at 30 °C/min heating rate.....	72
Table 7.23 Difference between experimental and calculated values of ignition temperatures for each fuel blend at 10 °C/min heating rate.....	73
Table 7.24 Activation energy of parent fuels from Arrhenius kinetic method.....	81
Table 7.25 Activation energy of biomass-Ulukışla blends from Arrhenius kinetic method.....	82
Table 7.26 Activation energy of biomass-Himmetoğlu from Arrhenius kinetic method.....	82
Table 7.27 Activation energy of parent fuels from Coats-Redfern kinetic method.....	83
Table 7.28 Activation energy of biomass-Ulukışla blends from Coats-Redfern kinetic method.....	83
Table 7.29 Activation energy of biomass-Himmetoğlu blends from Coats-Redfern kinetic method.....	84
Table 7.30 Activation energies of parent fuels from Kissinger method and Ozawa-Flynn-Wall method.....	85
Table 7.31 Activation energy of biomass-Ulukışla blends from Kissinger method and Ozawa-Flynn-Wall method.....	86
Table 7.32 Activation energy of biomass-Himmetoğlu blends from Kissinger method and Ozawa-Flynn-Wall method.....	86
Table 7.33 Statistical relations between physical properties of fuels.....	88
Table 7.34 Details of regression analysis.....	89
Table D.1. Repeatability Test Results.....	151
Table E.1 Results of other Turkish oil shale samples in the literature.....	155
Table E.2 Results of other oil shale samples in the literature.....	156

NOMENCLATURE

Abbreviations:

CH ₄	: Methane
CO ₂	: Carbon Dioxide
CHN	: Carbon, Hydrogen, and Nitrogen
DSC	: Differential Scanning Calorimeter
DTG	: Derivative Thermogravimetry
H ₂	: Hydrogen
H ₂ O	: Water
HR	: Heating Rate, °C/minute
MS	: Mass Spectrometry
MW	: Megawatt
R ²	: Coefficient of determination
SEM	: Scanning Electron Microscopy
TGA	: Thermogravimetric Analyzer

Symbols:

E	: Activation Energy, kJ/mol
T	: Temperature, °C
t	: Time, minute
R	: Ideal gas constant
wt.	: Weight
µm	: micro meter

Others:

Hm, Himmet	: Himmetoğlu Oil Shale
HS	: Hazelnut Shell
WB, Wheat	: Wheat Bran
Mis	: Miscanthus
Pop	: Poplar

CHAPTER 1

INTRODUCTION

Since the beginning of the industrial revolution, the global energy consumption has been growing steadily. Until the end of the nineteenth century biomass was the predominant fuel. In 1890 the consumption of fossil fuels roughly equaled the amount of biomass fuel burned in residential and industrial sectors. The twentieth century witnessed a rapid twentyfold increase in the use of fossil fuels. The current share of energy sources worldwide and in Turkey is shown in Table 1.1.

Table 1.1. Share of energy sources [IEA, 2012]

Fuel Type	Share, % (World)	Share, % (Turkey)
Oil	32.4	27.0
Gas	21.4	32.0
Coal	27.3	29.0
Hydroelectric	2.3	4.0
Nuclear	5.7	0
Geothermal, wind, solar	0.9	3.0
Biofuels and waste	10.0	5.0

The use of all energy sources are increasing over time. Based on the forecast of EIA2009 [EIA, 2009], world oil prices will remain relatively high through most of the projection period (2006-2030). Liquid fuels and other petroleum products are the world's slowest growing source of energy. Liquid fuel consumption will increase at an average annual rate of 0.9% as of 2006 up to 2030. Projected oil prices, the growing concern about the environmental impacts of fossil fuel use, and strong government encouragements for increasing renewable penetration in most countries around the world, is likely to improve the usage of renewable energy sources worldwide.

Renewable energy sources are the fastest-growing energy source for world electricity generation in the EIA2009 reference scenario, increasing by an average of 2.9% per year between the years 2006 and 2030. Renewable energy sources are composed of

biomass, biofuel, solar energy, geothermal, hydroelectricity, wind power, wave power, and tidal power. Hydroelectric power and wind power are responsible for much of the growth. Of the 3.3 trillion kilowatthours of new renewable energy generation to be added over the projection period, 1.8 trillion kilowatthours, 54% of total is due to hydroelectric power, and 1.1 trillion kilowatthours, or 33% of total, is due to wind power. Except hydroelectric power, it is difficult for most renewable technologies to compete economically with fossil fuels over the projection period. Government policies and supports typically are the main motivation factors for the construction of renewable generation facilities.

In addition to renewable energy sources, there is also an interest in so-called alternative energy sources due to the concern of potential energy shortages in the future. The demand for alternative energy in the transportation and power plant sectors is increasing. Research and development efforts for alternative energy have been intensified in the past few years [Lee et al, 2007]. The alternative energy includes oil shale, tar sand, extra heavy oil, shale gas, synthetic fuels from coal and nuclear energy.

Oil shale is an organic-rich fine-grained sedimentary rock containing significant amounts of kerogen and smaller amounts of bitumen. The kerogen in oil shale can be converted to shale oil through the chemical processes of pyrolysis. Oil shale can also be utilized by direct combustion. Tar sands are found in sand zones that contain naturally occurring mixtures of sand, clay, water, and a dense and extremely viscous form of petroleum, technically referred to as bitumen [Lee et al, 2007]. Extra heavy oils are extremely viscous and can be solids at room temperature. Heavy crude oils have a density approaching or exceeding that of water; and contain high concentrations of sulfur and metals.

In this study, the co-combustion of oil shale and some solid biomass fuels were investigated. The study differs from previous researches and publications in the literature, in that the samples were examined for co-combustion. There is lack of reported research on the co-combustion of oil shale and biomass fuels. Based on the results of this study, it can be claimed that the co-combustion oil shale and biomass will be feasible in the existing thermal power plants. Turkey has oil shale reserves and agricultural wastes in sufficient quantities. Utilizing them in thermal power plants will certainly improve the energy supply conditions in Turkey. Other than the economic contributions, the co-combustion will be environmentally friendly by low carbon emitting biomass blends to replace fossil sources.

CHAPTER 2

BIOMASS AND OIL SHALE RESOURCES

2.1 Biomass

All organic substances that can be used as fuel, including industrial, commercial, and agricultural wood and plant residues, organic waste, animal manure, and crops produced for energy purposes are called biomass [Capehart, 2007]. Biomass is available as solids (woody or herbaceous), liquids (biofuels), and gases (biogases).

Biomass can be processed to obtain heat or electricity either by thermochemical or biochemical conversion technologies. Biochemical conversion technologies include fermentation and other required stages. Thermochemical biomass conversion technologies include pyrolysis, gasification, direct combustion, and liquefaction. These technologies are in different stages of development, with combustion being the most developed, most applied, and generally most economic way [Van Loo and Koppejan, 2008].

2.1.1 Thermal Conversion of Biomass

There are four main thermal approaches that are commonly used to convert biomass into an alternative fuel. These are pyrolysis, gasification, liquefaction, and direct combustion [Van Loo and Koppejan, 2008].

2.1.1.1 Pyrolysis

Pyrolysis is the thermal degradation (devolatilization) of the material in the absence of an air or oxidizing agent. The products of pyrolysis are generally tar, carbonaceous charcoal, and low molecular weight volatile gases. Carbonmonoxide (CO) and carbondioxide (CO₂) can also be formed in significant amounts, especially from fuels having higher oxygen content like biomass. The liquid fuel called bio-oil is obtained after condensing the some products of pyrolysis process. Fuel type, temperature, pressure, heating rate, atmosphere are all parameters that affect the amounts and properties of the products formed.

2.1.1.2 Gasification

Gasification is the thermal degradation in the presence of a controlled amount of air or oxidizing agent which converts carbonaceous compounds (e.g. coal, petroleum, biomass etc.) into CO and H₂ at high temperatures. The operational temperatures are between 800 °C and 1100 °C. The product gases are generally CO, CO₂, H₂O, H₂, CH₄, and other hydrocarbons. The resulting gas mixture is called synthesis gas or syngas and is itself a kind of fuel that can be utilized in internal combustion engines. Gasification is a method for obtaining energy from many different types of organic materials.

2.1.1.3 Liquefaction

Liquefaction is a thermomechanical conversion in the liquid phase at low temperatures (250-350 °C) and high pressures (100-200 atm), typically with a high hydrogen partial pressure and a catalyst to increase the rate of reaction and/or to progress the selectivity of the process. Compared to pyrolysis process, liquefaction has a higher liquid yield, and results in a liquid with higher calorific value and lower oxygen concentration.

2.1.1.4 Combustion

Combustion is the complete oxidation of the fuel. It is a very complex process, which includes drying and pyrolysis followed by several exothermic reactions. The hot gases from the combustion are utilized for direct heating purposes in small combustion units, for heating water in small central heating boilers, to produce steam in boilers for electricity generation in larger units, and for heating water in larger central heating systems.

The heat released from combustion is utilized directly in thermal applications. It is used to drive turbines by steam engines to generate electricity [Miller and Tillman, 2008]. TGA and DSC can be used in the laboratory environment to simulate the combustion conditions in industrial combustion systems of solid fuels. There are three main combustion technology systems that are used to fire the solid fuels: fixed bed combustion, fluidized bed combustion, and pulverized fuel combustion [Van Loo and Koppejan, 2008 and Ots, 2009].

2.1.2 Biomass Model Compounds

Biomass fuels are chemically complex polymeric lignocellulosic materials. Lignocellulosic biomass is composed of cellulose, hemicellulose, and lignin. The carbohydrate polymers (cellulose and hemicellulose) are tightly bound to the lignin. These

model compounds form the physical and chemical properties of the biomass fuels based on their arrangement in the fuel.

2.1.2.1 Cellulose

Cellulose is the main constituent of biomass. It is a complex carbohydrate with the formula $(C_6H_{10}O_5)_n$. It is crystalline, strong, and resistant to hydrolysis, a polysaccharide with high molecular weight. It contains only anhydrous glucose. It is an unbranched structure with 7000-15000 glucose molecules per polymer [Sjostrom, 1993].

2.1.2.2 Hemicellulose

Hemicellulose can be any of several copolymers and is present in almost all plant cell walls along with cellulose. Hemicellulose has a random, amorphous structure with little strength. It contains many different sugar monomers. It has 500-3000 sugar units and has a branched structure. Like cellulose, most hemicelluloses function as supporting material in the cell walls [Sjostrom, 1993].

2.1.2.3 Lignin

Lignin is a complex chemical compound most commonly derived from wood, and is an integral part of the secondary cell walls of plants and some algae. Lignin fills the spaces in the cell wall between cellulose and hemicellulose. It is covalently linked to hemicellulose and thereby crosslinks different plant polysaccharides, conferring mechanical strength to the cell wall and, by extension, the plant as a whole [Sjostrom, 1993].

2.1.3 Biomass Usage

There are more than 3000 biomass power plants worldwide with a capacity of more than 40,000 MW [WEC, 2007]. Their generating capacities are between 1-80 MW due to the limited availability of biomass fuels within an economical milling and shipping distance [Bauen et al, 2004]. Some of these plants offer electricity for sale and some are used for own purposes by industry [Bain et al, 1998]. The biomass fuels utilized are agricultural residues and energy crops. The amount of biomass utilized to produce energy among some developed countries can be seen in Table 2.1.

Table 2.1. Biomass Utilization for Energy in Various Countries [Lee et al, 2007]

Country	Energy From Biomass Utilization (%)
Ireland	13.0
Sweden	13.0
Austria	4.0
Norway	4.0
Canada	3.0
U.S.A	2.8
Switzerland	1.6
Denmark	1.0
New Zealand	0.4
Belgium	0.2

2.1.4 Biomass Potential of Turkey

The biomass potential of Turkey from agricultural residues can be seen in Table 2.2 [Demirbaş, 2008]. There are different kinds of agricultural wastes in Turkey. The use of such resources can be important for Turkey. The total amount of those agricultural residues in Turkey is more than 16 millions of tones. This number may be increased by planned farming. The existing and potential numbers of biomass amounts prove to have enough quantity for the biomass supply in co-combustion projects. It is evident that biomass is a reliable source of energy for Turkey since it exists in available amounts on a yearly basis. It is also an advantage for biomass sources that they are distributed all along the country to reduce the transportation distance to power plants. The utilization of biomass sources in co-combustion projects will apparently increase the share of biomass sources in the energy production.

Table 2.2. Amounts of Agricultural Residues in Turkey [Demirbaş, 2008]

Crop Residues	Available Residues (tons)
Almond Shell	23,205
Almond Tree Pruning	22,800
Apricot Tree Pruning	69,571
Barley Straw	1,344,452
Cotton Ginning	585,776
Cotton Stalk	1,512,169
Grapefruit Tree Pruning	11,447
Groundnuts Shell	22,190
Hazelnut Shell	453,150
Hazelnut Tree Pruning	1,742,389
Maize Cop	1,144,384
Maize Straw	2,982,155
Mandarin Tree Pruning	82,744
Oats Straw	48,185
Olive Cake	746,834
Olive Tree Pruning	220,627
Orange Tree Pruning	82,744
Pistachio Tree Pruning	167,688
Pistachio Shell	4,202
Rice Husk	62,198
Rice Straw	125,719
Rye Straw	53,706
Sour Cherry Tree Pruning	17,120
Soybean Straw	13,123
Sunflower Stalk	1,355,472
Tobacco Stalk	246,467
Walnut Shell	60,633
Walnut Tree Pruning	25,240
Wheat Straw	3,514,486
TOTAL	16,740,876

2.2 Oil Shale

Oil shale is an organic-rich, fine-grained sedimentary rock. It contains considerable amounts of kerogen. It is a solid mixture of organic chemical compounds insoluble in normal organic solvents because of its huge molecular weight (carbon number greater than 200) and minor amounts of bitumen (carbon number greater than 25), and is a mixture of organic liquids that are very viscous, and black, sticky, entirely soluble in carbon disulfide. It is composed primarily of highly condensed polycyclic aromatic hydrocarbons [Andrews, 2006].

There are different methods to obtain energy from oil shale resources. The chemical process of pyrolysis can convert the kerogen in oil shale into synthetic crude oil. Heating oil shale to a high temperature in an inert atmosphere will form a vapor which can be distilled (retorted) to yield a petroleum-like shale oil -a form of non-conventional oil- and combustible shale gas (the term shale gas can also refer to gas occurring naturally in shales). Oil shale can be retorted by either above ground (ex-situ) or underground (in-situ) processing [Lee et al, 2007]. In above ground processing, shale is mined, transported to a processing facility, and then heated in retorting vessels. Underground retorting processes can be classified into two basic categories: (1) True in-situ (TIS) processing where an oil shale deposit is first fractured by explosives and then retorted underground, and (2) modified by (MIS) processing (modified in-situ), which is a more advanced in-situ technology where a portion of the deposit is mined and the rest turned into rubble using explosives and retorted underground. The crude shale oil can be burned as a boiler fuel, or can be further converted into syncrude by adding hydrogen [Lee, 1991].

Industry can also fire oil shale directly as a low-grade fuel for power generation and heating purposes, as discussed earlier. Beside energy, oil shale resources are also used as a raw material in chemical and construction materials processing. Oil shale is gaining attention as an energy resource as the price of conventional sources of petroleum has risen in the last decade, and as a way for some countries to form independence from external suppliers of energy. On the other hand, the mining and processing of oil shale comes with some environmental concerns, such as land use, waste disposal, water use, wastewater management, greenhouse-gas emissions and air pollution. Estonia and China have well-established oil shale industries, Brazil, Germany, Israel and Russia also utilize oil shale to some degree at power plants fired by oil shale.

The mineral components of oil shales vary according to depositional history. In some oil shales the major components are carbonates including calcite, dolomite, and

siderite, with lesser amounts of aluminosilicates. Silicates including quartz, feldspar, and clay minerals are major components in others with carbonates as a minor component. Many oil shale reserves contain small, widely abundant amounts of sulfides including pyrite and marcasite, which indicate that the sediments probably accumulated in dysaerobic to anoxic waters that prevented the destruction of the organic matter [USGS, 2005].

Organic matter in oil shale includes the residues of algae, spores, pollen, plant cuticle and corky fragments of herbaceous and woody plants, and other cellular remains of lacustrine, marine, and land plants. These materials are composed primarily of carbon, hydrogen, oxygen, nitrogen, and sulfur. Some organic matter preserves sufficient amount of biological structures that makes it possible to identify species and genus. In some oil shales, the organic matter is disordered and can be described as amorphous (bituminite). The history of this amorphous material is not well identified, but it is likely a mixture of degraded algal or bacterial remains. Some small amounts of plant resins and waxes also are a factor in the organic matter formation. Fossil shell and bone fragments, composed of phosphatic and carbonate minerals, are part of the mineral matrix of the oil shale [USGS, 2005].

Most of the organic matter in oil shales is from different types of marine and lacustrine algae [Yen and Chilingarian, 1976]. It is thought that organic matter may also include varied admixtures of biologically higher forms of plant debris depending on the depositional environment and geographic position [USGS, 2005].

Most of the organic matter in oil shale is not soluble in ordinary organic solvents, with the exception of bitumen which is present in small amounts and is soluble in certain organic solvents. Solid hydrocarbons including gilsonite, wurtzilite, grahamite, ozokerite, and albertite are present as veins or pods in some oil shales. Several such hydrocarbons with different chemical and physical characteristics have been mined at the commercial scale [USGS, 2005].

The amount of oil shale reserves worldwide is not certain. The amounts published by different sources, vary. Table 2.3 and Table 2.4 report the estimated amount of oil shale by United States Geological Survey [USGS, 2005] and United States Department of Energy [USDOE, 2005], respectively.

Table 2.3. World Oil Shale Reserves [USGS, 2005]

Country	%
U.S.A	70
Russia	15
Zaire	3.3
Brazil	2.7
Italy	2.4
Morocco	1.8
Jordan	1.1
Australia	1
Estonia	0.5
China	0.5
Canada	0.5
France	0.2

Table 2.4. World Oil Shale Reserves [USDOE, 2005]

Country	% of Reserves
U.S.A	72
Brazil	5.4
Jordan	4.2
Morocco	3.5
Australia	2.1
China	1.5
Estonia	1.1
Israel	0.3

2.2.1 Oil Shale Potential of Turkey

The amount of oil shale reserves in Turkey is also not certain and there is no comprehensive overview of the reserves. However, Table 2.5 provides at least some information on the oil shale reserves in Turkey.

Table 2.5. Oil Shale Reserves of Turkey [Altun et al, 2006 and Şengüler, 2007]

Name of the deposit	Geological Reserve (x10 ⁶ tones)	Possible Reserve (x10 ⁶ tones)	Total Reserve (x10 ⁶ tones)
Beypazari	327.68	-	327.68
Seyitomer	83.32	38.85	122.17
Himmetoglu	65.97	-	65.97
Hatildag	78.37	389.2	467.57
Mengen	-	50	50
Ulukisla	-	130	130
Bahcecik	-	42	42
Burhaniye	-	15.6	15.6
Beydili	-	300	300
Dodurga	-	138	138
Demirci	-	172	172
Saricakaya	-	300	300
Celtik	-	90	90
TOTAL	555.34	1665.65	2220.99

Oil shales are the second largest fossil fuel source in Turkey following the lignite reserves. Oil shale deposits in Turkey are widely distributed in middle and western Anatolia. They are lacustrine oil-shale deposits of Paleocene to Eocene age and of late Middle-Upper Miocene age. The information on the deposits is generally based on drilling data. The host rocks are marl and clays, in which organic matter is heterogeneously and finely dispersed.

2.3 Fuel Blending

In the context of solid fuels, blending involves two or more combustible materials: coals, biomass fuels, petroleum cokes to achieve a desired result [Miller and Tillman, 2008]. The basic principle of fuel blending is such that, simply by combining two or more different solid fuel types, a new fuel is produced. While many parameters reflect the weighted average of the parent fuels (with higher heating value), many other parameters reflect synergistic effects (interactions) between the fuels and as a consequence do not reflect the weighted average of the parent materials. Devolatilization patterns, total volatile evolution (% volatile matter), fuel nitrogen evolution, and ash fusion temperatures are among the parameters that reflect particle-particle interactions and do not reflect the weighted average of the parent materials. When blends of parent fuels are fired, the interactions between fuel types may

produce uncommon consequences, which can be frequently harmful but can also be advantageous.

Fuel blending can become attractive for a variety of economic reasons: fuel supply security, fuel cost, plant capacity goals, or similar plant objectives. Environmental reasons also support the practice of fuel blending. Environmental reasons, in general, focus on the reductions in greenhouse gas emissions and better management of particles.

Blending has become an important stage for controlling the solid fuel supply at electricity-generating utilities, process industries, and institutional establishments. It requires extensive equipment in the fuel yard and in the fuel transport system. It also requires considerable attention on controls for managing the flow of fuel.

When blending occurs, significant changes exist in the fuel to be fed to the boiler. These changes exist in the quality of the fuel and in the behavior of that fuel in a combustion setting. Operationally, these changes can influence management of the coal pile, the mills, the combustion system, and the post-combustion controls. Furthermore, the ability to adjust blending can influence operational practices.

Blending is increasingly practiced for both technical and economic reasons. It has an increasing potential for all solid fuel users but must be adapted to the design and operation of the combustion system, the utility boiler, the process industry boiler, or kiln, or the institutional system. Some technical advantages when biomass is added to coal in traditional power plants are the reduced CO₂ and SO₂ emissions due to the proportional decrease in coal feeding [Marcio, 2004]. In most of the cases, sulfur concentrations in coal vary from 1 to 5%. However, calcium and potassium oxides are excellent sulfur absorbers. Therefore, if biomass is present during the burning of coal, the generated ash can absorb some SO₂, producing a stable and environmentally harmless solid residue. Some constituents in the oil shale can also absorb SO₂, depending on their concentration.

CHAPTER 3

LITERATURE SURVEY

To date, there are many authors who have conducted numerous studies on the combustion of solid fuels (mostly coal or lignite fuels which are not in the scope of this study). There are many published articles on the thermal analysis of fossil fuels (such as, coal, lignite, and oil shale), biomass fuels (herbaceous, straw, and agricultural wastes), and to a lesser extent on blending of coal/lignite and biomass fuels. However, there is a very limited number of published works on the co-combustion of oil shale and biomass blends. The works are mentioned at the end of this chapter.

3.1 Biomass Combustion

Some important studies on biomass combustion are reviewed in this section. Ismail et al [1997] investigated the combustion of rice husk at heating rates of 50, 100, 150, 200 °C/min. using TGA at atmospheric pressure. They observed that ignition temperature increases as heating rate increases. Mansaray and Ghaly [1999] studied the combustion of rice husk using TGA at an atmospheric pressure at a heating rate of 20 °C/min. They observed two-step combustion as firing of volatiles and heavy fraction, respectively. Haykiri-Acma [2003] studied the combustion characteristics of different biomass materials using TGA. She performed TGA experiments on sunflower shell, colza seed, pine cone, cotton refuse, and olive refuse at a 20 °C/min. heating rate. She observed that the ignition temperatures of the biomass samples were all similar even though the proximate analysis results differ considerably. Demirbas [2004] investigated the combustion characteristics of different biomass fuels using proximate and ultimate analysis. He concluded as the previous researchers that biomass fuels have lower heating values compared to coals because they have higher moisture content and higher oxygen content, but biomass fuels have higher amount of volatile matter contents compared to that of coals. Biagini and Tognotti [2006] studied the combustion of biomass samples at different heating rates ranging between 5-100 °C/min. using a TGA, observing that the devolatilization and combustion behavior of solid fuels depend strongly on the conditions used. They concluded that at higher heating rates the separation of peaks in derivative weight loss curves can be easier; however, higher heating rates lead to less contact time between fuel and heater compared to lower heating rates until specified programmed temperature and this may result in possible thermal lags. Yu et al [2008] investigated the combustion characteristics of seaweed using TGA and DTA at a

heating rate of 20 °C/min for the particle size of 0.18mm from ambient temperature to 1200 °C and they observed that the initial part of combustion is pyrolysis followed by the combustion. They concluded that volatile matter content characterizes the combustion behavior of biomass fuels. Munir et al [2009] studied the combustion behaviors of cotton stalk and sugar cane using TGA. They performed TGA experiments at a 10 °C/min. heating rate from room temperature to 950 °C. They concluded that biomass behavior is complex due to different micro structural and elemental characteristics along with the type of reactive atmosphere. Otero et al [2011] studied the combustion of manure biomass and they also observed as many researchers that the initial part of combustion is pyrolysis followed by the combustion. Skreiberg et al [2011] investigated the combustion of different wood types using TGA at a heating rate of 5 °C/min. from ambient temperature to 900 °C using wood pellets (0.2mm x 2mm x 2mm). They concluded that the combustion behavior of biomass fuels depends on the type and concentration of model compounds (cellulose, hemicellulose, and lignin). Karampinis et al [2011] investigated the combustion properties of miscanthus and poplar using TGA at a heating rate of 10 °C/min at an atmospheric air. They characterized miscanthus and poplar as reactive fuels with high volatile matter and low ash content properties. Miranda et al [2012] investigated the combustion performance of some biomass fuels at 5.8 kW combustion stove and observed that the ratio of ash content and nitrogen content can limit the operation of the furnace. Tenorio and Moya [2013] investigated the combustion behavior of several biomass fuels using TGA at a heating rate of 20 °C/min. from ambient temperature to 950 °C and they observed that moisture content of fuels has the greatest impact on the combustion behavior with the minor effects of extractives. Yi et al [2013] studied the combustion of biomass (ramie residue) using TGA at a heating rate of 20 °C/min. from ambient to 800 °C and they observed that high oxygen content in biomass provides reactivity and better ignition. These are the studies of researchers to be mentioned on the biomass combustion area.

3.2 Oil Shale Combustion

Kok and Pamir [2000] made some investigations about the combustion kinetics of oil shale using TGA. They tested eight different oil shales from Turkey. They performed their tests at a 5 °C/min heating rate in air environment. They observed that the rate control mechanism was the chemical kinetics in the first reaction region due to lighter compounds, while diffusion was the rate controlling in the last stage of the reaction due to heavier compounds. Barkia et al [2003] investigated the kinetics of combustion of two oil shale types. They performed experiments using a TGA and DTA at different heating rates in an air atmosphere. They observed two different reaction regions in TGA and DTA profiles and noted that the reaction regions are more distinct as the heating rate increases. Kaljuvee et al [2004] performed TGA-FTIR combustion experiments on oil shale and observed CO₂ and

H₂O as the major emitted species with minor concentrations of CO, SO₂, HCL and some methane, ethane and etc. Han et al [2006] investigated the combustion mechanism of oil shale using TGA. He performed experiments at four different heating rates and at four different particle sizes in air environment. He observed two main reaction zones, as in previous studies, and also observed that particle size has little effect on combustion process of oil shale and that the ignition temperature and activation energy increases as heating rate increases. Han et al [2006] performed oil shale combustion experiments using TGA at a heating rate of 20 °C/min.. They observed two combustion regions corresponding to the combustion of light compounds between 280-500 °C and the combustion of heavy compounds between 620-730 °C like other researchers. Jiang et al [2007] investigated the combustion characteristics of oil shales in circulating fluidized bed and emphasized on the energy usage potential of all kinds of oil shale in circulating fluidized beds with satisfactory combustion efficiency. Kok [2007] investigated the kinetics of oil shales using DSC. He tested two different oil shale samples from Turkey at five different heating rates in air environment. He observed two reaction regions similar to other studies, first peak belonging to combustion of volatile matters and second one belonging to combustion of char material. Kaljuvee et al [2007] investigated oil shale combustion and emissions of gaseous compounds using TG-FTIR and DTA. He tested five different oil shale samples from different deposits at three different heating rates. They observed that the beginning and end point of the reaction interval increases as heating rate increases due to decreased contact time until programmed temperature. Yağmur and Durusoy [2009] performed oil shale combustion experiments at three different heating rates using a TGA between 25-900 °C for three different particle size range (-210+149), (-149+88), (-88) μm. They observed that particle size has a slight effect on the shape of the TGA curve. Kaljuvee et al [2010] also performed combustion experiments with oil shale at five different heating rates using TGA-DTA-FTIR. They identified three main regions during the combustion of oil shale: combustion of light compounds followed by combustion of heavy compounds and mineral decomposition. Syed et al [2011] also investigated the pyrolysis and combustion characteristics of oil shales. They did not observe any relationship between heating rate and activation energy values. Al-Makhadmeh et al [2013] performed combustion experiments using 20 kW reactor at a combustion temperature of 1200 °C and they concluded that the direct combustion of oil shale is feasible. Meriste et al [2013] performed TG-FTIR analysis on combustion of oil shale samples at a heating rate of 10 °C/min. from ambient temperature to 1000 °C and they observed that CO₂ and H₂O emissions during reactions cover the big part of emissions with some CH₄ emission. These compose the main publications in the oil shale combustion area.

3.3 Co-combustion

There are remarkably fewer publications in the literature on fossil fuel and biomass blends than on the parent fuels only. Most of the blending work involves coal or lignite as the fossil fuel whereas there is a wide diversity of biomass used. For example, Sami et al [2001] and Williams et al [2001] studied the co-firing of coal and biomass fuel blends. They observed that the addition of biomass for co-firing has environmental benefits because of reducing greenhouse gas emissions. Kastanaki and Vamvuka [2006] investigated the combustion behavior and kinetics of various biomass chars, a lignite and a hard coal char and their blends. They performed TGA experiments in an air atmosphere between the temperatures 25-850 °C at a heating rate of 10 °C/min. The biomass samples used are olive kernel, forest residue, cotton residue, and wood blended with coals at a ratio of 5, 10, and 20% by weight. They observed that the reactivity of biomass fuels is higher compared to lignite and hard coal. They observed that the ignition temperature of blends is lowered with the addition of biomass chars. They also concluded that some interactions between two components occurred during combustion based on the comparison of derivative weight loss curves of each fuel. Haykiri-Acma and Yaman [2008] investigated the combustion behavior of blending hazelnut shells with lignite. Lignite and hazelnut shell were mixed to obtain various blends of hazelnut shell in the ratios of 2, 4, 6, 8, 10, and 20% by wt. Activation energy, maximum burning rate, and temperature of maximum burning rate values were monitored. The addition of hazelnut shell up to 8 % by wt into Elbistan lignite provided higher burnouts than the expected theoretical ones. However, the addition of 10% biomass had less of a role on the burnout. Burnout characteristics of the blends up to 10% by wt during co-combustion can be concluded to show synergistic (interactive) effect, whereas additive effects are more favorable in the case of the blend having a biomass content of 20% by wt. Muthuraman et al [2009] investigated the effect of municipal solid waste (MSW) on the co-combustion characteristics with coals of varying rank using TGA and DTA. Blends containing 10% - 50% by the weight of MSW were tested. The ignition and burn-out temperature of each blend were determined. It was shown that blending of MSW with coal, improved the devolatilization properties of coal and the addition of MSW enhanced and supported the ignition of the blends indicating the feasibility of co-combustion. Gil et al [2010] investigated the thermal characteristics and kinetics of coal, biomass (pine sawdust), and their blends using a TGA under combustion conditions. Biomass was blended with coal in the range of 5-80 percent by weight to evaluate co-combustion behavior of two fuels. They observed no interaction between fuels during combustion based on the comparison of theoretical and experimental derivative weight loss curves. Varol et al [2010] investigated the combustion and co-combustion characteristics of three biomass fuels (wood chips, olive cake, and hazelnut shell) and three Turkish lignites using a TGA at a heating rate of 20 °C/min. starting from ambient temperature to 1100 °C. Samples were less than 250 µm in

size. They observed that as the volatile matter content of the sample increases, the ignition temperature decreases, and as the biomass content of the blend increases, the ignition temperatures of the mixtures approach to that of the biomass. Sahu et al [2010] investigated the combustion characteristics of blends of a coal with different biomass chars using simultaneous TGA-DSC at a heating rate of 10 °C/min. from ambient temperature to 750 °C with 212 µm sample particle size. They observed that information obtained through TGA experiments could not fully predict the burning characteristics of samples and also concluded that biomass char addition improved the combustion. Yüzbaşı and Selçuk [2011] investigated the co-combustion performance of olive residue and lignite. They performed TGA experiments in air for equal composition of blends, and observed an improvement in combustion performance based on the comparison of burnout temperatures and maximum weight loss rates. Vamvuka and Sfakiotakis [2011] investigated the combustion behavior of various biomass fuels (olive prunings, cotton residue, olive and peach kernels, pine needles, cardoon, and sewage sludge), one lignite, and lignite/biomass blends using a TGA. They checked the effects of heating rate, oxygen concentration, particle size and moisture content of the fuels on combustion performance. They observed that ignition temperature increased slightly with increasing particle size and moisture content, while it decreased with increasing oxygen concentration. They also observed that an increase in heating rate delayed ignition but increased the combustion performance. They concluded that blending lignite with biomass fuels increased its thermochemical reactivity. Idris et al [2012] investigated the combustion performance of different biomass fuels and different coal samples using a TGA at different heating rates. They observed that addition of biomass decreased the ignition temperature and activation energy of the blends without any interaction effects. Moon et al [2013] studied the co-combustion of different rank of coals and biomass (wood pellet) using TG-DSC at a heating rate of 10 °C/min. from ambient temperature to 800 °C/min. They blended biomass with coal in ratios of 10, 20, 30, 40% by wt. They observed that blending biomass with low-rank coal enhanced the combustion by lowering ignition temperature with interaction effect (10% biomass ratio has the significant impact).

3.4 Co-combustion of Oil Shale and Biomass

This study aims to contribute to the field of solid fuel combustion research in the area of the combustion of oil shale and biomass blends. There is limited number of published work on the co-combustion of oil shale and biomass blends. Recently, one similar study was published by Qing et al [2011]. They studied the combustion of biomass with oil shale semi coke. They studied the combustion behavior of different types of biomass (corn stalks, straw, rice husks, and sawdust) and oil shale semi coke. They performed experiments using a TGA with a heating rate of 20 °C/min. from ambient temperature to 850 °C and blends of 20% biomass – 80% oil shale by weight. An improvement in combustion (decrease in ignition

temperature) was observed when biomass was added to oil shale semi coke. Kask et al [2011] studied the combustion of oil shale and biomass at combustion burners from an environmental point of view. They blended wood with oil shale in ratios of 5, 10, 15% by wt. and performed experiments in a pulverized-fired boiler operated at 30 MW load capacity. They monitored emitted gaseous compounds using fourier transform infrared spectroscopy and observed a decrease in the emissions of carbon monoxide and total suspended particles as the biomass ratio increased in the blend. They also observed no negative effect on the combustion process and boiler operation during these tests. Wang et al [2013] studied the combustion of oil shale semi-coke with rice straw using a TGA with heating rates of 10, 20, 50, 80 °C/min. from 40 to 900 °C. They blended biomass with oil shale semi-coke in ratios of 10, 20, 30% by wt. They observed improvement in combustion (decrease in ignition temperature) and observed more stable and reactive combustion. Liu et al [2013] also studied the combustion of oil shale semi-coke with corn stalk using a TGA with a heating rate of 20 °C/min from ambient temperature to 850 °C. They blended biomass with oil shale semi-coke in ratios of 20, 30, 40, 50% by wt. They observed interactions during co-combustion with increased reactivity.

In the present study, the co-combustion of oil shale and biomass blends were investigated by using TGA and DSC analyzers at different heating rates and at blend proportions. TGA-MS and CHN analyzers were also used to provide more information on the combustion parameters to help the characterization of solid fuels. Evaluation of the co-combustion of oil shale and biomass will hopefully be the contribution of this thesis to the literature of solid fuel combustion area. This evaluation is detailed in the following chapters, Results and Discussion and is outlined in the conclusion part.

CHAPTER 4

STATEMENT OF THE PROBLEM

In this study, the thermal performance of co-combustion of biomass fuels and oil shales was investigated at different blend ratios (10, 20, and 50% by weight) and at different heating rates (10, 30, and 50 °C/minute) using a thermogravimetric analyzer (TGA) and a differential scanning calorimeter (DSC). At the same time, the effect of biomass addition on oil shale – biomass blend during co-combustion was investigated. Additive and interactive effects between the two types of fuels were studied. To make the evaluations, the ignition temperatures of each blend were compared and statistically analyzed. TGA coupled to a mass spectrometry (MS) and scanning electronic microscopy (SEM) were also used for confirmation of results and for provision of additional information on solid fuel properties. The obtained results can provide information on most suitable biomass types to be used with low grade oil shales and optimum biomass blending ratios, for the researchers in this area.

The aim was to search the effects of blending biomass with oil shale, to see if there will be a positive contribution to the combustion properties of oil shale by this procedure. In order to achieve this aim, experimental research with a statistical approach was held to try various combinations of the blends to find out the most appropriate biomass type and blend ratio.

CHAPTER 5

SAMPLES, EXPERIMENTAL EQUIPMENT & PROCEDURES

In this chapter, the experimental equipment, samples, experimental conditions and procedures used during the study are presented. Sample data, the experimental conditions and procedures about the equipment are explained after the information is given about the instruments.

5.1 Equipment

There is a variety of thermal analysis equipment in the thermal analysis area. Thermal analysis equipment provides extensive information based on different thermoanalytical techniques. In our study, a differential scanning calorimeter (DSC), thermogravimetric analyzer (TGA), a thermogravimetric analyzer coupled to a mass spectrometry (TGA-MS), scanning electron microscope (SEM), and carbon-hydrogen-nitrogen (CHN) analyzer were used. The detailed information about equipment can be seen in Appendix A.

5.2 Samples

In the study, two oil shale samples and four biomass samples were used. Oil shale sources are found in central and west-central part of Turkey. Oil shales in Turkey are lacustrine deposits of Paleocene to Eocene age and late Miocene age. Ulukışla oil shale sample was obtained from the city of Niğde located in the south part of central Turkey. Himmetoğlu oil shale sample was obtained from the city of Bolu located in the North West part of central Turkey. The Himmetoğlu formation occurs in a succession of predominantly brown and brownish-grey oil shale layers between pyroclastic outcrops around the margin of the basin, which is bordered in north and south by uplift areas. Himmetoğlu oil shale formation has been deposited from late Miocene age. The Ulukışla oil shale deposit underlying conglomeratic rocks has 13 meters average thickness of bed [Şener et al, 1995]. Ulukışla oil shale formation has been deposited from Miocene age. Himmetoğlu formation is older than Ulukışla formation.

Wheat bran samples were taken from the central Anatolian part of Turkey. Hazelnut shell samples were taken from east black sea region of Turkey. Miscanthus and poplar wood samples, which are potential energy crops in Turkey because of suitable climate conditions, were taken from Italy within the scope of a technical cooperation.

General information about the samples was given in Table 5.1. The detailed information about the samples can be reached at the "Results and Discussion" part of the thesis.

Table 5.1. Information about samples

Sample Name	Sample Type	Location	Formation Period
Himmetoğlu	Oil Shale	Bolu, Turkey	Late Miocene Age
Ulukışla	Oil Shale	Niğde, Turkey	Miocene Age
Hazelnut Shell	Biomass	Black Sea Region, Turkey	Perennial
Miscanthus	Biomass	Italy	Perennial
Poplar	Biomass	Italy	Perennial
Wheat Bran	Biomass	Central Anatolia, Turkey	Perennial

5.2.1 Sample Preparation

All solid fuel samples were ground and sieved between 50-80 mesh sizes before the experiments following ASTM D2013 standard.

Oil shale samples were obtained as grounded; miscanthus and poplar wood samples were also obtained in grounded state from Italy but hazelnut shell and wheat bran samples were grounded in Middle East Technical University – Mining Engineering Department using ball mill grinder because of fibrous structure of biomass fuels which makes the milling process of biomass not possible in conventional grinders.

5.3 Experimental Conditions & Procedures

The experimental conditions and procedures for DSC, TGA, TGA-MS, and CHN analyzer are provided in this section.

In DSC experiments, the maximum operation temperature was 600 °C. Experiments were carried out at atmospheric pressure and in an air environment. The flow rate of air was 50 ml/min. Experiments were performed at three different heating rates (10, 30, 50 °C/min.). Sample size varied between 2-4 mg. and particle sizes were 50-80 mesh sizes. For each experiment, the samples were held isothermal at 110 °C for 5 minutes to remove the moisture. The experimental conditions for the TGA were similar to the conditions of DSC. The only difference was that the maximum temperature used had been 800 °C for the TGA experiments. Experiments showed good repeatability within a confidence interval of 95% (as given in the Appendix D).

The experimental condition for TGA-MS was different compared to the DSC and TGA because of the high sensitivity of the equipment to sample mass and heating rate to obtain accurate results. There was no isothermal step to prevent the accumulation of volatiles in the capillary tube. The heating rate was 20 °C/min, which was the optimum rate for the operation of the instrument to detect the emitted gases. The temperature range was from ambient temperature to 1000 °C. The combustion environment was O₂/Ar (20-80 in volume), and the flow rate of gas was 100 ml/min. The sample weight was much higher, 100 mg, to generate detectable gaseous compounds, and the sample particle sizes were 50-80 mesh size. The experiments were performed at atmospheric pressure.

The procedure for proximate analysis is as follows: the amount of moisture and volatile matter in a sample of a solid fuel is determined by measuring the weight loss in a nitrogen environment at 110 °C for 1 hour and in an inert gas at 900 C +/- 20 °C for 7 minutes, respectively. The amount of fixed carbon content corresponds to the weight loss after further heating in air at 815 +/- 10 °C for 1 hour, and the residual is regarded as ash. The combustible matter comprises volatile matter, which easily volatilizes to the gas phase, and fixed carbon, which remains in the char even at high temperature [Keating, 1993]. Although this procedure is per ASTM standards, there can be some differences in practice.

To perform CHN analyzer experiments, 10 mg sample was used to detect elemental ratios accurately. Rapid combustion is performed in the instrument, setting the temperature to 1000 °C from ambient temperature in a second at atmospheric pressure to attain the conditions for complete combustion. Sample particle sizes were again between 50-80 mesh size.

The detailed information about the repeatability tests on experimental runs can be seen in the Appendix D.

CHAPTER 6

SAMPLE ANALYSES

In this section, the information on the sample properties of solid fuels such as the ignition temperature, proximate analysis, ultimate analysis, and activation energy is introduced. These are important indicators to evaluate the combustion performance of the solid fuels. The ignition temperature, proximate and ultimate analyses are determined using the thermal analysis instruments; activation energy calculation is based on the kinetic analysis of the experimental output data.

6.1 Ignition Temperature

Ignition temperature is the lowest temperature at which combustion occurs. However, the ignition temperature of solid fuels can not be given in exact terms since it depends upon several conditions. Heating rate and particle size have a significant influence on ignition temperature. For example, pulverized solid fuels ignite at a lower temperature compared to solid fuels having higher particle size.

Ignition temperature is directly proportional to the oxidative stability of a sample. Lower ignition temperature means lower oxidative stability. Solid fuel combustion is primarily governed by its ignition temperature. Ignition temperature is not only an important parameter for the characterization of the solid fuel but also crucial for the design of the boiler equipment of thermal power plants.

6.2 Proximate and Ultimate Analysis

In this part, proximate and ultimate analyses which are fingerprinting techniques for solid fuel analysis are explained.

6.2.1 Proximate Analysis

One of the most common and useful methods for analyzing the solid fuels is proximate analysis. Proximate analysis is performed by the help of TGA.

Proximate analysis is used to calculate the amounts of moisture, volatile matter, fixed carbon, and ash contents. Moisture is water trapped within a fuel sample. Volatiles are components that evaporate during low-temperature heating of the fuel; while ash is inorganic mineral impurities or incombustible residue left when a fuel has been completely burned. The fixed carbon is a cokelike residue fuel resource, left after the removal of water vapor, volatiles, and ash [Masuda et al, 2006].

The amount of volatile matter -like the ignition temperature- in a sample is important to characterize the solid fuel and to design the boiler equipment. They set the minimum limit on the furnace height and volume. High volatile matter content plays a key role in improving the combustion performance in the system; it helps to keep the combustion continuously.

6.2.2 Ultimate Analysis

One of the most common and useful methods for analyzing the solid fuels is ultimate analysis. The contents of the main elements such as, carbon, hydrogen, oxygen, nitrogen, and sulfur in solid fuels are determined using the ultimate analysis. A CHN analyzer instrument is used to perform the required experiments. The analyzer executes a rapid combustion process and then quantifies compounds by infrared spectroscopy. Evaluation of the accurate energy characteristics of solid fuels requires a complete knowledge of the weight ratio of all constituents (carbon, hydrogen, oxygen, nitrogen, and sulfur) in ultimate analysis. However, proximate analysis could be mostly sufficient for engineering consideration to identify the fuel's combustion characteristics [Keating, 1993].

6.3 Activation Energy

Activation energy is a term defined as the energy that must be overcome in order for a chemical reaction to occur. Activation energy may also be defined as the minimum energy required in order to start a chemical reaction. The activation energy of a reaction is generally symbolized by E_a , and given in units of kilojoules per mole.

Activation energy can be considered as the height of the energy barrier separating two minima of potential energy (of the reactants and products of a reaction). For a chemical reaction to progress at a reasonable rate, there should exist a noticeable number of molecules with energy equal to, or greater than the activation energy.

6.3.1 Kinetic Analysis

To perform a kinetic analysis based on TGA and DSC output data; there are different kinetic methods available in the thermal analysis literature. In this study, five different kinetic methods were used. The methods used to perform the kinetic analysis were: Coats & Redfern method and Arrhenius method from a single TGA curve, Ozawa-Flynn-Wall method from TGA curves, and Kissinger method and ASTM method from DSC curves which are isoconversional methods (data at different heating rates).

6.3.1.1 Coats & Redfern Method (Single TGA curve)

To derive the activation energy (E_a) from single TGA curve, the Coats & Redfern method was used. This is one of the most commonly used methods in thermal analysis [Kok et al, 2004]. Equations 6.1 and 6.2 can be used to implement Coats & Redfern kinetic method. Equation 6.1, which assumes first order kinetics, was preferred for calculating the activation energies. When the sample size is small, and with an excess air supply, the process of the combustion reaction is independent of the concentration of oxygen, and it is therefore reasonable to assume that oxidation can be described by first order kinetics method [Kok et al, 2004]. Also, equation 6.2 was used to check the best linear fit to determine the optimum reaction order number, and it was observed that the best fit was provided for the first order kinetics which is in conformity with the equation 6.1.

$$\ln\left[\frac{-\ln(1-\alpha)}{T^2}\right] = \ln\left[\frac{A.R}{\beta.E_a}\left(1 - \frac{2.R.T}{E_a}\right)\right] - \frac{E_a}{R.T} \quad \text{for } n = 1 \quad (6.1)$$

$$\ln\left[\frac{1-(1-\alpha)^{1-n}}{T^2(1-n)}\right] = \ln\left[\frac{A.R}{\beta.E_a}\left(1 - \frac{2.R.T}{E_a}\right)\right] - \frac{E_a}{R.T} \quad \text{for } n \neq 1 \quad (6.2)$$

A = the 'frequency' or 'pre-exponential' factor linked to reactant particle collision.

E_a = activation energy in J/mol

R = ideal gas constant = 8.314 Jmol⁻¹K⁻¹

T = temperature in K (Kelvin = °C + 273)

β = heating rate in °C/min

n = reaction order

α = fraction of material conversion

TGA output data gives the fraction of material conversion (α) in the specified reaction region. The fraction of material conversion (α) is placed in equation 6.1. Then, plotting the left hand side of equation 6.1 versus the reciprocal temperature in Kelvin, gives E_a from the slope and A from intercept, respectively.

6.3.1.2 Arrhenius Method (Single TGA curve)

Swedish scientist Arrhenius observed that rate constants for most chemical reactions follow the relationship shown in equation 6.3. It is a simple and powerful formula for the temperature dependence of the reaction rate constant [Skoog et al, 1998].

$$k = Ae^{-E_a/RT} \quad (6.3)$$

where,

A= frequency factor

E_a = activation energy in J/mol

R = ideal gas constant = 8.314 Jmol⁻¹K⁻¹

T = temperature in K

In logarithmic form,

$$\ln k = \ln A - E_a/RT \quad (6.4)$$

where,

$$k = \frac{\Delta[w]}{\Delta t.w} \quad (6.5)$$

w= weight

From the plot of $\ln k$ vs $1/T$, activation energy can be calculated.

6.3.1.3 Ozawa-Flynn-Wall Method (TGA conversion, isoconversional)

The Ozawa-Flynn-Wall method and Kissinger methods are based on the distributed activation energy model (DAEM). It is a simplified model for determining kinetic parameters for complex reactions [Miura and Maki, 1998]. This simplified model does not

require a priori assumption and mathematical model fitting for obtaining the kinetic parameters. Only a set of experimental data obtained at three different heating profiles are required. DAEM assumes a set of irreversible first-order reactions that have different activation energies. After some simplifications and approximations, activation energy of reactions can be calculated using the Ozawa-Flynn-Wall method and Kissinger method based on DAEM. The DAEM is represented as follows:

$$1 - X = \int_0^{\infty} \exp\left(-\int_0^T \frac{k_o}{\beta} e^{-E/RT} dT\right) f(E) dE \quad (6.6)$$

The derivation of the model can be seen in the Appendix Part B.

For Ozawa-Flynn-Wall method, several TGA curves (three or more) can be used simultaneously to determine the activation energy values. The TGA curves move to higher temperatures with increasing heating rates. At the same conversion, the following relationship can be obtained from the P function of Doyle's approximate expression in equation 6.7.

$$\frac{d(\log \beta)}{d(1/T)} = 0.4565(E / R) \quad (6.7)$$

where,

E_a = activation energy in J/mol

R = ideal gas constant = 8.314 Jmol⁻¹K⁻¹

T = temperature in K (Kelvin = °C + 273) corresponding to the measured heating rate at same conversion

β = heating rate in °C/min.

From the slope of the plot $\log(\beta)$ vs $1/T$ at given conversions, E can be calculated.

6.3.1.4 Kissinger Method (DSC/DTG peak, isoconversional)

In this method, the peak temperature from the DSC or DTG curve and heating rate for several thermal analysis curves are correlated and the activation energy can be calculated based on the equation 6.8 [Skoog et al, 1998].

$$\frac{d(\ln \beta / T_p^2)}{d(1/T_p)} = -E / R \quad (6.8)$$

where,

E_a = activation energy in J/mol

R = ideal gas constant = 8.314 Jmol⁻¹K⁻¹

T_p = peak temperature in K (Kelvin = °C + 273)

β = heating rate in °C/min

From the slope of the plot $\ln(\beta/T_p^2)$ vs $1/T_p$, E can be calculated.

6.3.1.5 ASTM Method (DSC peak, isoconversional)

In this method, the sample temperature is increased at linear heating rates and exothermic peaks are recorded [ASTM, 1979 and Skoog et al, 1998]. A trial and error procedure is used for the determination of activation energy. The procedure is as follows:

The reciprocals of temperatures at which reaction maximum occur are plotted as a function of the logarithm of the respective heating rates ($\log \beta$ vs. $1/T_p$). Then, approximate value of activation energy is calculated by the equation below,

$$\frac{d(\log \beta)}{d(1/T_p)} = -E / 2.19R \quad (6.9)$$

To refine E , E/RT_p is calculated approximately. The corresponding value of D is obtained from equation;

$$D = -d[\ln g(x)]/dx \quad (6.10)$$

Assuming,

$$g(x) = (x+2)^{-1} (x^{-1}) (e^{-x}) \quad (6.11)$$

Then, new value of E is evaluated from:

$$\frac{d(\log \beta)}{d(1/T_p)} = -E.D / 2.303R \quad (6.12)$$

These steps must be repeated until E values obtained by these two ways become equal to each other.

CHAPTER 7

RESULTS AND DISCUSSION

In this section, the results from the study are presented and discussed. Firstly, proximate and ultimate analysis of samples were considered. Then, DSC and TGA curves of parent fuels, blended fuels, and biomass model compounds were presented. TGA-MS curves and SEM images of some samples were also given. Kinetic and statistical analysis of obtained output data were discussed at the last part of the section.

7.1 Proximate Analysis

One of the most common and useful methods for analyzing the solid fuels is proximate analysis. Proximate analysis is performed by the help of TGA and is used to calculate the amounts of moisture, volatile matter, fixed carbon, and ash contents. The result of each fuel's proximate analysis is given in Table 7.1a. The biomass fuels have high volatile matter contents. The ash content of the Ulukışla oil shale is very high compared to the biomass fuels. The Ulukışla oil shale's ash content was a challenging factor for its combustion. The Ulukışla oil shale is a low-quality oil shale whereas the Himmetoğlu oil shale is a high-quality oil shale due to their different volatile matter and ash contents as a result of their different depositional history, maturity age, and original organic content. Himmetoğlu oil shale has an increased carbonization of organic material owing to its older age of formation than Ulukışla oil shale.

The biomass fuels have very high volatile matter content and very low ash content as a typical property to yield in easier combustion as shown in the below Table 7.1a. Unlike oil shales, biomass fuels disregarding their location have close properties owing to their similar formation origins.

Table 7.1a. Proximate analysis of fuels (wt. %)

Fuel Type	Moisture	Volatile Matter	Fixed Carbon	Ash
Ulukışla Oil Shale	7.0	8.4	0.1	84.5
Himmetoğlu Oil Shale	5.0	63.0	13.5	18.5
Hazelnut Shell	1.5	69.5	28.9	0.1
Miscanthus	2.0	80.5	16.0	1.5
Poplar	1.0	74.0	24.0	1.0
Wheat Bran	8.0	65.0	24.1	2.9

7.2 Ultimate Analysis

An ultimate analysis was also performed to obtain carbon, nitrogen, and hydrogen contents of each fuel. Because there was only a small amount of sample to work with, sulfur content was not determined. Sulfur contents of these feedstocks are typically low, hence the difference is mostly due to oxygen content. In Table 7.1b the results of each fuel's ultimate analysis can be seen. Ulukışla oil shale is a low grade fuel because of its low carbon and high ash content; on the contrary Himmetoğlu oil shale is high grade fuel having high carbon and low ash content. The difference is due to their depositional history and maturity age. Himmetoğlu oil shale is an older formation than Ulukışla oil shale. This fact naturally increases the carbonization of organic material of Himmetoğlu oil shale. Moreover, Himmetoğlu oil shale is also richer in organic content due to the original formation history.

The combination of high carbon and high oxygen content is also a typical property of biomass fuels as shown in the Table 7.1b.

Table 7.1b. Ultimate analysis of fuels (wt. %)

Fuel Type	C	H	N	O +S (by difference)
Ulukışla Oil Shale	3.75	1.05	0.22	10.48
Himmetoglu Oil Shale	53.30	6.13	1.73	20.54
Hazelnut Shell	50.50	5.63	0.18	43.59
Miscanthus	45.20	5.28	0.01	48.01
Poplar	46.60	5.71	0.45	46.24
Wheat Bran	43.20	6.19	2.58	45.13

7.3 Heat Content

The heat contents of fuels (higher heating value) are presented in Table 7.2 based on bomb calorimeter tests performed in TÜBİTAK – Research Center. Heat content is an indicator of the exothermicity (energy release) of the fuel during combustion. As can be seen in the table, Ulukışla oil shale has the lowest, Himmetoğlu oil shale and hazelnut shell have the highest heat contents among all fuels due to their higher carbon contents and higher combustible volatile contents.

The same samples were also studied by other researchers in the literature (İscan et al, 2007; Altun, 2006; Phyllis, 2013). The results were given in Table 7.3. Information about other oil shale samples studied in the literature is given in the appendix part E. The results of ash contents and heat contents show high match with our results. It is also clear that biomass fuels have no sulfur contents; however Himmetoğlu oil shale and Ulukışla oil shale has 3.1% and 0.8% sulfur contents by weight.

Table 7.2. Heat content of fuels (HHV)

Fuel Type	Heat Content (MJ/kg)	Heat Content (kcal/kg)
Ulukışla Oil Shale	2.60	621.0
Himmetoğlu Oil Shale	20.9	4991.9
Hazelnut Shell	20.4	4872.5
Miscanthus	18.1	4323.1
Poplar	18.7	4466.1
Wheat Bran	17.2	4108.1

Table 7.3. Samples studied by others (İscan et al, 2007; Altun, 2006; Phyllis, 2013)

Fuel Type	Ash Content (wt.%)	Heat Content (MJ/kg)	Sulfur Content (wt.%)
Himmetoğlu Oil Shale	34.8	18.1	3.1
Ulukışla Oil Shale	75.5	3.5	0.8
Hazelnut Shell	1.3	19.3	0
Miscanthus	1.5	18.9	0
Poplar	1.1	19.2	0
Wheat Bran	7.0	17.6	0

7.4 DSC Analysis

DSC curves were used to evaluate the combustion of the fuels. The portion of the curve above '0' on the y-axis of the DSC curves -that shows the heat flow- indicates that the reaction is exothermic; while the portion of the curve below represents an endothermic reaction.

7.4.1 DSC Curves of Parent Fuels

In this part, DSC curves of oil shale and biomass samples are given. The reaction intervals, peak temperatures, and ignition temperatures of each sample at different heating rates are presented. The start and end points in reaction intervals can be identified from the start and end points of shoulders in DSC curves. It is to be noted that the start point of "combustion of light compound" region in oil shale and biomass is the ignition temperature of the samples. The combustion properties of the model compounds of biomass fuels are also presented with DSC curves.

7.4.1.1 Oil Shale

Oil shale combustion is a complex process, and involves a series of parallel reactions [Ots, 2009]. Oil shale combustion is a two-step process: first combustion of light hydrocarbon fractions (bitumen) from the shale organic matter takes place. Combustion of the heavy hydrocarbon fractions (kerogen) follows next. Two reaction regions were identified at intervals of 300-425 °C and 425-600 °C at 50 °C/min. heating rate, first one belonging to the combustion of bitumen in oil shale and second one to the kerogen in oil shale, referring to the studies of other researchers; Kok [2007], Han et al [2006], Kaljuvee et al [2007]. The presentation of reaction regions at DSC profile of Ulukışla oil shale at a heating rate of 50 °C/min. can be seen in Figure 7.1. The figure shows the combustion profile at a high heating rate on purpose, since at higher heating rates the distinction of peaks in DSC curves is observed to be more clear, as also observed by Biagini and Tognotti [2006]. The combustion profiles of Ulukışla and Himmetoğlu oil shales at different heating rates can be seen in the appendix in Figure C.1 and Figure C.2, respectively.

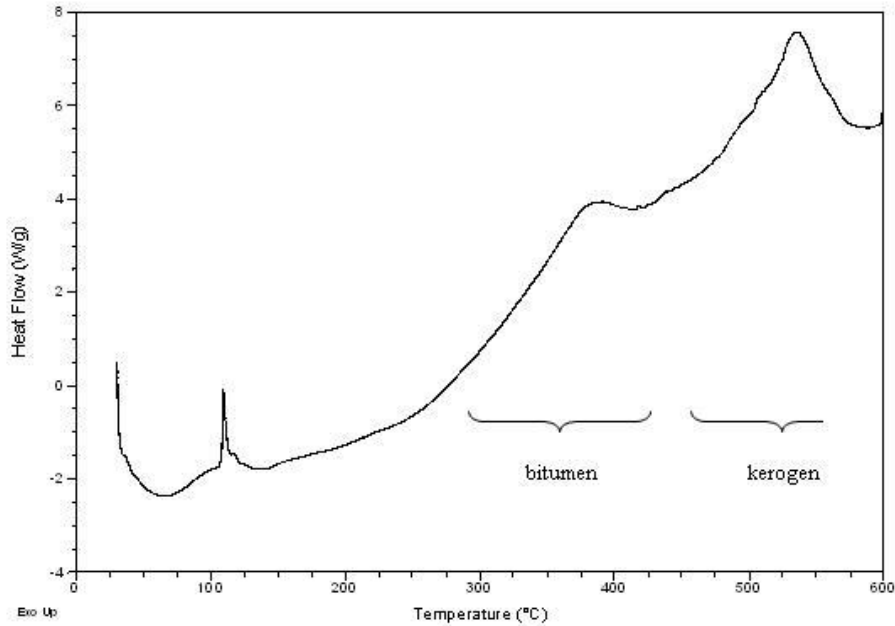


Figure 7.1. Reaction regions in DSC curve of Ulukışla oil shale at 50 °C/min

The same reaction regions observed for the combustion of Ulukışla oil shale (Figure 7.1) are observed for Himmetoğlu oil shale as shown in Figure 7.2. However, the combustion of the Himmetoğlu oil shale is more exothermic (more energetic) compared to Ulukışla oil shale combustion. This fact can be verified by semi-quantitative analysis based on the peak heat flow values in DSC curves, 120 W/g for Himmetoğlu and 8 W/g for Ulukışla oil shale, respectively or it can also be verified by the heat liberated values during reactions given in Table 7.6. Two main reaction regions for both oil shales were identified in intervals of 230-425 °C and 425-600 °C at 50 °C/min. heating rate, first one due to the combustion of bitumen in oil shale and the second one to the kerogen combustion in oil shale. The formation of the two peaks in the second reaction region is due to the combustion of different types of kerogens.

The reaction regions of Ulukışla and Himmetoğlu oil shales at different heating rates are given in Table 7.4. The differences between reaction regions of oil shales are due to their different carbon and volatile matter contents. Kök and Pamir [1998] observed two reaction regions for the combustion of oil shale between around 250-400 °C and 400-600 °C depending on the quality of the oil shale and heating rate of the system which shows good match with the results in Table 7.4.

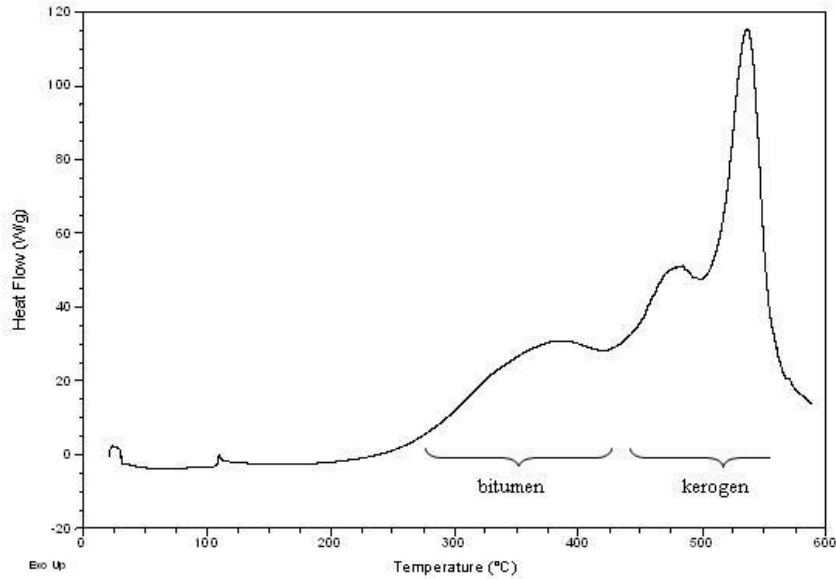


Figure 7.2. Reaction regions in DSC curve of Himmetoğlu oil shale at 50 °C/min

Table 7.4. Reaction regions of oil shale samples

Heating Rate	Fuel Type	Reaction Intervals, C		
		Vaporization of moisture and devolatilization of volatile matter	Combustion of light compounds	Combustion of heavy compounds
50 °C/min	Ulukışla Oil Shale	25-302	302-425	425-600
	Himmetoğlu Oil Shale	25-231	231-425	425-600
30 °C/min	Ulukışla Oil Shale	25-296	296-425	425-550
	Himmetoğlu Oil Shale	25-224	224-410	410-600
10 °C/min	Ulukışla Oil Shale	25-244	244-400	400-550
	Himmetoğlu Oil Shale	25-197	197-375	375-600

7.4.1.2 Biomass

The combustion of biomass fuels is highly exothermic, and their ignition temperature is lower compared to Ulukışla oil shale. However, the ignition temperatures of biomass fuels are higher, compared to Himmetoğlu oil shale due to Himmetoğlu oil shale's higher reactivity as a result of the high carbon and hydrogen content. The DSC combustion profiles of biomass fuels at 50 °C/min heating rate can be seen in the following figures; 7.3, 7.4, 7.5, 7.6. Other DSC profiles at different heating rates can be seen in the appendix part between Figure C.3-C.6.

In the combustion experiments of biomass fuels, two main exothermic peaks were identified between the temperature intervals 250-400 °C and 450-550 °C, respectively which are very close to the results of Grotkjaer et al [2003]. DSC profile of the model compounds are to be investigated for a better perception of the DSC of the biomass fuels. When the two main peaks in DSC of the biomass fuels are checked, it will be noticed that the shape and temperature interval of peaks are similar with the DSC profile of hemicellulose (one of the model compounds in biomass) in Figure 7.15. It can be said that the two main peaks in the DSC profile of biomass fuels are the results of combustion of hemicellulose. However, the height and the width of the peaks in the DSC profile of biomass fuels are different due to the existence of cellulose, lignin, and extractives apart from hemicellulose. The height of the peaks (indication of calorific value) in biomass fuels are lower compared to that of hemicellulose due to the existence of other model compounds and extractives which have lower calorific value.

The ignition temperature of biomasses -although the hemicellulose and lignin content is a factor for the reactivity and lower oxidation stability- is shifted to a slightly higher temperature due to the existence of cellulose (which has higher ignition temperature) and due to the chemical bonds between cellulose, hemicellulose, and lignin that make biomass more difficult to burn. The information about the combustion profile of the model compounds will be given later in the sub-chapters 7.6 and 7.7.4.

Observations in DSC experiments reveal that the reactions between the two main intervals are due to the combustion of lignin taking place in the long interval between the 265-600 °C and combustion of cellulose 385-460 °C. The combustion profiles of biomass samples show close match to other studies in the literature; Biagini and Tognotti [2006], Grotkjaer et al [2003]. The combustion takes in this order according to other researchers as widely reported: at the first stage devolatilization takes place and then combustion of light volatile matters proceed. Finally, combustion ends for biomass with the combustion of heavy volatile matters as stated also in the study of Liang and Kozinski [2000].

It can be inferred from DSC curves that the reactivity of biomass fuel is due to the combustion of light volatiles; however the energy release of biomass fuels is mainly due to the combustion of heavy volatiles based on the larger area of second peak compared to the first peak under DSC curves.

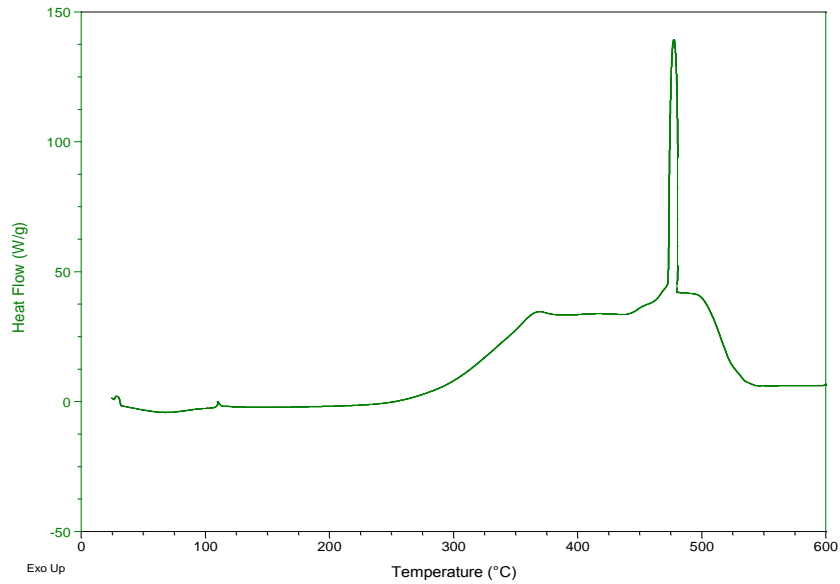


Figure 7.3. DSC curve of hazelnut shell at 50 °C/min

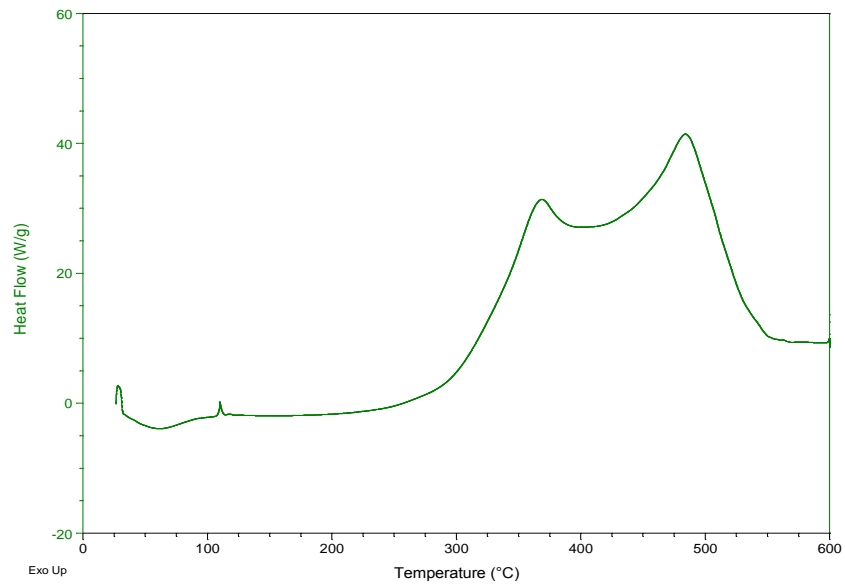


Figure 7.4. DSC curve of miscanthus at 50 °C/min

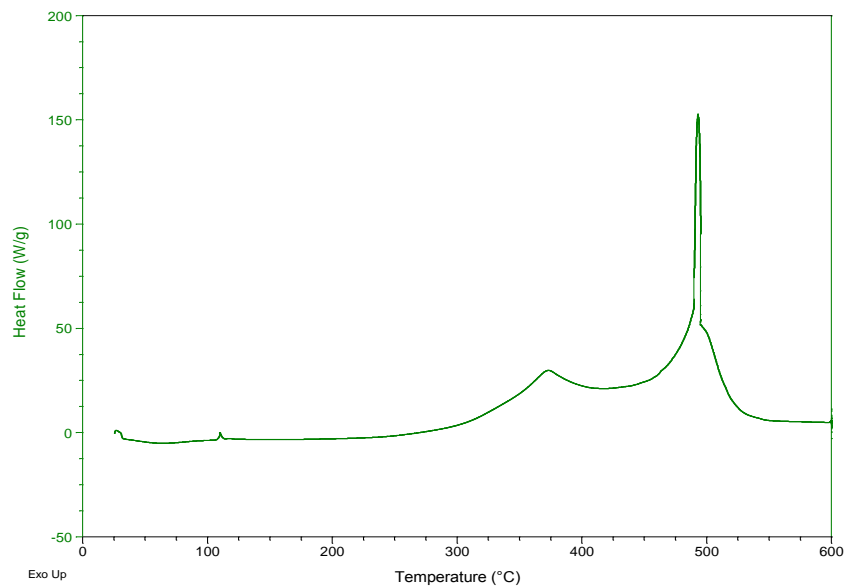


Figure 7.5. DSC curve of poplar at 50 °C/min

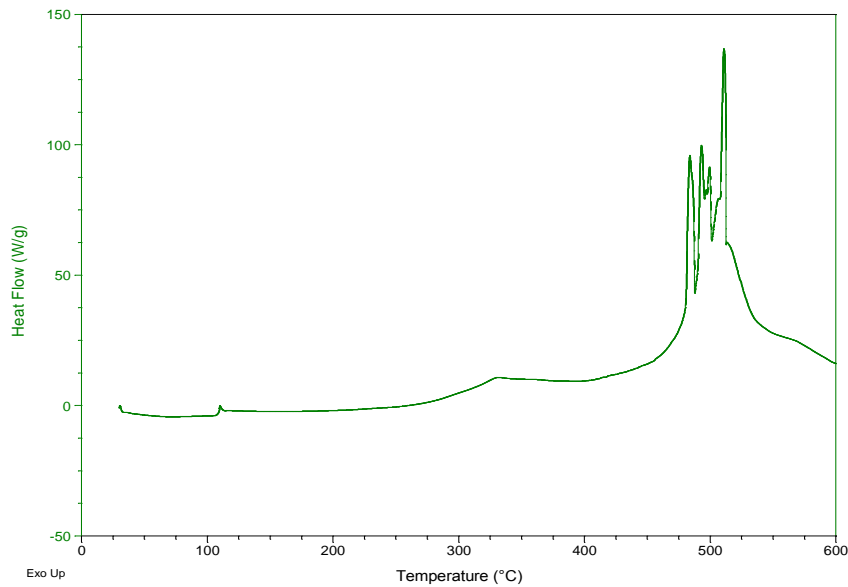


Figure 7.6. DSC curve of wheat bran at 50 °C/min

The reaction regions of hazelnut shell, wheat bran, miscanthus, and poplar at different heating rates are given in Table 7.5. It is clear that as heating rate decreases, also lower start and end points of the reaction intervals (temperature interval) are observed due to the decrease of temperature gradients in samples which form at higher heating rates. Munir et al [2009] identified two main reaction regions appearing between around 250-400 °C and 400-550 °C for different biomass fuels which verifies the results in Table 7.5. The reaction regions for biomass fuels using a heating rate of 50 °C/min. can be seen in Figure 7.7, which indicates that biomass samples have similar combustion behaviors with some minor variances because of matching elemental content and molecular structure.

Table 7.5. Reactions regions of biomass fuels

Heating Rate	Fuel Type	Reaction Intervals, °C		
		Vaporization of moisture and devolatilization of volatile matter	Combustion of light compounds	Combustion of heavy compounds
50 C/min	Hazelnut Shell	25-252	252-400	400-600
	Wheat Bran	25-260	260-400	400-600
	Miscanthus	25-253	253-400	400-600
	Poplar	25-250	250-400	400-600
30 C/min	Hazelnut Shell	25-240	240-400	400-525
	Wheat Bran	25-255	255-400	400-600
	Miscanthus	25-251	251-400	400-525
	Poplar	25-249	250-400	400-525
10C/min	Hazelnut Shell	25-224	224-355	355-500
	Wheat Bran	25-233	233-355	355-550
	Miscanthus	25-220	220-355	355-500
	Poplar	25-219	219-355	355-500

The peak temperatures in DSC curves were also presented in Table 7.6. They have the same tendency with the reaction regions. As heating rate increases both of them increase due to the temperature gradient. Oil shale samples have high and similar peak temperatures because of kerogen's aromatic structure. Biomass samples have lower peak temperatures compared to oil shale's temperatures caused by the high presence of volatiles in biomass. The differences in peak temperatures of biomass samples result from the heavy volatile matters included in samples. Hazelnut shell and miscanthus have the lowest peak temperatures; wheat bran has the highest peak temperature among biomass fuels which have similar tendencies also for the ignition temperatures.

Kök and Pamir [1998] and Yağmur and Durusoy [2009] observed peak temperature values between 400-550 °C for the combustion of Turkish oil shales (Çan, Göynük, Himmetoğlu, and Mengen); depending on the heating rate and Senneca et al [2002] observed peak temperature values between 430-480 °C for the combustion of biomass fuels depending on the heating rate which is consistent with the results in Table 7.6.

Table 7.6. Peak temperatures and heat values obtained from DSC curves

	Peak Temperatures, °C			Heat liberated, kJ/kg		
	HR10	HR30	HR50	HR10	HR30	HR50
Ulukışla	487	517	535	1001	983	932
Himmetoğlu	487	519	536	14084	13910	10764
Hazelnut Shell	454	475	477	12270	8027	7974
Miscanthus	436	468	484	7859	6206	6101
Poplar	456	478	493	8580	6357	6299
Wheat Bran	472	490	511	7667	6278	6019
Ulu-HS10	457	493	506	1761	2123	1448
Ulu-HS20	459	492	498	4383	3332	3105
Ulu-HS50	461	475	498	5620	4919	4568
Ulu-Mis10	452	495	529	2001	1461	1285
Ulu-Mis20	445	495	482	3031	2251	2154
Ulu-Mis50	439	465	482	4351	4195	3764
Ulu-Pop10	459	500	506	2042	1809	1499
Ulu-Pop20	460	485	500	2937	2823	2624
Ulu-Pop50	457	477	497	4711	4055	4017
Ulu-Wheat10	477	516	504	2093	1720	1258
Ulu-Wheat20	477	494	503	2733	2656	2621
Ulu-Wheat50	475	493	500	5411	4086	3128
Hm-HS10	484	518	531	13359	12216	11042
Hm-HS20	483	517	530	12637	11898	11526
Hm-HS50	481	509	529	11020	10370	9885
Hm-Mis10	485	522	540	13407	11804	11707
Hm-Mis20	485	516	536	12953	11728	11490
Hm-Mis50	482	514	533	12380	9758	9734
Hm-Pop10	484	518	538	13417	11942	10622
Hm-Pop20	484	518	538	12567	11243	11055
Hm-Pop50	483	517	534	11211	10560	10356
Hm-Wheat10	487	518	536	13591	11919	10207
Hm-Wheat20	485	518	536	12620	11702	10308
Hm-Wheat50	485	517	535	10842	9018	8125

In Table 7.6 for each fuel and blend, the heat liberated during combustion is given at each heating rate, for comparison. The heat values are calculated based on the area under DSC curve. However, because the mass loss occurs during the combustion all the time, the

values can be used only for comparison among fuels; they can not be used to determine the energy contents of fuels. Although the heat liberated for parent fuels are different compared to results from bomb calorimeter as expected, the results from DSC are consistent to make comparison among fuels and to determine the exothermicity of fuels. The observation that Himmetoğlu oil shale and hazelnut shell have the highest heat contents among the parent fuels is verified with the results in Table 7.2 and Table 7.6.

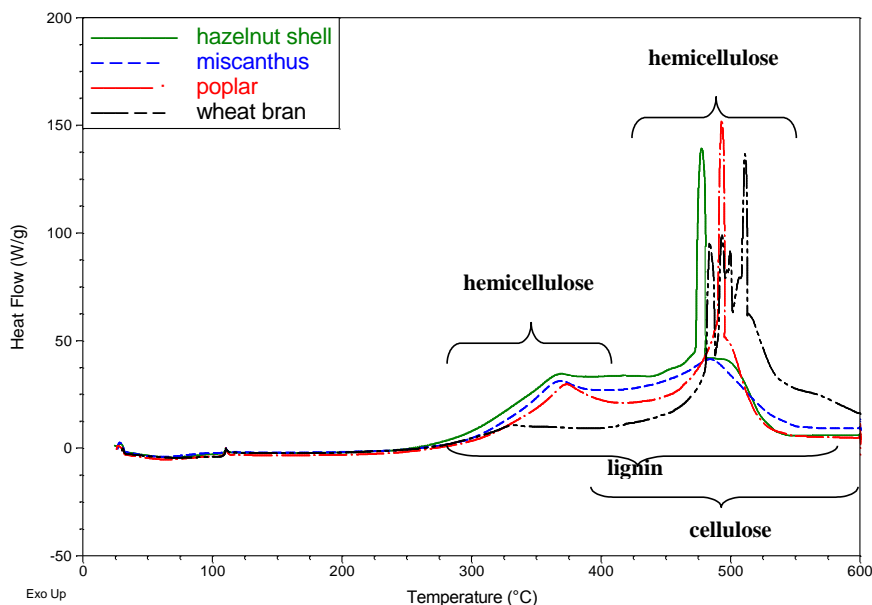


Figure 7.7. Reaction regions in DSC curve of biomass fuels at 50 °C/min

7.4.2 DSC Curves of Blended Fuels

The co-combustion experiments of biomass fuels and oil shale blends using different biomass proportions (10, 20, 50 % by weight) were performed at different heating rates (10, 30, 50 °C/min.). It was observed that as the biomass ratio increased in biomass-Ulukışla oil shale blends, the ignition temperature of the blend decreased because Ulukışla oil shale has higher ignition temperature compared to biomass fuels. On the other hand, for the biomass–higher quality Himmetoğlu oil shale blends the opposite trend was observed, due to the fact that the ignition temperature of Himmetoğlu oil shale is lower than that of biomass blended. Therefore, the addition of biomass is reasonable for the low quality oil shale or oil shale

which has higher ignition temperatures compared to biomass blended. The DSC profiles for each blend at different heating rates are presented in the appendix in Figures C.7-C.30.

7.4.3 Comparison of DSC Curves

In this section, blends at different biomass proportions (10%, 20%, and 50% by weight) are investigated. The DSC curves are presented for the 50 °C/min heating rate for each biomass type and oil shale. It can be seen that the addition of biomass improved the combustion for the Ulukışla oil shale–biomass blends by lowering the ignition temperature. Since biomass fuels contain more energy on a mass basis than Ulukışla oil shale, the energy released during the reactions increases as the ratio of biomass increases in the Miscanthus-Ulukışla oil shale blend as observed from the increased area under the curves in the Figure 7.8. The data of this figure is also tabulated in Table 7.6. However, since the Himmetoğlu oil shale has energy content close to the biomass fuels, the DSC curves of blends of Himmetoğlu oil shale and Miscanthus are similar as can be seen in Figure 7.9. DSC profiles for the co-combustion between other biomass fuels and oil shales are provided in the appendix in Figures C.31-C.36 that confirms the above observations as well.

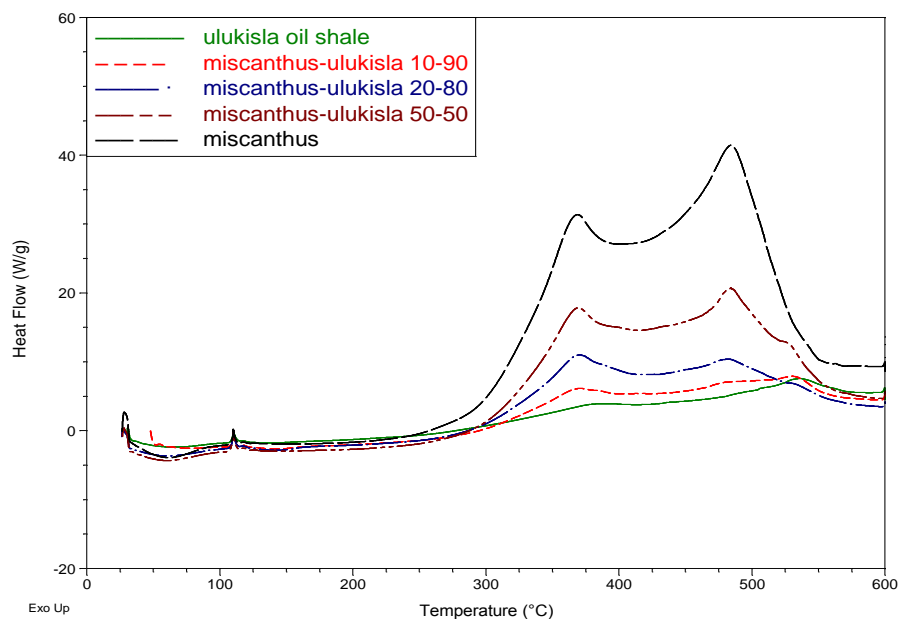


Figure 7.8. Comparison of DSC curves for miscanthus-Ulukışla at 50 °C/min

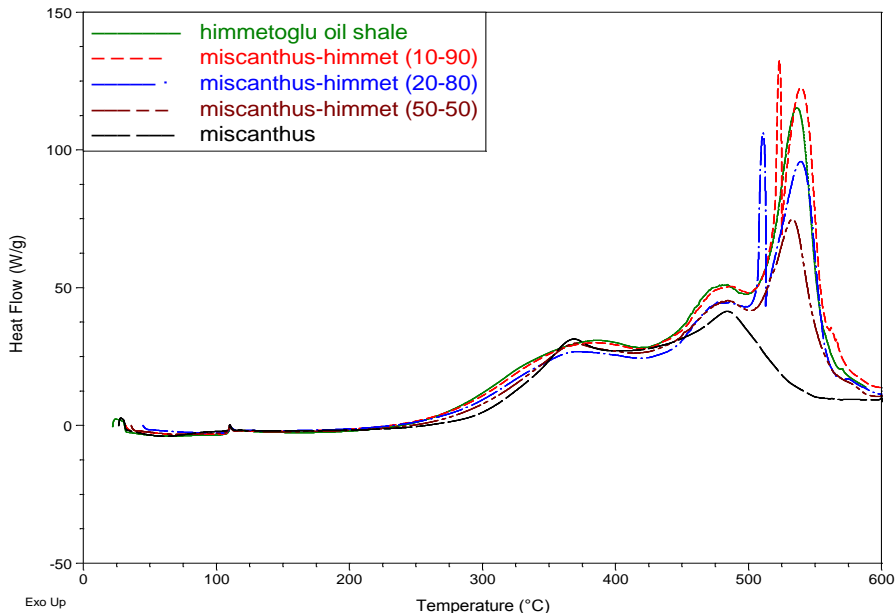


Figure 7.9. Comparison of DSC curves for miscanthus- Himmetoğlu at 50 °C/min

7.5 Ignition Temperature

Ignition temperature is the lowest temperature at which combustion starts to occur and stay self-sustained. It can be an indicator for the degree of difficulty of a combustion process. As ignition temperature decreases, combustion occurs more easily. Determining of ignition temperature is complicated since the ignition temperature is not a fundamental parameter of the fuel; it can depend on the sample mass, the particle size, the heating rate of the particle, the pressure of environment, and the surrounding gas [Zhang and Wall, 1994]. Consequently, different experimental techniques may lead to very different ignition temperatures for the same fuel [Grotkjaer et al, 2003]. Some experimental techniques to determine ignition temperature include: detection of a flame, an increase in sample temperature, an increase in the CO_2/CO ratio, laser-induced ignition, and determination from TGA or DSC curves [Zhang and Wall, 1994].

In this work, ignition temperatures of each fuel are tabulated in Tables 7.7, 7.8, and 7.9. They were determined from DSC curves, which is a useful technique also used by others [Leroy et al, 2006]. DSC curves are preferred for determination since determining ignition temperature using TGA and DTG is not as accurate because the pyrolysis and devolatilization reactions occurring before the onset combustion make it difficult to identify the ignition temperature. There are also different determination methods for each

experimental technique to obtain ignition temperature. For example, extrapolation method or first deviation from baseline method can be used when working with DSC. When using a DSC in this study, the ignition temperature is based on the first deviation from the baseline instead of applying an extrapolation method, which is common when using a TGA or DTG. The DSC equipment has high sensitivity and its use eliminates high errors common with the extrapolation method as reported by other researchers [Boettinger, 2006 and Wiley, 2008]. The extrapolation method is not a reliable method and its uncertainty is difficult to estimate [Ferreira, 2010].

The blending ratios are presented (in the parenthesis in terms of weight percentages) in the following tables (Tables 7.8, 7.9, 7.10) and it can be observed that increase of biomass content in the blends decreases the ignition temperature of the Ulukışla oil shale – biomass blends; however, the opposite effect is observed for Himmetoğlu oil shale – biomass blends. This is due to the higher ignition temperature and ash content of Ulukışla oil shale and lower ignition temperature and ash content of Himmetoğlu oil shale compared to the biomass fuels' ignition temperatures.

It is also observed that as the heating rate increases, the ignition temperature values increases. This is due to the shorter residence times for fuels at higher heating rates.

Table 7.7. Ignition temperatures of the parent fuels at different heating rates

Parent Fuels	10 °C/min	30 °C/min	50 °C/min
Ulukışla Oil Shale	244	296	302
Himmetoğlu Oil Shale	197	224	231
Hazelnut Shell	224	240	252
Wheat Bran	233	255	260
Poplar	219	249	250
Miscanthus	220	251	253

Table 7.8. Ignition temperatures of the blend of Ulukışla oil shale and other biomass fuels at different heating rates

Ignition Temperatures of Ulukışla oil shale and biomass fuels			
Blends, in wt. %	10 °C/min	30 °C/min	50 °C/min
Oil Shale-Hazelnut Shell (90-10)	243	266	283
Oil Shale-Hazelnut Shell (80-20)	236	260	271
Oil Shale-Hazelnut Shell (50-50)	235	244	257
Oil Shale-Wheat Bran (90-10)	239	275	295
Oil Shale-Wheat Bran (80-20)	236	269	279
Oil Shale-Wheat Bran (50-50)	235	260	269
Oil Shale-Miscanthus (90-10)	238	285	295
Oil Shale-Miscanthus (80-20)	236	276	287
Oil Shale-Miscanthus (50-50)	233	264	278
Oil Shale-Poplar (90-10)	241	263	290
Oil Shale-Poplar (80-20)	221	256	279
Oil Shale-Poplar (50-50)	220	250	272

Table 7.9. Ignition temperatures of the blend of Himmetoğlu oil shale and other biomass fuels at different heating rates

Ignition Temperatures of Himmetoğlu oil shale and biomass fuels			
Blends, in wt. %	10 °C/min	30 °C/min	50 °C/min
Oil Shale-Hazelnut Shell (90-10)	206	226	232
Oil Shale-Hazelnut Shell (80-20)	208	227	233
Oil Shale-Hazelnut Shell (50-50)	220	228	239
Oil Shale-Wheat Bran (90-10)	199	225	232
Oil Shale-Wheat Bran (80-20)	201	227	239
Oil Shale-Wheat Bran (50-50)	207	228	245
Oil Shale-Miscanthus (90-10)	197	232	231
Oil Shale-Miscanthus (80-20)	201	238	240
Oil Shale-Miscanthus (50-50)	212	241	247
Oil Shale-Poplar (90-10)	198	229	232
Oil Shale-Poplar (80-20)	199	230	233
Oil Shale-Poplar (50-50)	204	231	234

To evaluate the ignition temperatures of the Ulukışla oil shale / biomass blends, the effect of increasing biomass ratio on the blends are presented graphically. This was not done with the Himmetoğlu oil shale and biomass blends because of the negative effect of the biomass on ignition temperature. In Figures 7.10, 7.11, and 7.12, ignition temperature profiles of each biomass – Ulukışla oil shale blend can be seen for different heating rates.

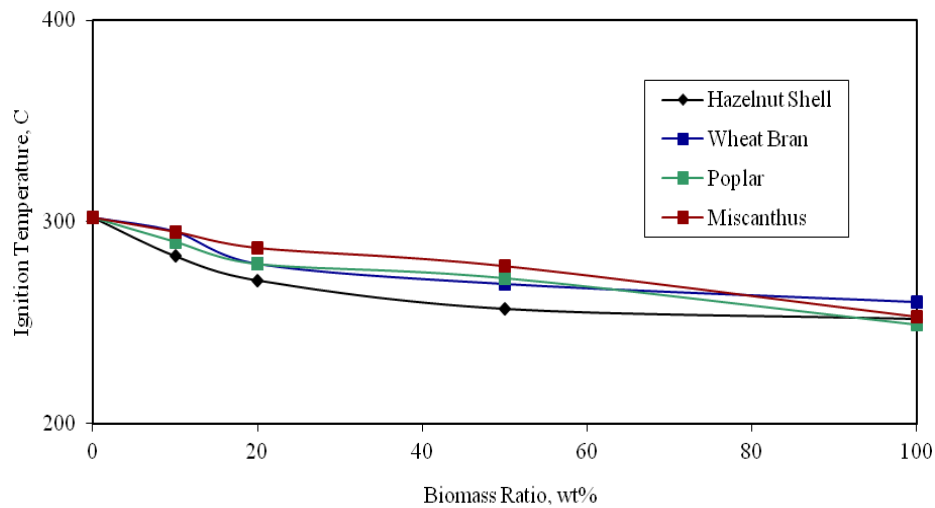


Figure 7.10, Change of ignition temperature of Ulukışla oil shale-biomass blend with biomass ratio (10, 20, 50%) at 50 °C/min

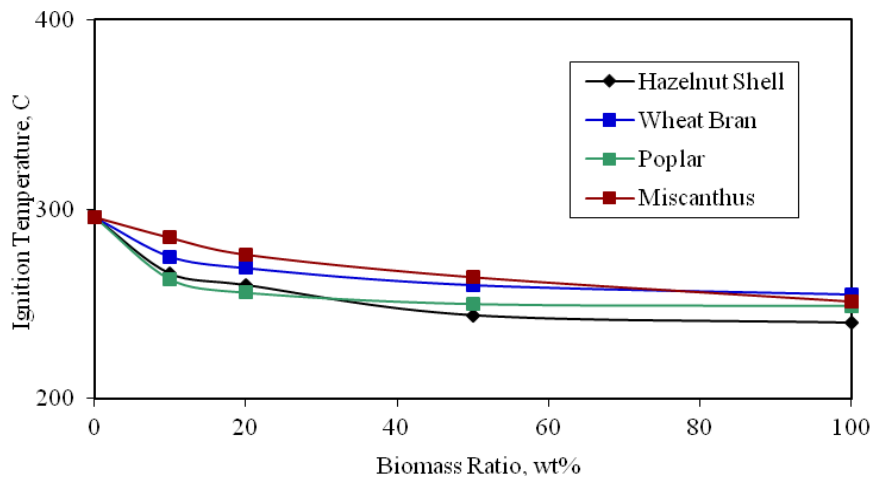


Figure 7.11, Change of ignition temperature of Ulukışla oil shale-biomass blend with biomass ratio (10, 20, 50%) at 30 °C/min

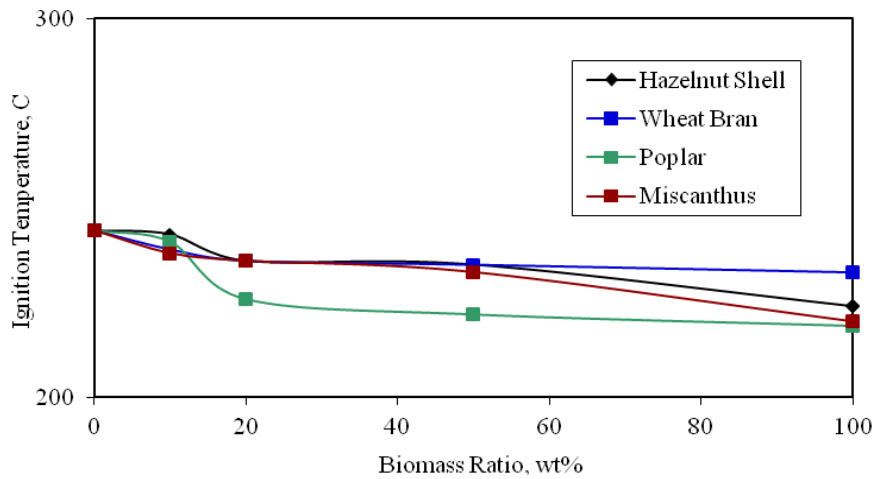


Figure 7.12, Change of ignition temperature of Ulukışla oil shale-biomass blend with biomass ratio (10, 20, 50%) at 10 °C/min

It is observed in the Figures 7.10, 7.11 and 7.12 that the change in ignition temperature up to 20% biomass ratio in the blends is high. However, when biomass ratio is increased over 20%, the rate of change of the ignition temperature decelerates. There is almost no change in the ignition temperatures of blends with 50% and more biomass. The ignition temperature stabilizes after that proportion. This is the impact of biomass domination in the blends.

The trendline of ignition temperature with volatile matter content at different heating rates is given in Figure 7.13. It can be seen in Figure 7.13 that the ignition temperature decreases as volatile matter content increases. The rate of ignition temperature decreases plateaus after 40% by weight of volatile matter content and the ignition temperature is stabilized.

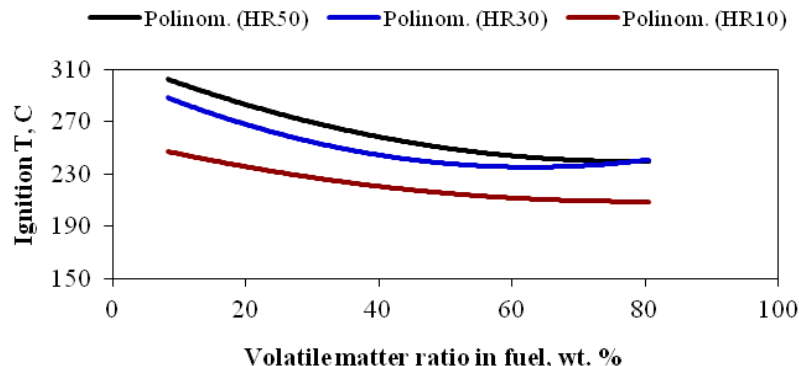


Figure 7.13. Variation of ignition temperature with volatile matter content

7.6 Biomass Model Compounds

The ignition temperatures of biomass model compounds are given at different heating rates in Table 7.10, as obtained from the DSC. The concentrations of biomass components in each biomass fuel are given in Table 7.11 following the lab procedures of Sluiter et al [2005]. There are numerous types of model compounds. In this study the model compounds tested are CF11 fibrous cellulose powder, hemicellulose (xylan) from birchwood, and loblolly pine lignin. The composition of model compounds can be deterministic on the ignition temperature of the fuel. So, model compounds were tested individually. Among the three components, cellulose was the most difficult one to combust.

Table 7.10. Ignition temperatures of biomass model compounds at different HR

Samples	10 °C/min	30 °C/min	50 °C/min
Cellulose	273	369	383
Hemicellulose	210	238	251
Lignin	240	252	264

Table 7.11. Lignocellulosic contents of biomass fuels
(provided by Pisa University – Department of Chemical Engineering and Penn State EMS
Energy Institute)

Biomass Fuels	Cellulose Cont., wt.%	Hemicellulose Cont., wt.%	Lignin Cont., wt.%	Extractives, wt.%
Hazelnut Shell	26.2	22.1	36.5	15.2
Miscanthus	27.7	33.9	18.7	19.7
Poplar	43.8	22.0	11.1	23.1
Wheat Bran	12.0	36.0	3.0	49.0

7.6.1 DSC curves of biomass model compounds

The DSC curves for cellulose, hemicellulose, and lignin are presented in Figures 7.14 through 7.16. Hemicellulose exhibited highly exothermic combustion compared to lignin and cellulose. Cellulose has a higher ignition temperature and the lowest heat of reaction among the model compounds as seen in the Figures 7.14 through 7.16. Because hemicellulose is composed of highly branched polymers of carbon sugars, it is easily oxidized during combustion so that it has the lowest ignition temperature among the model compounds. During the combustion of hemicellulose, light compounds burn first, and the combustion of heavy compounds occur later, as can be seen in the DSC profile of hemicellulose (Figure 7.15). The combustion of cellulose occurs in the interval 385-460 °C, between 460-600 °C with the oxidation of degraded fragments and depolymerization reactions occurring. The combustion of lignin occurs in the long interval between 265-600 °C in two stages with the consumption of light compounds (265-400 °C) followed by the heavy compounds (400-600 °C). If the DSC profiles of model compounds and biomass fuels are compared, it can be seen that the DSC profile of wheat bran and hemicellulose show high similarity. This is due to the high hemicellulose content of wheat bran among the biomass fuels. Same reaction intervals for the combustion of model compounds and similar DSC profiles can be seen in the study of Ramiah [1970] and Shukry et al [1991]. It can be inferred that the composition of model compounds can be deterministic on the ignition temperature and combustion behavior of fuels so that model compound composition of fuels should also be tested in order to have a clear idea.

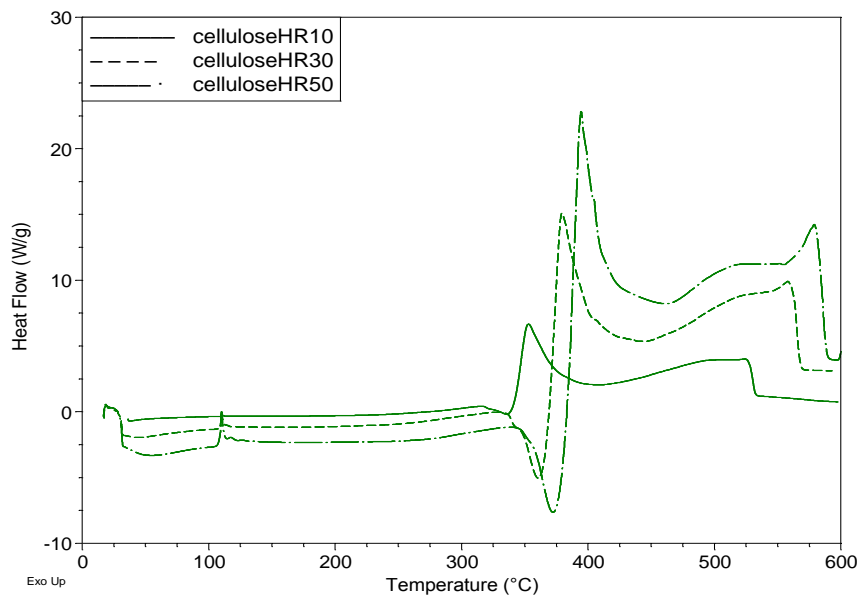


Figure 7.14. DSC curve of cellulose

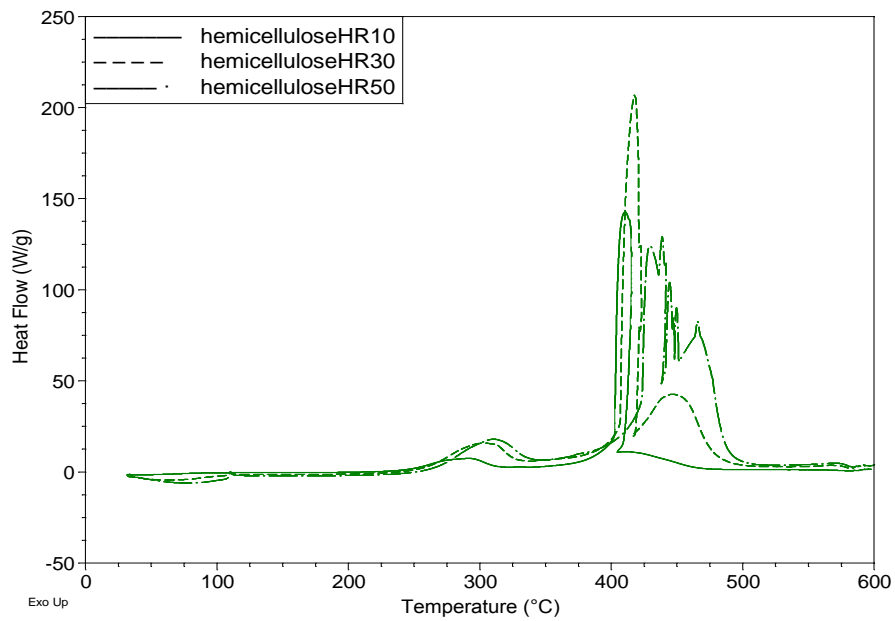


Figure 7.15. DSC curve of hemicellulose

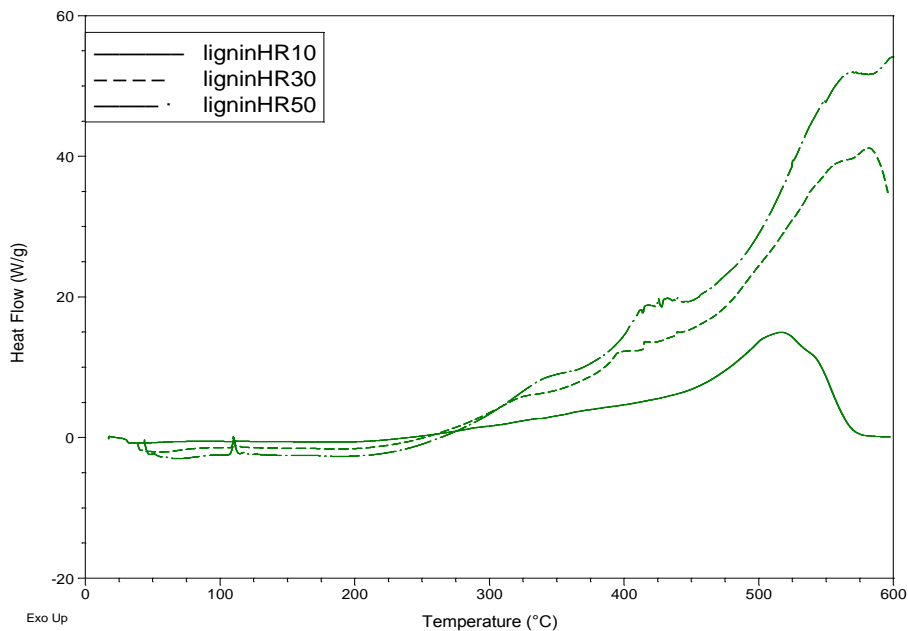


Figure 7.16. DSC curve of lignin

7.7 TGA Analysis

In this section, the results from TGA analysis of parent fuels and blends and later, comparisons of TGA curves are presented. The TGA curves are presented with weight loss in percentage and derivative thermogram (DTG) versus temperature. In TGA curves, weight loss values can be seen in the left side of the figures and derivative weight loss rates (DTG) can be seen in the right side of the figures. The reaction regions, peak temperatures, and weight loss ratios of each sample at different heating rates are presented. The combustion properties of the model compounds of biomass fuels are also presented with TGA curves.

7.7.1 TGA Curves of Parent Fuels

The combustion profile of oil shales in a TGA operated at 50 °C/min. heating rate can be seen in Figures 7.17 and 7.18. The TGA profiles using different heating rates are provided in the Appendix in Figures C.37-C.38. From the combustion profile of the Ulukışla oil shale, it is clear that as the heating rate increases the rate of DTG increases in the specific interval. This is the result of high heating leading to higher mass loss rate. At 110 °C, a sharp loss in mass can be observed because moisture is evolved at this point. The system is kept

isothermal for 5 minutes to drive off the moisture. Similar to the DSC profiles of the Ulukışla oil shale, two reaction regions can be identified between the intervals 300-425 °C and 425-600 °C when using a heating rate of 50 °C. The first period represents the combustion of bitumen while the second one identifies combustion of kerogen. After 600 °C, mineral decomposition occurs. It is clear that between 600 °C and 800 °C, mineral decomposition occurs. Same reaction regions were observed in the study of Kaljuvee et al [2007].

From the TGA profile of the Himmetoğlu oil shale, it was observed that the combustion of Himmetoğlu oil shale is more exothermic compared to the Ulukışla oil shale. The DTG peak of Himmetoğlu oil shale is much higher than that of Ulukışla oil shale. The TGA profile of Himmetoğlu oil shale shows three main peaks. The first peak is probably due to the combustion of light volatiles like bitumen. The other two peaks in the reaction region is clear and possibly due to the combustion of different types of kerogens. The reaction regions of the oil shale samples can be seen in Figure 7.17 and Figure 7.18.

The combustion profile of the parent biomass fuels using a TGA at 50 °C/min. heating rate can be seen in Figures between 7.19 and 7.22. The TGA profiles generated at different heating rates are provided in the appendix in Figures C.39-C.42. It is clear that all have similar combustion TGA profiles. They have two main reaction regions which can be verified by DTG peaks. The first peaks are the beginning part of devolatilization prior to combustion. The point where the reaction passes from devolatilization to combustion can be verified with the DSC data. The reaction regions of the biomass fuels showing the regions where the various constituents react as identified by model compounds can be seen in Figure 7.23.

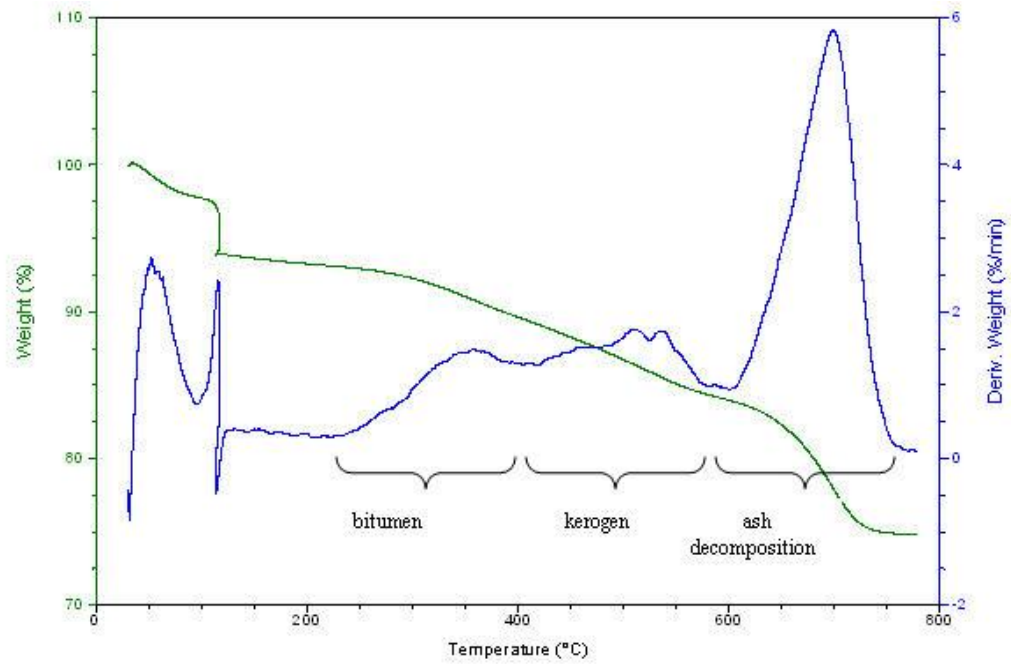


Figure 7.17 Reaction regions in TGA curve of Ulukışla oil shale at 50 °C/min

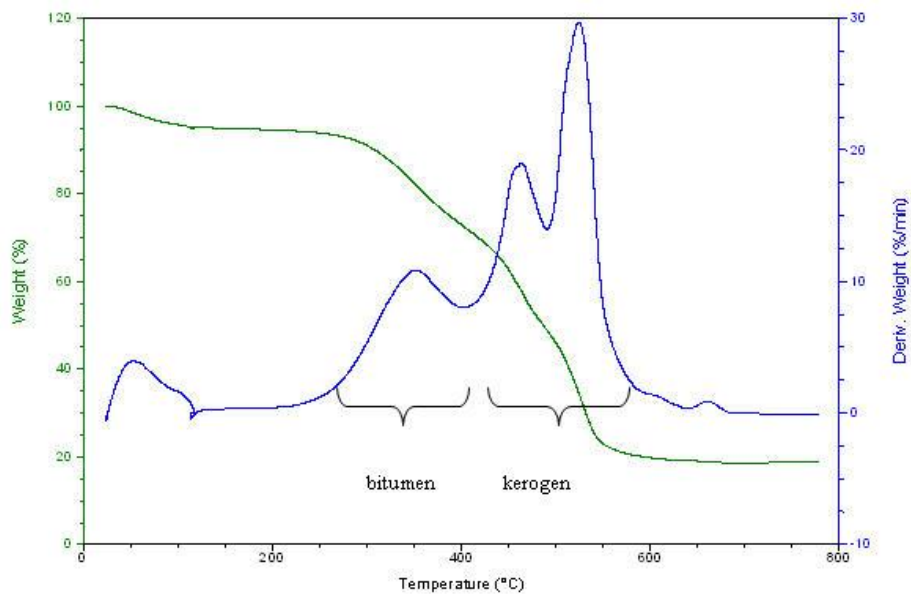


Figure 7.18 Reaction regions in TGA curve of Himmetoğlu oil shale at 50 °C/min

The reaction regions and the weight loss of the oil shales in the reaction regions at different heating rates can be seen in Table 7.12 and 7.13, respectively. Although TGA is useful for determining the reaction intervals, it is not as accurate as DSC so that the values were reported with approximation. The reaction intervals obtained from TGA are quite similar to those obtained from DSC as in Table 7.4. The weight loss amounts during combustion are much higher for Himmetoğlu oil shale compared to Ulukışla oil shale. This is due to high volatile matter and high fixed carbon content of Himmetoğlu oil shale with its lower ash content. It is clear that the Himmetoğlu oil shale has more light and heavy compounds compared to the Ulukışla oil shale from Table 7.13. The amount of heavy compounds (kerogen) is greater than light compounds (bitumen) amount for both oil shale samples as well. It was observed that the total weight loss during the combustion of each oil shale is almost the same for each heating rate so that no relationship was observed connected with heating rate due to the partial mixing of reaction regions at higher heating rates. K k and Pamir [1998] observed two reaction regions for the combustion of oil shale between around 250-400  C and 400-600  C depending on the quality of the oil shale and heating rate of the system which shows good match with the results in Table 7.12.

Table 7.12. Reaction regions of oil shale samples

Heating Rate	Fuel Type	Reaction Intervals, �C		
		Vaporization of moisture and devolatilization of volatile matter	Combustion of light compounds	Combustion of heavy compounds
50 �C/min	Ulukışla Oil Shale	25-300	300-425	425-600
	Himmetoğlu Oil Shale	25-230	230-425	425-600
30 �C/min	Ulukışla Oil Shale	25-300	300-425	425-550
	Himmetoğlu Oil Shale	25-225	225-410	410-600
10 �C/min	Ulukışla Oil Shale	25-245	245-400	400-550
	Himmetoğlu Oil Shale	25-200	200-375	375-600

Table 7.13. Weight loss of oil shales in the reaction regions

Heating Rate	Fuel Type	Weight Loss, %		
		Vaporization of moisture and devolatilization of volatile matter	Combustion of light compounds	Combustion of heavy compounds
50 °C/min	Ulukışla Oil Shale	7.8	3.3	5.0
	Himmetoğlu Oil Shale	5.9	25.5	48.9
30 °C/min	Ulukışla Oil Shale	9.1	2.4	3.5
	Himmetoğlu Oil Shale	3.8	23.7	48.9
10 °C/min	Ulukışla Oil Shale	7.5	2.8	3.2
	Himmetoğlu Oil Shale	5.0	20.7	48.3

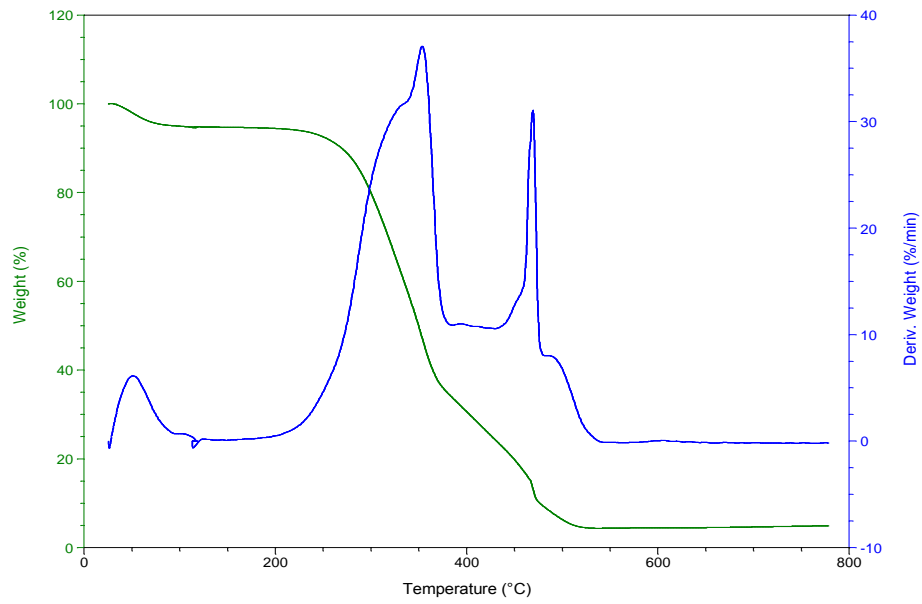


Figure 7.19. TGA curve of hazelnut shell at 50 °C/min

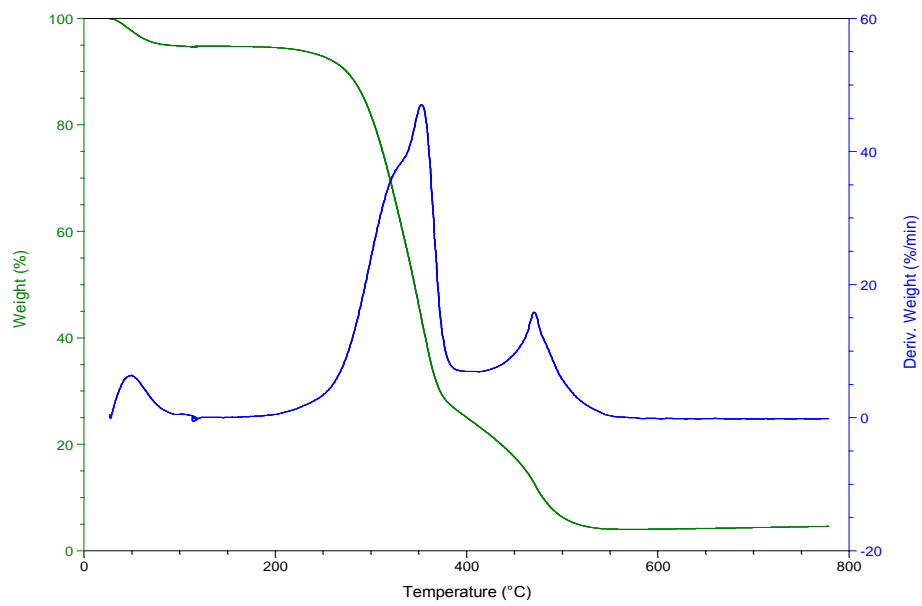


Figure 7.20. TGA curve of miscanthus at 50 °C/min

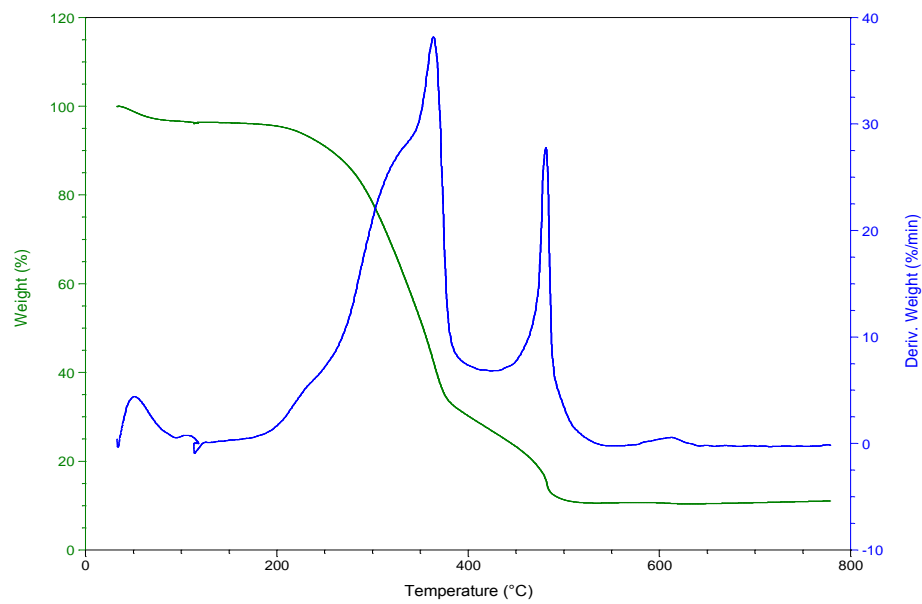


Figure 7.21. TGA curve of poplar at 50 °C/min

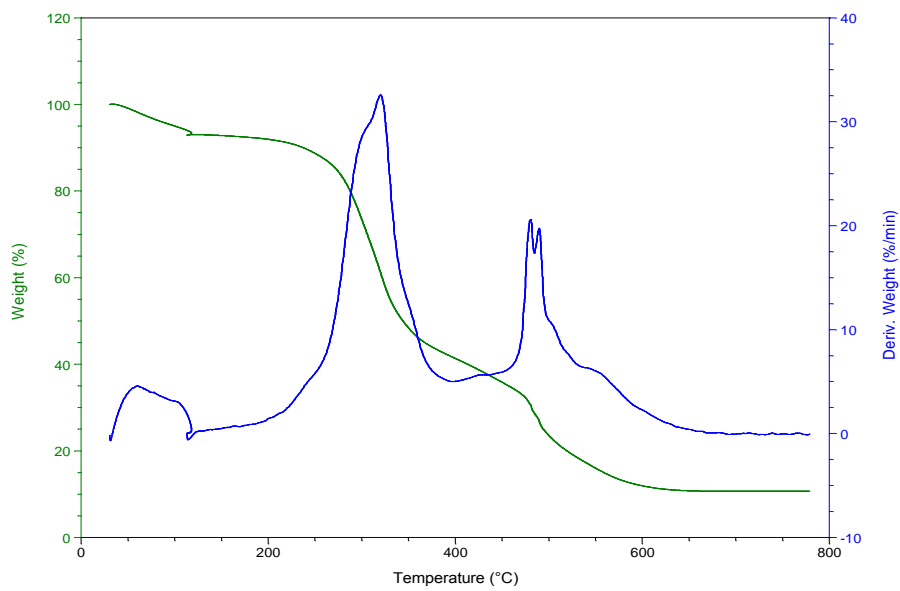


Figure 7.22. TGA curve of wheat bran at 50 °C/min

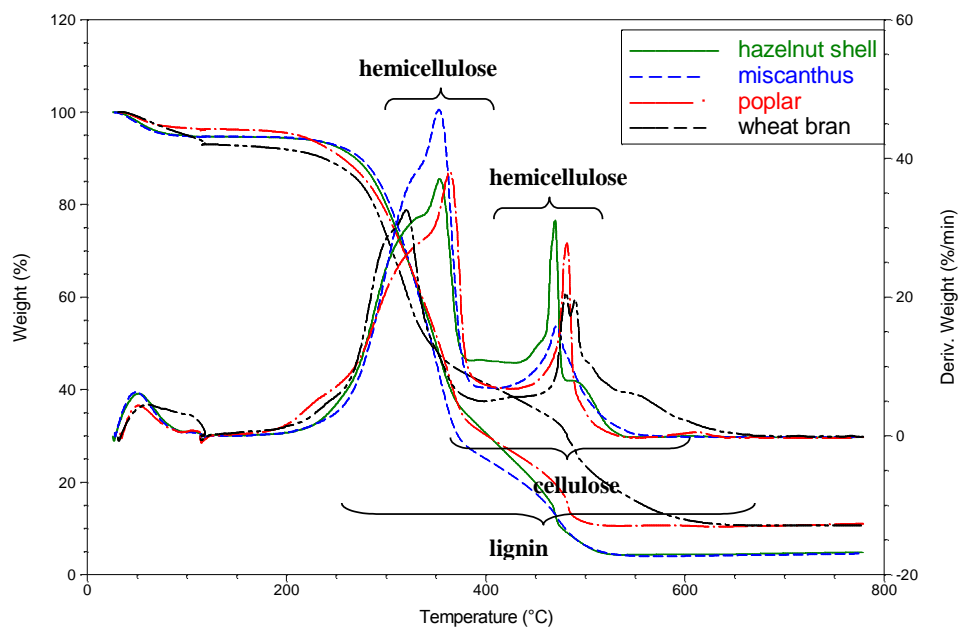


Figure 7.23. Reaction regions in TGA curve of biomass fuels at 50 °C/min

The reaction regions and the weight loss of the biomass fuels in the reaction regions at different heating rates can be seen in Table 7.14 and 7.15, respectively. As mentioned, although TGA is useful for determining the reaction intervals, it is not as accurate as DSC so that the values were reported with approximation. The reaction intervals obtained from TGA are quite similar to those obtained from DSC as in Table 7.5. It is clear that in biomass fuels the quantity of light compounds is considerably greater than the amount of heavy compounds. The high amount of light compounds in biomass provides reactivity at the early stage of the combustion. It was observed that the heating rate is important for the combustion of heavy compounds in biomass. As heating rate decreases weight loss increases for the combustion of heavy compounds as can be seen in the table, because time needed is higher for the destruction of the heavy compounds. However, no relationship can be set for the reaction in the devolatilization and combustion of light compounds with heating rate because of biomass volatiles' less dependence on heating rate due to their reactivity and mixing of reaction regions at higher heating rates.

Table 7.14. Reactions regions of biomass fuels

Heating Rate	Fuel Type	Reaction Intervals, C		
		Vaporization of moisture and devolatilization of volatile matter	Combustion of light compounds	Combustion of heavy compounds
50 C/min	Hazelnut Shell	25-250	250-400	400-600
	Wheat Bran	25-260	260-400	400-600
	Miscanthus	25-250	250-400	400-600
	Poplar	25-250	250-400	400-600
30 C/min	Hazelnut Shell	25-240	240-400	400-525
	Wheat Bran	25-255	255-400	400-600
	Miscanthus	25-250	250-400	400-525
	Poplar	25-250	250-400	400-525
10C/min	Hazelnut Shell	25-225	225-355	355-500
	Wheat Bran	25-235	235-355	355-550
	Miscanthus	25-220	220-355	355-500
	Poplar	25-220	220-355	355-500

Munir et al [2009] identified two main reaction regions appearing between around 250-400 °C and 400-550 °C for different biomass fuels which verifies the results in Table 7.14

Table 7.15. Weight loss of biomass fuels in the reaction regions

Heating Rate	Fuel Type	Weight Loss, %		
		Vaporization of moisture and devolatilization of volatile matter	Combustion of light compounds	Combustion of heavy compounds
50 C/min	Hazelnut Shell	7.5	62.2	26.0
	Wheat Bran	12.5	46.1	29.3
	Miscanthus	7.2	67.9	20.9
	Poplar	9.0	60.9	19.5
30 C/min	Hazelnut Shell	8.5	64.1	23.4
	Wheat Bran	12.7	48.1	30.5
	Miscanthus	5.6	74.5	20.7
	Poplar	12.2	64.0	19.8
10C/min	Hazelnut Shell	3.7	58.9	33.8
	Wheat Bran	10.6	43.9	36.8
	Miscanthus	3.1	65.8	22.8
	Poplar	6.1	68.6	24.7

The peak temperatures of each fuel and blends in TGA curves are presented in Table 7.16. The results of peak temperatures in TGA curves are similar to those in DSC curves presented in Table 7.6. However, there are some minor differences between results. This is due to the fact that, in DSC curves peak temperatures are the result of maximum energy given by combustion (it only includes exothermic reactions, not devolatilization reactions); however, in TGA curves peak temperatures is the result of maximum weight loss due to combustion and devolatilization reactions. The parallel devolatilization reactions can affect results slightly in TGA curves. The results of the study of K k and Pamir [1998], Yađmur and Durusoy [2009] for the combustion of Turkish oil shales and Senneca et al [2002] for the combustion of biomass fuels are consistent with the results in Table 7.16.

Table 7.16. Peak temperatures obtained from TGA curves

	HR10	HR30	HR50
Ulukışla	473	522	538
Himmetoğlu	483	514	525
Hazelnut Shell	447	456	469
Miscanthus	441	467	470
Poplar	452	464	481
Wheat Bran	474	489	490
Ulu-HS10	456	485	492
Ulu-HS20	456	481	491
Ulu-HS50	455	477	482
Ulu-Mis10	451	470	479
Ulu-Mis20	445	470	477
Ulu-Mis50	442	469	476
Ulu-Pop10	460	487	492
Ulu-Pop20	459	480	492
Ulu-Pop50	455	472	481
Ulu-Wheat10	477	509	518
Ulu-Wheat20	477	506	505
Ulu-Wheat50	472	504	495
Hm-HS10	483	511	525
Hm-HS20	482	509	525
Hm-HS50	480	503	490
Hm-Mis10	483	509	520
Hm-Mis20	482	508	504
Hm-Mis50	481	505	503
Hm-Pop10	483	512	513
Hm-Pop20	483	505	513
Hm-Pop50	481	504	504
Hm-Wheat10	483	516	529
Hm-Wheat20	483	515	529
Hm-Wheat50	483	515	529

7.7.2 TGA Curves of Blended Fuels

Co-combustion experiments of biomass fuels and oil shale blends were performed using different biomass proportions (10, 20, 50 % by weight) and different heating rates (10, 30, 50 °C/min.). It was observed that the degree of derivative weight increases as the heating

rate increases due to the higher contacted temperature at specified temperature interval. It is also observed that the ash contents are not severely affected by the heating rates. The heating rates are sufficient to complete the combustion. There are slight differences between the ash contents of same samples/blends at different heating rates due to experimental error and sample heterogeneity. However, at 10 °C/min. heating rate, ash contents are generally slightly lower due to the longer exposure time to combustion. Low heating rate eases the destruction of compounds due to higher contact time and leads to lesser amount of incombustible materials. The TGA profiles of combustion of each blend at different heating rates are presented in the appendix part between Figure C.43-C.66. The reaction regions observed in the TGA curves of parent fuels (oil shale and biomass samples) are also observed in the TGA curves of blended fuels; however the interval of reaction regions and the shape of DTG shoulders in the blends are partly distorted as a result of the partial overlapping of reaction regions of oil shale and the biomass.

7.7.3 Comparisons of TGA Curves

In this section, blends at different biomass proportions for each fuel type are discussed. TGA graphs using the 50 °C/min heating rate are presented because they exhibited better combustion conditions as evidenced by the decrease in organic matter loss from devolatilization at the higher heating rates. For the blend of miscanthus and the two oil shales, the TGA curves are presented in Figure 7.24 and Figure 7.25. Blends between other biomass types and oil shales are provided in the appendix in Figures C.67-C.72. As the biomass ratio increases in the blends, the ash content of the each blend decreases, because of the lower ash content of biomass fuels. Since the biomass fuels have higher reactivities compared to the Ulukışla oil shale, the addition of biomass also increases the mass loss rate (DTG) in the blend of biomass and Ulukışla oil shale at every proportion.

However, the addition of biomass only increases the rate of mass loss during the early stages of combustion in the blends of biomass and Himmetoğlu oil shale because the high volatile matter content of the biomass devolatilized at the beginning of combustion (Table 7.17). During the later stages, there is almost no difference in the DTG curves because of similar reactivities of the oil shale and biomass.

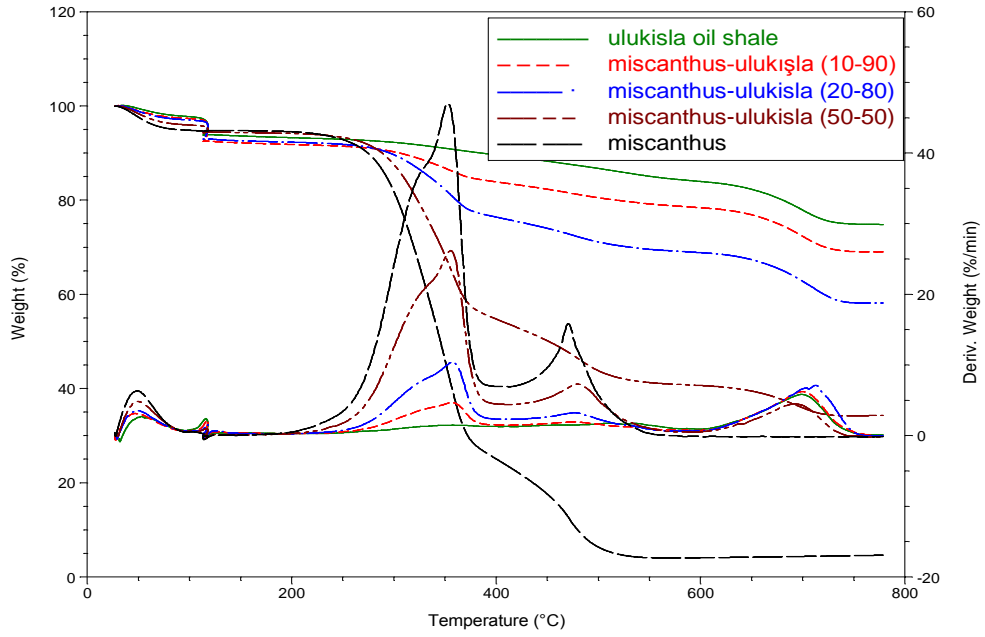


Figure 7.24. Comparison of TGA curves for miscanthus-Ulukışla at 50 °C/min

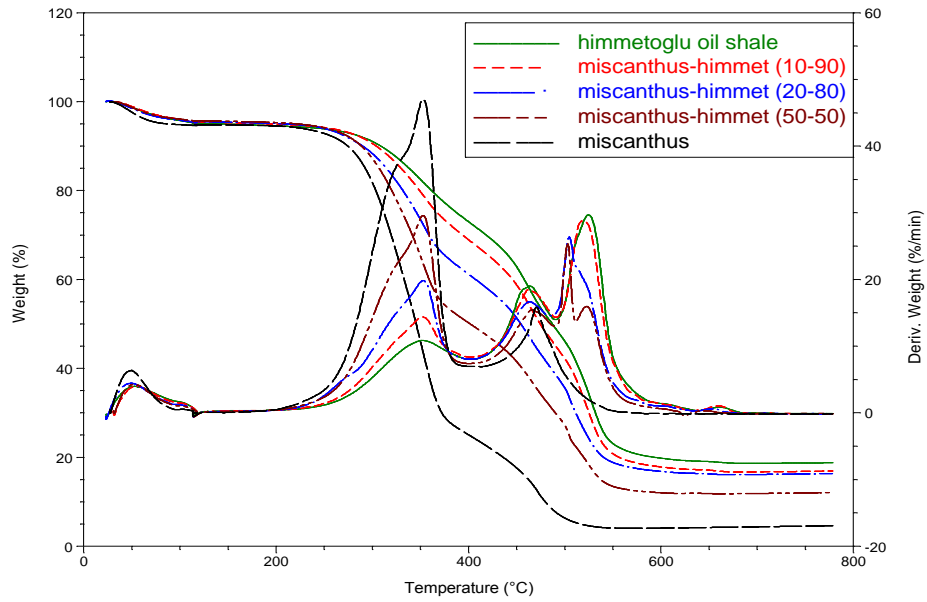


Figure 7.25. Comparison of TGA curves for miscanthus-Himmetoğlu at 50 °C/min

Table 7.17. Weight loss of blends in the reaction regions, %

Fuel Type	50 °C/minute			30 °C/minute			10 °C/minute		
	V	C1	C2	V	C1	C2	V	C1	C2
H.S10-Ulukisla90	6.4	8.9	5.9	5.1	8.5	6.0	5.1	8.0	6.5
H.S20-Ulukisla80	6.6	15.7	9.1	6.1	17.3	10.6	6.1	17.2	10.2
H.S50-Ulukisla50	5.9	32.0	15.2	5.1	30.9	16.5	5.1	31.3	16.2
H.S10-Himmetoğlu90	4.4	29.5	47.1	4.5	28.3	47.7	4.7	27.2	48.7
H.S20-Himmetoğlu80	4.2	33.1	45.8	4.8	32.5	47.7	5.0	31.8	48.1
H.S50-Himmetoğlu50	4.4	45.1	42.7	3.7	42.8	47.0	3.6	43.7	46.2
W.B.10-Ulukisla90	5.6	8.3	6.9	5.8	5.7	5.2	5.8	5.6	5.3
W.B.20-Ulukisla80	7.2	14.9	9.5	6.6	12.4	9.2	6.6	12.5	9.0
W.B.50-Ulukisla50	8.5	26.8	18	6.3	27.3	16.1	6.3	26.8	16.7
W.B.10-Himmetoğlu90	4.6	25.0	50.5	4.8	25.0	50.4	4.6	24.5	51.0
W.B.20-Himmetoğlu80	4.7	29.3	45.3	4.4	31.4	48.6	4.5	31.3	48.5
W.B.50-Himmetoğlu50	5.0	37.3	42.5	6.2	38.4	43.5	6.1	38.3	42.9
Mis10-Ulukisla90	7.5	8.9	5.1	7.4	9.4	4.1	7.4	9.2	4.3
Mis20-Ulukisla80	7.0	17.0	7.2	3.4	17.0	8.0	3.5	17.1	7.7
Mis50-Ulukisla50	5.6	40.0	13.8	6.6	36.6	12.9	6.6	37.1	12.4
Mis10-Himmetoğlu90	4.5	26.9	50.8	3.8	28.4	45.7	3.8	28.2	46.6
Mis20-Himmetoğlu80	4.5	34.6	44.0	4.5	27.3	46.4	4.7	27.1	46.5
Mis50-Himmetoğlu50	4.3	45.1	38.5	4.6	45.3	37.0	4.6	45.5	37.0
Poplar10-Ulukisla90	6.1	6.6	4.1	5.6	11.9	6.7	5.6	12.0	6.5
Poplar20-Ulukisla80	6.1	19.3	8.3	7.0	20.5	7.4	6.9	20.7	7.5
Poplar50-Ulukisla50	4.0	30.5	10.1	4.8	36.7	12.4	4.8	36.1	13.0
Poplar10-Himmetoğlu90	3.4	30.5	49.0	2.3	27.8	47.2	2.2	27.6	47.4
Poplar20-Himmetoğlu80	3.5	34.6	45.4	3.8	33.2	46.8	3.9	32.9	47.0
Poplar50-Himmetoğlu50	5.3	45.5	37.0	5.3	45.6	35.0	5.6	45.4	35.2

V: Vaporization

C1: Combustion of light compounds

C2: Combustion of heavy compounds

H.S: Hazelnut Shell

W.B: Wheat Bran

Mis: Miscanthus

7.7.4 TGA curves of biomass model compounds

The TGA curves of cellulose, hemicellulose, and lignin are presented in Figures 7.26 through 7.28. All model compounds have almost no ash contents. Cellulose has one main peak because of its structure in a good order without branches; while hemicellulose and lignin have two main peaks due to the presence of light and heavy compounds in their complex branched structures, so that combustion of hemicellulose and lignin occurred in a wide range. Same peaks/intervals and similar TGA/DTG profiles were observed by Ramiah [1970] and Shukry et al [1991].

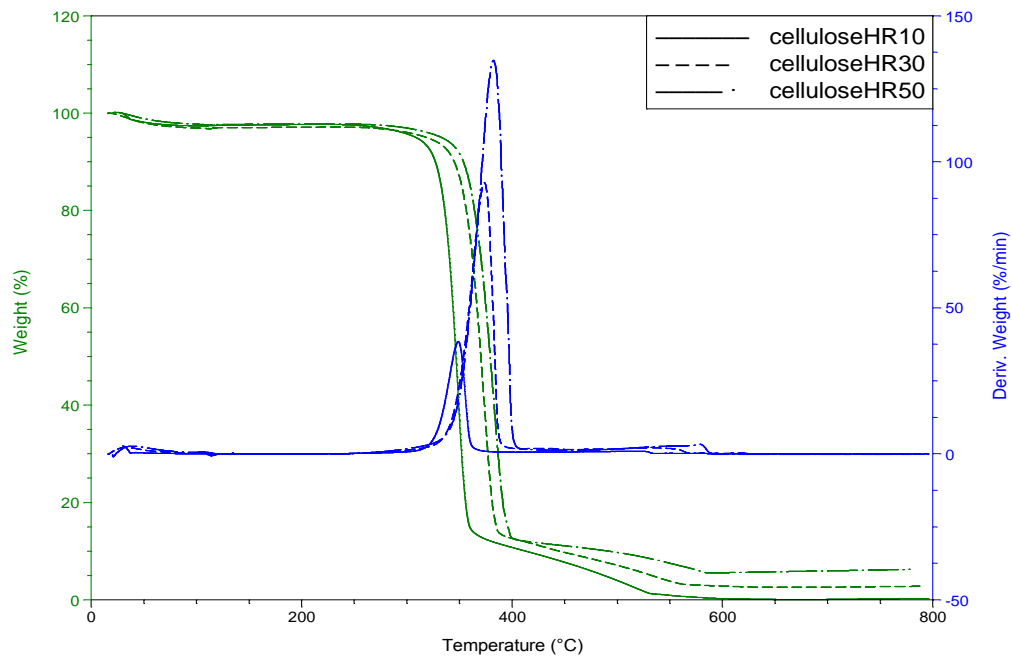


Figure 7.26. TGA curve of cellulose

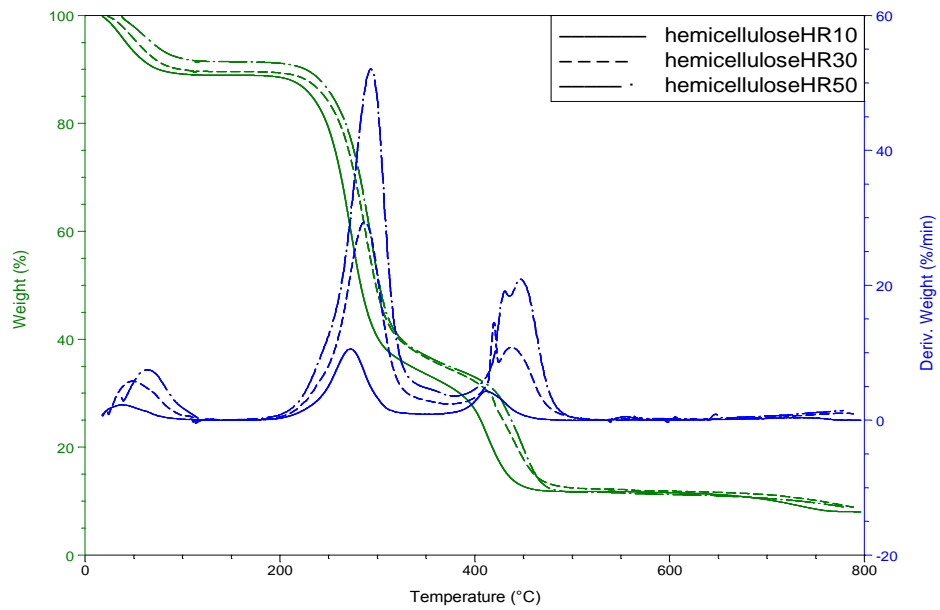


Figure 7.27. TGA curve of hemicellulose

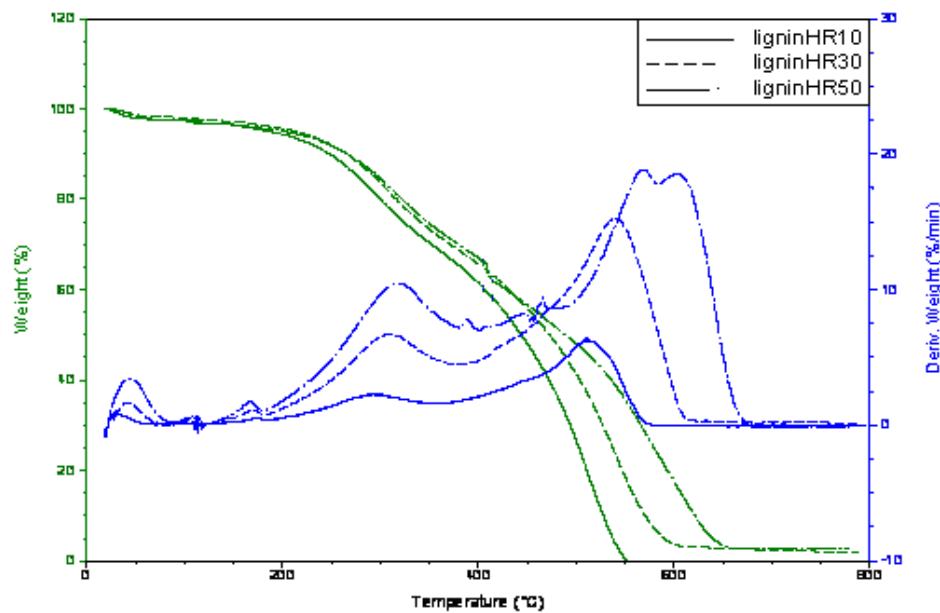


Figure 7.28. TGA curve of lignin

7.8 Additive or Interactive Effect

Deviations between calculated and experimental values of the ignition temperatures of each blend were determined to investigate whether interaction existed between oil shale and biomass fuels during combustion. A similar method to clarify the additive/interactive effects during cofiring of wood waste, switchgrass and coal was used by other researchers [Duong et al, 2010]. They observed interaction for blends during the ignition. The method was used for the evaluation of our experimental results. For the calculation of calculated values, the parent fuels, oil shale and biomass fuels were used. Calculated values of ignition temperatures for the blends are determined using equation 7.1. The calculation is based on the values of parent fuels' experimental values using arithmetic average method. The procedure is used to calculate each blend's ignition temperature. Deviation between experimental values and calculated values for each blend is determined using equation 7.2.

$$\text{CalculatedIgnitionTemperatureValue for blend} = \text{IgnitionTemperatureValue}_{\text{OilShale}} \times (\text{Wt. Percent of Oil Shale}) + \text{IgnitionTemperatureValue}_{\text{Biomass}} \times (\text{Wt. Percent of Biomass}) \quad (7.1)$$

$$\text{Deviation} = \frac{\text{IgnitionTemperatureValue}_{\text{Experimental}} - \text{IgnitionTemperatureValue}_{\text{Calculated}}}{\text{IgnitionTemperatureValue}_{\text{Calculated}}} \quad (7.2)$$

The experimental and calculated values for the ignition temperature and the deviation between them are tabulated and are listed in Tables 7.18-7.23 for three different heating rates. Negative values indicate that the ignition temperature was lower than the expected value. This can be the evidence for the blend improving ignition. Positive values indicate an increase in ignition temperature or a negative effect. A zero value indicates the blend behave as an arithmetic average. It should be noted that at a heating rate of 30 °C/min., more material stay in the pan and do not undergo a change to gaseous form when compared to samples exposed to a heating rate of 50 °C/min. At a heating rate of 10 °C/min., escaping combustible volatiles (because of devolatilization) that occur before combustion are higher due to the long heat-up time so that good ignition condition is partly assured.

As the biomass ratio increases in the Ulukışla oil shale – biomass blend, the ignition temperature decreases more than expected as can be seen in the Tables 7.18 through 7.20. Because the biomass fuels included have a high oxygen content compared to the oil shale, the additional oxygen may improve the combustion. This is valid for each blend at heating rates of 30 °C/min. and 50 °C/min. as well as for many of the blends at the 10 °C/min. heating rate despite poorer ignition conditions at lower heating rates. Combustion

performance improves as the biomass ratio increases; however after 20% biomass addition the improvement stabilizes. Changes in performance at 50% biomass addition are generally lower than or equal to changes in performance in 20% biomass addition. This is likely a volume issue. The density of the biomass fuels are between 0.6-0.8 g/cm³ while the density of the oil shales are around 2 g/cm³; hence the biomass occupies more than 2 times the volume of oil shale for a 50% by weight blend [Van Loo and Koppejan, 2008]. Although higher biomass quantities improve the combustion, the large volume of biomass at some point may prevent the oxygen consumption by oil shale, and the positive effect of the biomass is reduced at this ratio.

Tests were repeated on some runs (as given in the Appendix D) in order to verify probable experimental errors. Based on these repeatability tests, good repeatability was observed within a confidence interval of 95%. It is clear that blending improves the combustion by observing the ignition temperatures and the deviation. The deviations are mostly negative which means blending improves combustion more than expected. For the Himmetoğlu oil shale-biomass blends, the addition of biomass increases the ignition temperature of the blend due to higher ignition temperature of biomass fuels as mentioned before. Therefore, the study was focused on Ulukışla oil shale-biomass blends. However, the comparisons for Himmetoğlu oil shale-biomass were still made and the results are presented in Table 7.21, 7.22, and 7.23, and it can be seen that the deviations are in the range of experimental errors or positive indicating that the addition of biomass doesn't make any synergistic improvement for the co-firing with Himmetoğlu oil shale.

Table 7.18. Difference between experimental and calculated values of ignition temperatures for each fuel blend at 50 °C/min heating rate (Ulukışla + Biomass)

Fuel Type	T_{Ignition}, °C (exp.)	T_{Ignition}, °C (calculated)	Deviation, %
Ulu-HS10	283	297.0	-4.9
Ulu-HS20	271	292.0	-7.7
Ulu-HS50	257	277.0	-7.8
Ulu-Mis10	295	297.1	-0.7
Ulu-Mis20	287	292.2	-1.8
Ulu-Mis50	278	277.5	0.2
Ulu-Pop10	290	296.7	-2.3
Ulu-Pop20	279	291.4	-4.4
Ulu-Pop50	272	275.5	-1.3
Ulu-Wheat10	295	297.8	-0.9
Ulu-Wheat20	279	293.6	-5.2
Ulu-Wheat50	269	281.0	-4.5

Table 7.19. Difference between experimental and calculated values of ignition temperatures for each fuel blend at 30 °C/min heating rate (Uluğişla + Biomass)

Fuel Type	T_{Ignition}, °C (exp.)	T_{Ignition}, °C (calculated)	Deviation,%
Ulu-HS10	266	290.4	-9.2
Ulu-HS20	260	284.8	-9.5
Ulu-HS50	244	268.0	-9.8
Ulu-Mis10	285	291.5	-2.3
Ulu-Mis20	276	287.0	-4.0
Ulu-Mis50	264	273.5	-3.6
Ulu-Pop10	263	291.3	-10.8
Ulu-Pop20	256	286.6	-12.0
Ulu-Pop50	250	272.5	-9.0
Ulu-Wheat10	275	291.9	-6.1
Ulu-Wheat20	269	287.8	-7.0
Ulu-Wheat50	260	277.5	-6.0

Table 7.20. Difference between experimental and calculated values of ignition temperatures for each fuel blend at 10 °C/min heating rate (Uluğişla + Biomass)

Fuel Type	T_{Ignition}, °C (exp.)	T_{Ignition}, °C (calculated)	Deviation,%
Ulu-HS10	243	242.0	0.4
Ulu-HS20	236	240.0	-1.7
Ulu-HS50	235	234.0	0.4
Ulu-Mis10	238	241.6	-1.5
Ulu-Mis20	236	239.2	-1.4
Ulu-Mis50	233	232.0	0.4
Ulu-Pop10	241	241.5	-0.2
Ulu-Pop20	221	239.0	-8.1
Ulu-Pop50	220	231.5	-5.2
Ulu-Wheat10	239	242.9	-1.6
Ulu-Wheat20	236	241.8	-2.5
Ulu-Wheat50	235	238.5	-1.5

Table 7.21. Difference between experimental and calculated values of ignition temperatures for each fuel blend at 50 °C/min heating rate (Himmetoğlu + Biomass)

Fuel Type	T_{Ignition}, °C (exp.)	T_{Ignition}, °C (calculated)	Deviation, %
Hm-HS10	232	233.1	-0.5
Hm-HS20	233	235.2	-0.9
Hm-HS50	239	241.5	-1.0
Hm-Mis10	231	233.2	-1.0
Hm-Mis20	240	235.4	1.9
Hm-Mis50	247	242.0	2.0
Hm-Pop10	232	232.8	-0.3
Hm-Pop20	233	234.6	-0.7
Hm-Pop50	234	240.0	-2.6
Hm-Wheat10	232	233.9	-0.8
Hm-Wheat20	239	236.8	0.9
Hm-Wheat50	245	245.5	-0.2

Table 7.22. Difference between experimental and calculated values of ignition temperatures for each fuel blend at 30 °C/min heating rate (Himmetoğlu + Biomass)

Fuel Type	T_{Ignition}, °C (exp.)	T_{Ignition}, °C (calculated)	Deviation, %
Hm-HS10	226	225.6	0.2
Hm-HS20	227	227.2	-0.1
Hm-HS50	228	232.0	-1.8
Hm-Mis10	232	226.7	2.3
Hm-Mis20	238	229.4	3.6
Hm-Mis50	241	237.5	1.5
Hm-Pop10	229	226.5	1.1
Hm-Pop20	230	229.0	0.4
Hm-Pop50	231	236.5	-2.4
Hm-Wheat10	225	227.1	-0.9
Hm-Wheat20	227	230.2	-1.4
Hm-Wheat50	228	239.5	-5.0

Table 7.23. Difference between experimental and calculated values of ignition temperatures for each fuel blend at 10 °C/min heating rate (Himmetoğlu + Biomass)

Fuel Type	T_{Ignition}, °C (exp.)	T_{Ignition}, °C (calculated)	Deviation,%
Hm-HS10	206	199.7	3.1
Hm-HS20	208	202.4	2.7
Hm-HS50	220	210.5	4.3
Hm-Mis10	197	199.3	-1.2
Hm-Mis20	201	201.6	-0.3
Hm-Mis50	212	208.5	1.7
Hm-Pop10	198	199.2	-0.6
Hm-Pop20	199	201.4	-1.2
Hm-Pop50	204	208.0	-2.0
Hm-Wheat10	199	200.6	-0.8
Hm-Wheat20	201	204.2	-1.6
Hm-Wheat50	207	215.0	-3.9

7.9 TGA-MS Curves

TGA-MS was used to obtain information on the gases emitted during the combustion of the fuels. Ulukışla oil shale, hazelnut shell, wheat bran, and the 50-50 weight percentage blends of Ulukışla oil shale with hazelnut shell and wheat bran were investigated. Higher sample mass is required in TGA-MS experiments compared to that of DSC and TGA experiments to generate a sufficient quantity of gases. The heating rate has to be kept relatively low in order to detect the emitted gases accurately to secure reliable test results.

In this study, a comparison of the intensity peak areas of the different samples was performed using a semi-quantitative analysis. The shape and the characteristics temperatures of the peaks were compared. Hydrogen (H₂), methane (CH₄), water vapor (H₂O), and carbon dioxide (CO₂) were monitored, among the emitted gases.

In complete combustion water and carbon dioxide are the only products, though in practice it is almost impossible to achieve. The analytical modelling of solid fuel combustion is very complex. During combustion most of the intermediate products are burnt and some - such as hydrogen and methane- escape as emissions without burning. Methane and hydrogen are formed and released due to reforming/charring reactions during combustion. In Figures 7.29 and 7.30, the emissions of hydrogen and methane for selected fuel types can be seen,

respectively. In these figures, the emissions of hydrogen and methane at biomass combustion are very high compared to the emissions at Ulukışla oil shale combustion due to the high volatile matter content of biomass fuels. This high emission may indicate that high volatile matter content has influence on the formation of hydrogen and methane during combustion. This observation is consistent with the amounts of volatile matters of biomass fuels measured from the proximate analysis.

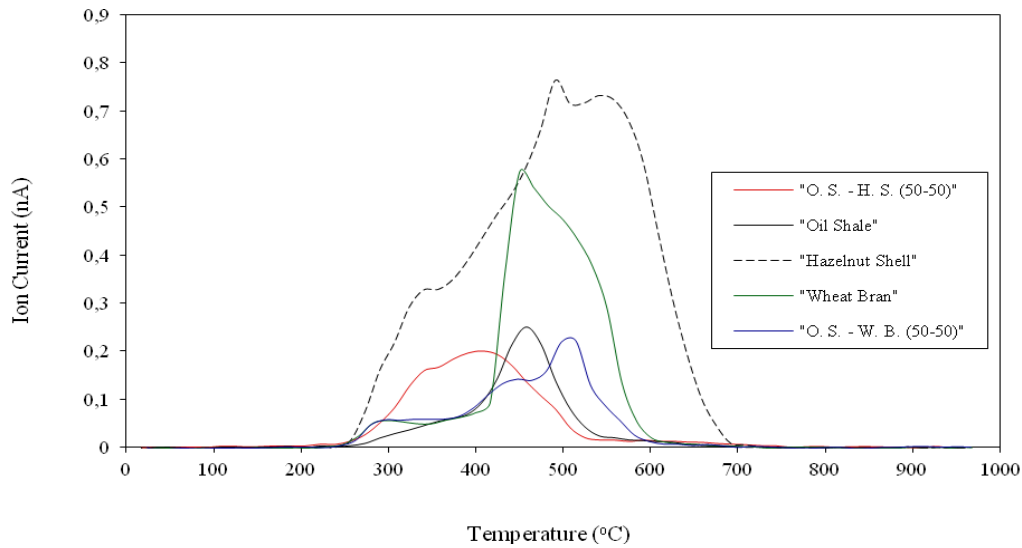


Figure 7.29. TGA-MS curve of hydrogen

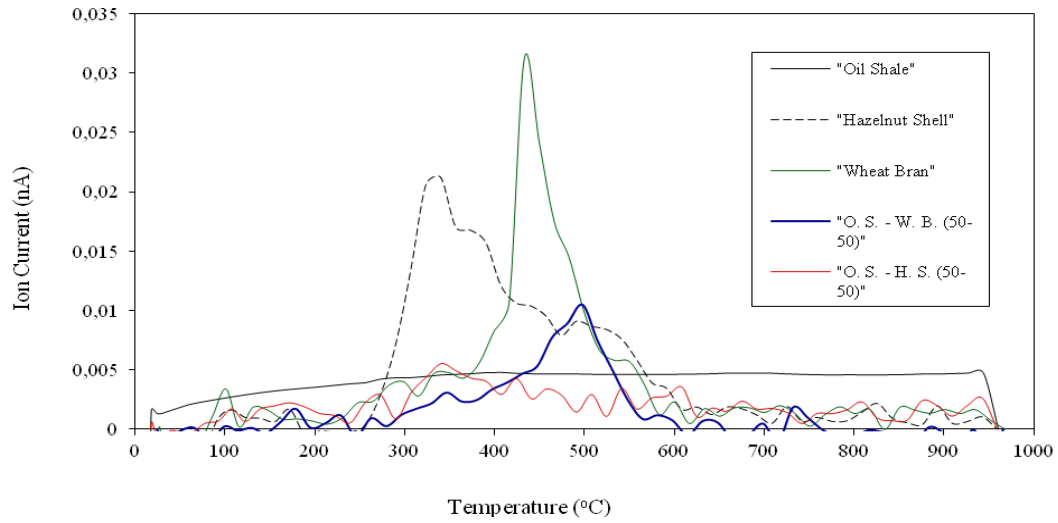


Figure 7.30. TGA-MS curve of methane

In Figure 7.31, the emissions of water for selected fuel types can be seen. Between 110 °C and 150 °C, first water loss was observed for each selected fuel type. The water in this region is due to physical adsorption (physisorption). The second water loss region was observed around 180 °C for oil shale and 300 °C for biomass fuels. The water in this region is due to reaction water and chemisorption which is characterized by a strong interaction between an adsorbate and a substrate surface, compared to physisorption which is controlled by weak Van der Waals forces.

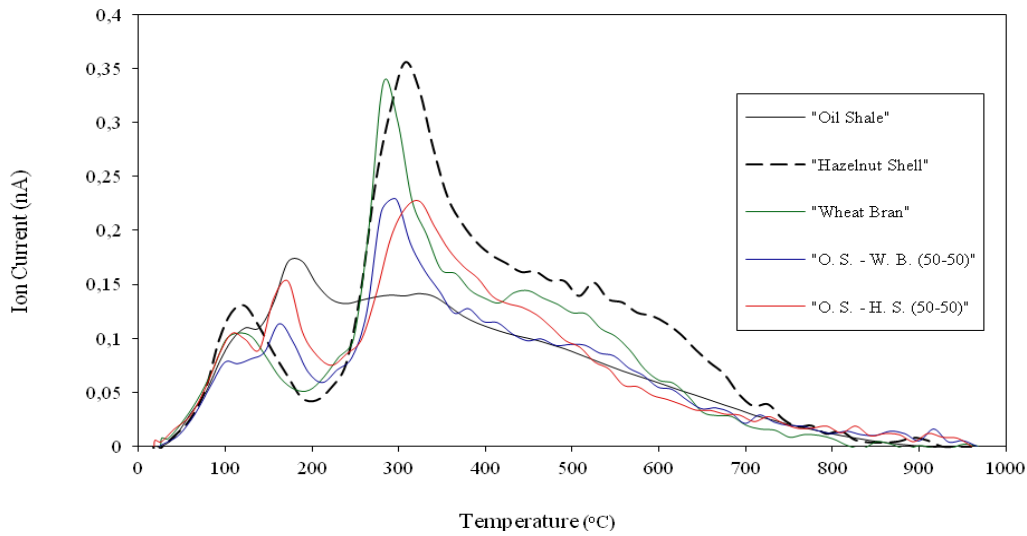


Figure 7.31. TGA-MS curve of water

In Figure 7.32, the emissions of carbon dioxide for selected fuel types can be seen. Carbon dioxide in the emissions is a primary product of combustion. Higher carbon dioxide emissions mean better energy content in the fuel in the combustion interval. Side reactions (cracking, polymerization, reforming, and etc.) -different from combustion reactions- may also partially lead to formation of carbon dioxide in the reaction interval, as well. In the figure, as expected, the carbon dioxide emission is higher for biomass fuels compared to the emission in Ulukışla oil shale because of higher exothermic behavior of biomass fuels.

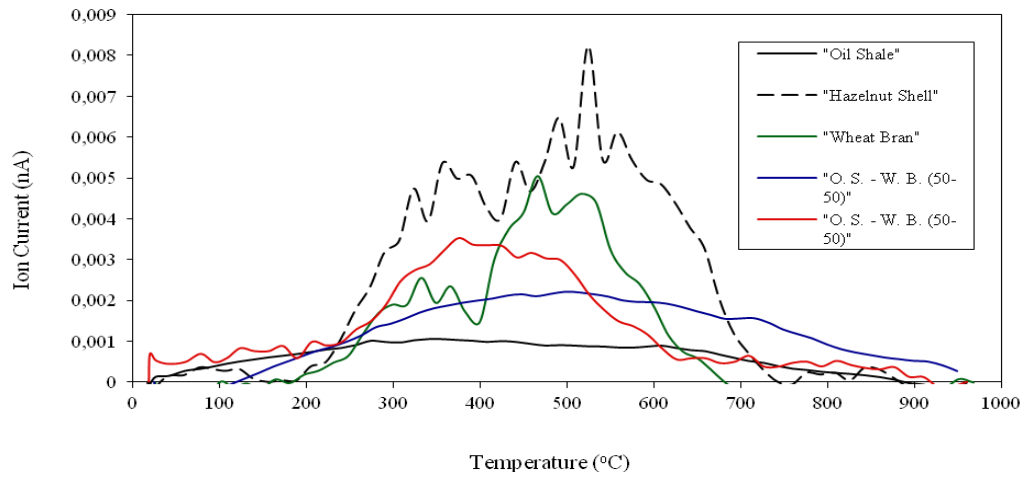


Figure 7.32. TGA-MS curve of carbondioxide

7.10 SEM Images

SEM images were taken to obtain information on the structure of solid fuels. The SEM image of Ulukışla oil shale and some biomass fuels are provided to show the structures of the fuels. Oil shale has a rounded shape structure, as seen in Figure 7.33 and Figure 7.34, which were taken at different magnifications. Biomass fuels have long, fibrous structures. In Figures 7.35, 7.36, 7.37 and 7.38, the structure of miscanthus and poplar can be seen at different magnifications. Since biomass is generally more reactive than oil shale, the particle size for biomass can be larger than oil shale at the preparation of blends for the combustion. The fibrous structure of biomass can be challenging during the milling process of samples.

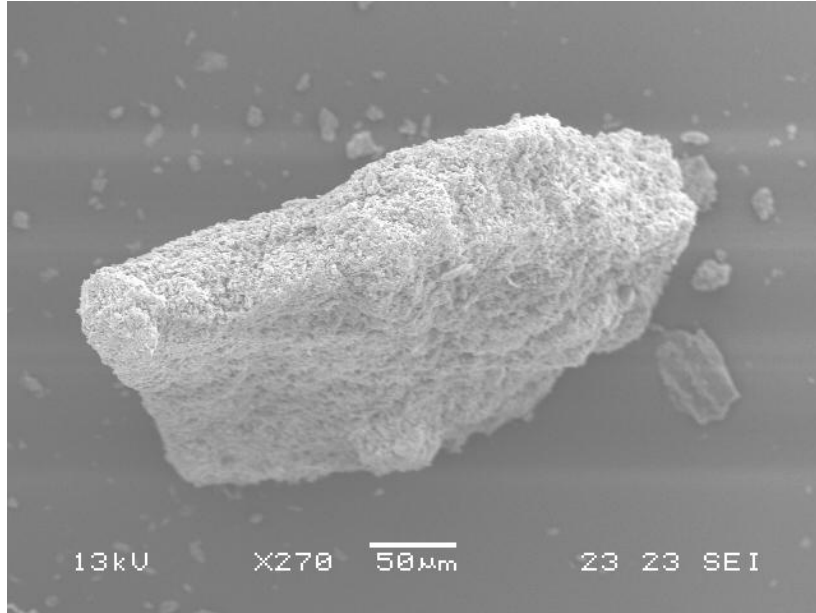


Figure 7.33. SEM image of Ulukışla oil shale (x270)

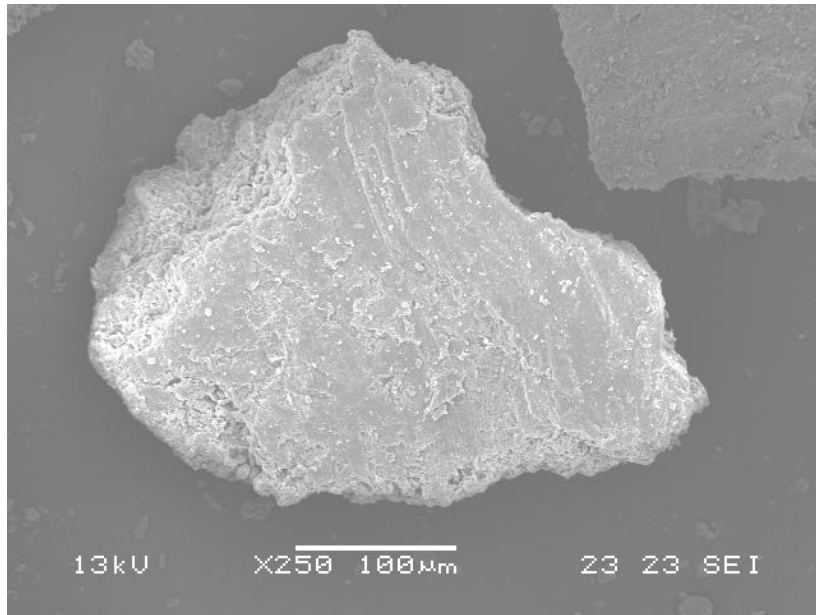


Figure 7.34. SEM image of Ulukışla oil shale (x250)

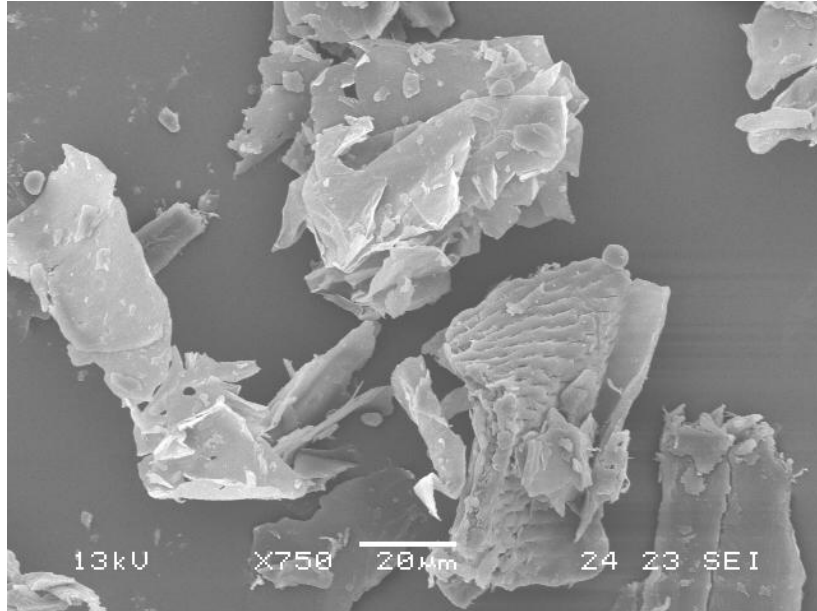


Figure 7.35. SEM image of miscanthus (x750)

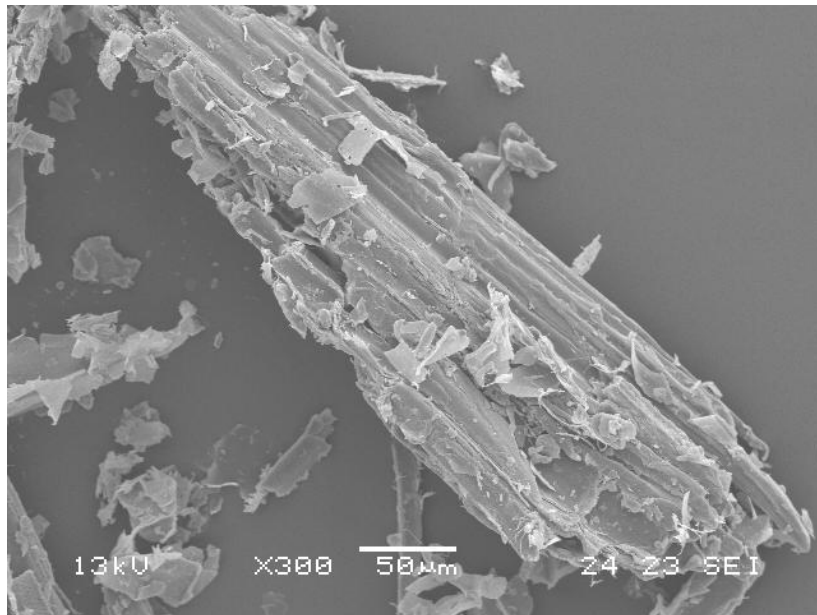


Figure 7.36. SEM image of miscanthus (x300)

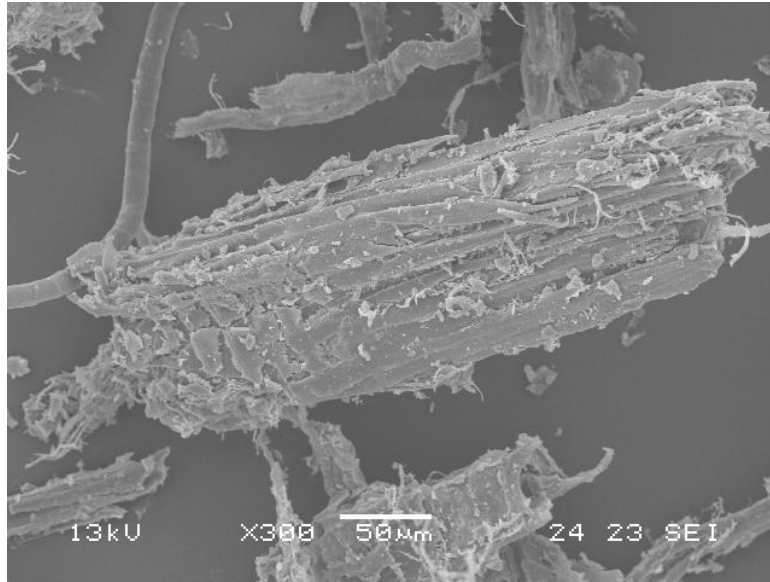


Figure 7.37. SEM image of poplar (x300)

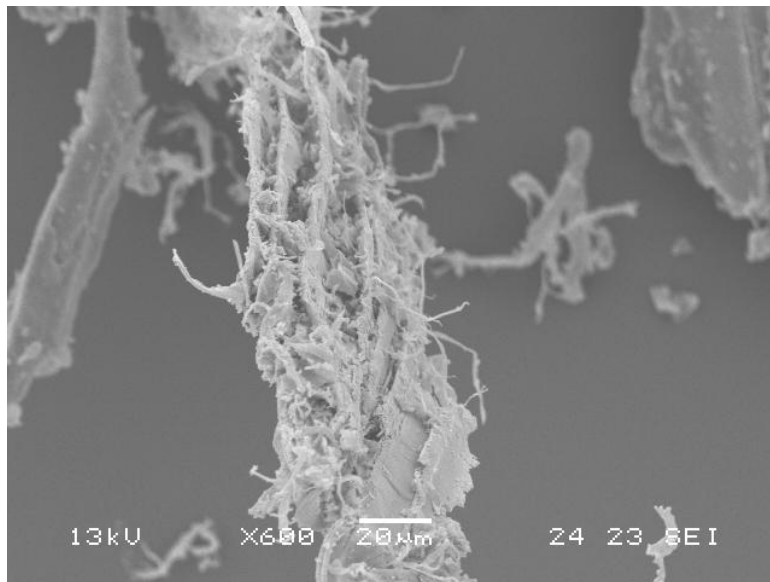


Figure 7.38. SEM image of poplar (x600)

7.11 Kinetic Analysis

It is difficult to report specific activation energy of solid fuel combustion reactions since each kinetic method may give different results. Solid fuels are not homogeneous and the results are sensitive to experimental conditions, material characteristics and the kinetic methods used in the calculation. Thus the results can vary accordingly. Therefore, instead of focusing on an activation energy value, one should be interested in the comparative values when using the same kinetic method [Haines, 2002]. It is recommended that multiple heating rate programs should be used for the kinetic computations [Brown et al, 2000 and Vyazovkin et al, 2011]; however, single heating rate methods can be performed to evaluate activation energies. Both techniques were used in this study.

Activation energies based on Arrhenius, Coats&Redfern, Kissenger, Ozawa-Flynn-Wall, and ASTM methods are listed in Tables between 7.24-7.32. For the Coats&Redfern method, equation 7.1 was used due to the better correlation results for the reaction order “one”. Ulukışla oil shale has the highest activation energy value, as expected, due to its difficult combustion characteristics. It is observed that the activation energy decreases gradually when adding more biomass for the biomass-Ulukışla oil shale blends because of the lowered ignition temperatures. However, the opposite effect is observed for the biomass-Himmetoğlu oil shale blends, as expected, because biomass addition increases the ignition temperature of the blends as the biomass fuels have higher ignition temperatures compared to that of Himmetoğlu oil shale. The results demonstrated that the sequence of activation energies showed parallel distribution with that of ignition temperatures. Also, no relationship was observed between the heating rate and activation energy as noted by other researchers [Syed et al, 2011].

Table 7.24. Activation energy of parent fuels from Arrhenius kinetic method

Fuel Type (kJ/mol)	10 °C/min.	30 °C/min.	50 °C/min.
Ulukışla Oil Shale	102.2	100.5	101.3
Himmetoğlu Oil Shale	68.8	66.4	69.5
Hazelnut Shell	72.8	70.3	71.3
Wheat Bran	81.9	85.2	84.1
Poplar	75.5	79.6	80.4
Miscanthus	75.8	80.6	82.5

Table 7.25. Activation energy of biomass-Ulukışla blends from Arrhenius kinetic method

Fuel Type (kJ/mol)	10 °C/min.	30 °C/min.	50 °C/min.
Oil Shale-Hazelnut Shell (90-10)	91.6	91.7	93.4
Oil Shale-Hazelnut Shell (80-20)	85.0	88.7	84.9
Oil Shale-Hazelnut Shell (50-50)	81.0	88.3	83.1
Oil Shale-Wheat Bran (90-10)	92.5	96.8	95.2
Oil Shale-Wheat Bran (80-20)	88.0	86.3	90.7
Oil Shale-Wheat Bran (50-50)	86.3	85.8	88.1
Oil Shale-Miscanthus (90-10)	92.1	91.4	92.0
Oil Shale-Miscanthus (80-20)	87.0	90.6	87.2
Oil Shale-Miscanthus (50-50)	84.2	84.7	85.0
Oil Shale-Poplar (90-10)	91.2	90.1	90.2
Oil Shale-Poplar (80-20)	86.5	85.6	88.8
Oil Shale-Poplar (50-50)	84.3	84.3	85.4

Table 7.26. Activation energy of biomass-Himmetoğlu from Arrhenius kinetic method

Fuel Type (kJ/mol)	10 °C/min.	30 °C/min.	50 °C/min.
Oil Shale-Hazelnut Shell (90-10)	69.2	70.3	70.7
Oil Shale-Hazelnut Shell (80-20)	70.9	70.3	70.8
Oil Shale-Hazelnut Shell (50-50)	72.1	71.4	71.6
Oil Shale-Wheat Bran (90-10)	70.5	69.7	70.3
Oil Shale-Wheat Bran (80-20)	75.0	76.3	73.9
Oil Shale-Wheat Bran (50-50)	80.7	82.0	80.3
Oil Shale-Miscanthus (90-10)	69.8	70.1	70.4
Oil Shale-Miscanthus (80-20)	74.6	73.6	72.3
Oil Shale-Miscanthus (50-50)	75.8	75.7	75.9
Oil Shale-Poplar (90-10)	69.1	69.3	69.0
Oil Shale-Poplar (80-20)	72.0	73.0	72.5
Oil Shale-Poplar (50-50)	73.7	73.1	76.5

Table 7.27. Activation energy of parent fuels from Coats-Redfern kinetic method

Fuel Type (kJ/mol)	10 °C/min.	30 °C/min.	50 °C/min.
Ulukışla Oil Shale	106.3	102.7	106.2
Himmetoğlu Oil Shale	73.6	72.5	75.8
Hazelnut Shell	77.3	77.8	77.5
Wheat Bran	82.3	85.4	83.3
Poplar	82.7	85.9	80.7
Miscanthus	85.2	83.7	81.3

Table 7.28. Activation energy of biomass-Ulukışla blends from Coats-Redfern kinetic method

Fuel Type (kJ/mol)	10 °C/min.	30 °C/min.	50 °C/min.
Oil Shale-Hazelnut Shell (90-10)	95.4	101.0	97.3
Oil Shale-Hazelnut Shell (80-20)	86.0	93.3	89.5
Oil Shale-Hazelnut Shell (50-50)	85.2	82.4	83.3
Oil Shale-Wheat Bran (90-10)	91.2	96.2	97.1
Oil Shale-Wheat Bran (80-20)	87.3	90.3	93.1
Oil Shale-Wheat Bran (50-50)	87.6	88.1	89.1
Oil Shale-Miscanthus (90-10)	96.0	97.1	96.7
Oil Shale-Miscanthus (80-20)	93.4	96.9	90.2
Oil Shale-Miscanthus (50-50)	88.8	87.6	82.3
Oil Shale-Poplar (90-10)	92.7	94.0	94.6
Oil Shale-Poplar (80-20)	85.5	87.2	87.5
Oil Shale-Poplar (50-50)	83.4	86.3	81.4

Table 7.29. Activation energy of biomass-Himmetoğlu blends from Coats-Redfern kinetic method

Fuel Type (kJ/mol)	10 °C/min.	30 °C/min.	50 °C/min.
Oil Shale-Hazelnut Shell (90-10)	73.7	75.2	77.0
Oil Shale-Hazelnut Shell (80-20)	75.8	75.3	77.5
Oil Shale-Hazelnut Shell (50-50)	77.2	76.1	79.5
Oil Shale-Wheat Bran (90-10)	75.9	73.6	76.7
Oil Shale-Wheat Bran (80-20)	78.1	75.2	76.9
Oil Shale-Wheat Bran (50-50)	78.5	76.8	82.5
Oil Shale-Miscanthus (90-10)	79.9	77.0	76.4
Oil Shale-Miscanthus (80-20)	80.6	79.1	77.3
Oil Shale-Miscanthus (50-50)	81.2	80.5	80.4
Oil Shale-Poplar (90-10)	78.6	73.0	76.1
Oil Shale-Poplar (80-20)	79.2	75.7	77.8
Oil Shale-Poplar (50-50)	80.8	79.9	78.4

The results from the single heating rate kinetic methods (Arrhenius and Coats-Redfern) and multiple heating rate kinetic methods (Kissenger, Ozawa-Flynn-Wall, and ASTM) are very different. These differences are explained by the different equation parameters and assumptions that these methods are based on [Kök and Pamir, 2000].

Many researchers performed Arrhenius and Coats-Redfern kinetic methods for the determination of activation energy of oil shale combustion [Kök et al, 1998; Kök and İşcan, 2007; Yağmur and Durusoy, 2009]. The results of the activation energies for the combustion of oil shale given by the above researchers are in the range of 59-102 kJ/mol and 22-91 kJ/mol comparable (except for some variances) with those of this study which are in the range of 99-107 kJ/mol and 66-76 kJ/mol, respectively for Arrhenius and Coats-Redfern kinetic methods.

The Arrhenius and Coats-Redfern kinetic method were also used for the determination of activation energy of biomass combustion by other researchers [Wang et al, 2008 and Gil et al, 2010]. The results of the activation energies for the combustion of biomass given by the above researchers are in the range of 22-103 kJ/mol similar with those of this study which are in the range of 72-85 kJ/mol for Arrhenius and Coats-Redfern kinetic methods.

For the isoconversional kinetic methods on oil shale combustion, Kk and Pamir [1998] used Kissinger method (DSC) for the combustion of different different oil shales at different heating rates. Biagini et al [2008] compared the results of the Kissinger kinetic method and the Ozawa-Flynn-Wall kinetic method for different biomass fuels. They found that the values obtained from the Kissinger method are considerably lower than that of the Ozawa-Flynn-Wall method, which is due to the methodology of the Kissinger method focusing on the temperature at maximum weight loss rate.

The results of isoconversional kinetic methods in the literature are parallel to those of the present study for the most of the values in Tables 7.30, through 7.32, which are in the range of 101-284 kJ/mol by Kissinger method, 113-184 kJ/mol for ASTM method and in the range of 176-302 kJ/mol by Ozawa-Flynn-Wall method for oil shale; and in the range of 129-222 kJ/mol by Kissinger method, 139-151 kJ/mol for ASTM method and 184-198 kJ/mol by Ozawa-Flynn-Wall method for biomass. It can be deduced that the results in our study are consistent and reasonable for the activation energy output data.

The results also show that the trend of activation energy data is same for each kinetic method as mentioned in the beginning of the chapter. However, Kissinger kinetic method based on DSC output data has the lowest variances among the activation energy values in the study and closer activation energy values to the values reported in the literature. The correlation between peak temperatures and heating rates using DSC data strengthen the Kissinger kinetic method by only considering the combustion process, on the contrary, in kinetic methods using TGA data, devolatilization reactions can also be included in the calculations which can give more erroneous activation energy results.

Table 7.30. Activation energies of parent fuels from Kissinger method and Ozawa-Flynn-Wall method

Fuel Type (kJ/mol)	Kissinger Method (DSC)	Kissinger Method (DTG)	Ozawa-Flynn-Wall Method	ASTM Method
Ulukışla Oil Shale	156.6	283.2	301.8	156.1
Himmetođlu Oil Shale	101.3	121.6	175.8	113.5
Hazelnut Shell	129.2	150.4	184.6	139.3
Wheat Bran	145.8	221.5	197.8	150.6
Poplar	133.0	157.0	187.3	144.4
Miscanthus	130.3	150.6	190.5	143.9

Table 7.31. Activation energy of biomass-Ulukışla blends from Kissinger method and Ozawa-Flynn-Wall method

Fuel Type (kJ/mol)	Kissinger Method (DSC)	Kissinger Method (DTG)	Ozawa-Flynn-Wall Method	ASTM Method
O. Shale-H. Shell (90-10)	146.1	181.7	279.0	151.1
O. Shale-H. Shell (80-20)	143.4	177.2	254.1	146.3
O. Shale-H. Shell (50-50)	134.5	163.8	197.8	142.5
O. Shale-W. Bran (90-10)	156.6	260.4	292.9	154.9
O. Shale-W. Bran (80-20)	152.4	256.6	266.5	153.0
O. Shale-W. Bran (50-50)	149.4	233.6	232.3	152.2
O. Shale-Miscanthus (90-10)	148.1	185.3	278.9	153.2
O. Shale-Miscanthus (80-20)	138.5	176.5	274.7	147.1
O. Shale-Miscanthus (50-50)	135.6	167.9	244.4	145.5
O. Shale-Poplar (90-10)	152.9	165.4	277.7	152.9
O. Shale-Poplar (80-20)	146.3	161.0	272.4	148.8
O. Shale-Poplar (50-50)	139.8	160.5	244.2	145.4

Table 7.32. Activation energy of biomass-Himmetoğlu blends from Kissinger method and Ozawa-Flynn-Wall method

Fuel Type (kJ/mol)	Kissinger Method (DSC)	Kissinger Method (DTG)	Ozawa-Flynn-Wall Method	ASTM Method
O. Shale-H. Shell (90-10)	107.1	131.1	180.3	114.1
O. Shale-H. Shell (80-20)	108.1	133.8	183.8	119.1
O. Shale-H. Shell (50-50)	126.5	141.7	187.7	134.3
O. Shale-W. Bran (90-10)	102.8	203.5	175.8	117.1
O. Shale-W. Bran (80-20)	108.8	207.6	181.5	118.9
O. Shale-W. Bran (50-50)	114.6	215.7	184.9	144.5
O. Shale-Miscanthus (90-10)	108.0	142.6	179.4	114.3
O. Shale-Miscanthus (80-20)	112.2	148.6	182.2	115.4
O. Shale-Miscanthus (50-50)	129.1	149.9	189.9	143.1
O. Shale-Poplar (90-10)	101.6	146.3	176.2	113.6
O. Shale-Poplar (80-20)	101.9	147.4	181.8	121.1
O. Shale-Poplar (50-50)	122.2	147.8	185.3	133.3

7.12 Statistical Analysis

The statistical software Minitab was used to identify possible relationships between the properties of the samples and the combustion. The relationship of ignition temperature to carbon, hydrogen, nitrogen, volatile matter, fixed carbon, and ash contents was investigated for six parent fuels and each blend. A total of 200 data points were checked statistically. Multiple regression analysis was performed on all the data. The results are given in Table 7.33. The results are tabulated with their p-values and R^2 values. The ignition temperature is the dependent parameter and the other parameters are independent ones. The lower p-values indicate statistical significance for independent parameters. The confidence interval was selected as 95%. All p-values are lower than the alpha level (acceptable level for analysis) of 0.05 which shows a good statistical significance for independent parameters. R-squares (R^2) values, coefficient of determination, show the strength of linear relationship between dependent and independent parameters. In general, the higher the R^2 , the better the model fits the data. Besides R^2 , adjusted R^2 values were also calculated. The adjusted R^2 is a useful tool to compare the explanatory power of models with different numbers of predictors. Some increases in R^2 may be due to chance alone, the adjusted R^2 will increase only if the new term improves the model more than that would be expected by chance. It will decrease when a predictor improves the model less than expected by chance.

For solid fuels, it is observed that carbon content and volatile matter content are the most deterministic parameters for the ignition temperature of fuels. Carbon content and volatile matter content has a reducing effect on ignition temperature. On the other hand, no strong correlation was observed for the other parameters (moisture, ash content, hydrogen content) which are out of confidence interval. Based on Table 7.33, it is observed that as the heating rate increases, the dependence of ignition temperature on carbon content and volatile matter content increases. This is most strongly due to the better ignition conditions at higher heating rates due to the decrease in the loss of volatile matter content before combustion occurs at higher heating rates. At higher heating rates, the system reaches ignition temperature quicker, and this decreases the loss of volatiles during the devolatilization stage. The details of regression analysis are given in Table 7.34 with regression equations, variances, correlation factors, and confidence intervals for each heating rate.

Table 7.33. Statistical relations between physical properties of fuels

Dependent Parameter	Independent Parameter	Heating Rate	P-values	R²	R²(adj)
Ignition Temperature	Carbon Content	50	0	94	93.5
	Volatile Matter Content		0.001		
Ignition Temperature	Carbon Content	30	0	84.1	82.9
	Volatile Matter Content		0.004		
Ignition Temperature	Carbon Content	10	0	76.7	75
	Volatile Matter Content		0.008		
Ignition Temperature	Hydrogen Content Nitrogen Content Moisture Content Fixed Carbon Content Ash content	10, 30, 50	>>0.05	No statistical relationship	
	Cellulose Content Hemicellulose Content Lignin Content				
Ignition Temperature	Cellulose Content Hemicellulose Content Lignin Content	10, 30, 50	>>0.05	No statistical relationship	

Table 7.34. Details of regression analysis

<u>Regression Analysis: Ignition Temperature at HR 50 versus Carbon Content, Volatile Matter</u>		
The regression equation: Ignition Temperature = 295 - 2.03 Carbon Content + 0.704 Volatile Matter		
Predictor	Coefficient	P (confidence interval)
Constant	294.596	0.000
Carbon Content	-2.0325	0.000
Volatile Matter	0.7041	0.001
S (variance) = 6.12030 R-Sq = 94.0% R-Sq(adj) = 93.5%		
<u>Regression Analysis: Ignition Temperature at HR 30 versus Carbon Content, Volatile Matter</u>		
The regression equation: Ignition Temperature = 272 - 1.79 Carbon Content + 0.778 Volatile Matter		
Predictor	Coefficient	P (confidence interval)
Constant	271.653	0.000
Carbon Content	-1.7897	0.000
Volatile Matter	0.7781	0.004
S (variance) = 7.77278 R-Sq = 84.1% R-Sq(adj) = 82.9%		
<u>Regression Analysis: Ignition Temperature at HR 10 versus Carbon Content, Volatile Matter</u>		
The regression equation: Ignition Temperature = 240 - 1.64 Carbon Content + 0.764 Volatile Matter		
Predictor	Coefficient	P (confidence interval)
Constant	240.379	0.000
Carbon Content	-1.6389	0.000
Volatile Matter	0.7645	0.008
S (variance) = 8.42049 R-Sq = 76.7% R-Sq(adj) = 75.0%		

CHAPTER 8

CONCLUSIONS

In this study, co-combustion of oil shale and biomass fuels were investigated by using TGA, DSC, and TGA-MS methods at different biomass proportions. The following conclusions were reached with the observations of this study:

- Himmetoğlu oil shale sample proved to have lower ignition temperature compared to biomass fuels due to its high carbon and low ash content; whereas tested Ulukışla oil shale sample showed the highest ignition temperature among the all solid fuels in the study.
- The ignition temperature of fuels increase as the heating rate of the experiment increases as expected, due to the thermal lag effect. The lower quality Ulukışla oil shale has narrower reaction interval with higher oxidative stability, while higher quality oil shale Himmetoğlu and biomass fuels have wider reaction interval with lower oxidative stability.
- Biomass fuels were characterized as low ash content fuels; however, Himmetoğlu oil shale and Ulukışla oil shale were observed to have medium and high ash contents, respectively.
- Since the combustion of biomass fuels showed high exothermicity based on DSC output data, biomass fuels could serve as fine heating fuels for co-firing operations.
- It was observed experimentally that cellulose was the most difficult one to combust among biomass model compounds because of its strong structure. Biomass fuels having high volatile matter content and low cellulose content are good options for co-firing with oil shale.

- The biomass fuels improved combustion interactively (in a synergistic manner) for low grade Ulukışla oil shale by lowering ignition temperature more than the expected based on the results of arithmetic average of ignition temperature values of parent fuels.
- An operational range using up to 20% biomass proportion by weight is a good option for co-combustion due to the sufficient volatile matter content in the blend for maintaining the stability of combustion and the low amount of biomass required.
- The high reactivity of biomass fuels is caused by light compounds: however, the high energy release is due to the heavy compounds.
- It was observed that activation energies were in direct relation with the ignition temperatures for each kinetic methods. The results demonstrated that the sequence of activation energies showed parallel distribution with that of ignition temperatures.
- The relationship between the sample properties (output results of ultimate and proximate analysis) and the ignition temperature was investigated using statistical approach. It was observed that carbon content and volatile matter content are the most deterministic parameters on the ignition temperature.
- It was observed that the blending of high volatile biomass with an oil shale having high ash content and low volatile matter content always lowers the ignition temperature of the system.
- It was noticed that co-combustion of biomass and tested low grade Ulukışla oil shale is technically feasible for tested samples.

CHAPTER 9

RECOMMENDATIONS

Based on the laboratory experiments, the results for the co-combustion of oil shale and biomass are promising. If full scale tests can be performed in real combustion units (thermal power plants or small scale test units), better test results can be obtained. The use of a drop tube furnace and TGA coupled to a fourier transform infrared spectroscopy technique for the tests can provide more information about combustion data (oxidative stability, energy input/output, products, and etc.). Moreover, the laboratory experiments can be performed at different conditions (pressure, air ratio, and etc.) to see the effects of these parameters on combustion performance.

REFERENCES

- Aboulkas, A., El-Harfi, K., El-Bouadili, A., Benchanaa, M., Mokhlisse, A., Outzourit, A., Kinetics of co-pyrolysis of Tarfaya (Morocco) oil shale with high-density polyethylene, *Oil Shale*, Vol. 24, No:1, pg. 15-23, 2007
- Abu-Qudais, M., Jaber, J.O., Sawalha, S., Kinetics of pyrolysis of Attarat oil shale by thermogravimetry, *Oil Shale*, Vol. 22, No: 1, pg. 51-63, 2005
- Alali, J., Jordan oil shale, availability, distribution, and investment opportunity, *International Conf. on Oil Shale: "Recent Trends in Oil Shale"*, 7-9 Nov.2006, Jordan
- Al-Ayed, O.S., Variable reaction order for kinetic modeling of oil shale pyrolysis, *Oil Shale*, Vol. 28, No: 2, pg. 296-308, 2011
- Al-Makhadmeh, L., Maier, J., Al-Harashseh, M., Scheffknecht, G., Oxy-fuel technology: An experimental investigations into oil shale combustion under oxy-fuel conditions, *Fuel*, Vol. 103, pg. 421-429, 2013
- Altun, N.E., Hicyilmaz, C., Hwang, J.Y., Bagci, A.S., Kok, M.V., Oil shales in the world and Turkey; reserves, current situation and future prospects: a review, *Oil Shale*, Vol. 23, No. 3, pp. 211-227, 2006
- Altun, N.E., "Beneficiation of Himmetoglu and Beypazari oil shales by flotation and their thermal characterization as an energy source", PhD Thesis, METU, Ankara, 2006
- Amer, M.W., Marshall, M., Fei, Y., Jackson, W.R., Gorbaty, M.L., Cassidy, P.J., Chaffee, A.L., A comparison of the structure and reactivity of five Jordanian oil shales from different locations, *Fuel*, Vol. 119, pg. 313-322, 2014
- Andrews, A. *Oil Shale: History, Incentives, and Policy*. Congressional Research Service. Report Number :RL33359, 2006
- ASTM E 698 - 79, Standard Test Method for Arrhenius Kinetic Constants for Thermally Unstable Materials, ANSI/ASTM, Philadelphia, 1979
- Avid, B., Purevsuren, B., Paterson, N., Zhuo, Y., Peralta, D., Herod, A., Dugwell, D.R., Kandiyoti, R., An exploratory investigation of the performance of Shivee-Ovoo coal and Khoot oil shale from Mongolia, *Fuel*, Vol. 83, pg. 1105-1111, 2004

Bain, R. L., Overend, R. P., Craig, K. R., Biomass-fired power generation, Fuel Processing Technology, Vol. 54, pg. 1-16, 1998

Barkia, H., Belkbir, L., Jayaweera, S.A.A, Oxidation kinetics of Timahdit and Tarfaya Moroccan oil shales, Journal of Thermal Analysis and Calorimetry, Vol.71, pg. 97-106, 2003

Bauen, A., Woods, J., Hailes, R., A Biomass Blueprint to Meet 15% of OECD Electricity Demand by 2020, Report by ICEPT and E4TECT, 2004

Bhadeshia, H.K.D.H., Lecture Notes in Materials Science & Metallurgy – University of Cambridge, 2009

Biagini, E. and Tognotti, L., Comparison of devolatilization/char oxidation and direct oxidation of solid fuels at low heating rate, Energy&Fuels, Vol.20, pg. 986-992, 2006

Biagini, E., Fantei, A., Tognotti, L., Effect of the heating rate on the devolatilization of biomass residues, Thermochimica Acta, Vol. 472, pg. 55-63, 2008

Boettinger, W.J., Kattner, U.R., Moon, K.W., Perepezko, J.H., DTA and heat-flux DSC measurements of alloy melting and freezing, National Institute of Standards and Technology – Special Publication 960-15, 2006

Brown, M.E., Maciejewski, M., Vyazovkin, S., Nomen, R., Sempere, J., Burnham, A., Opfermann, J., Strey, R., Anderson, H.L., Kemmler, A., Keuleers, R., Janssens, J., Desseyne, H.O., Li, C., Tang, T.B., Roduit, B., Malek, J., Mitsuhashi, T., Computational aspects of kinetic analysis Part A: The ICTAC kinetics project-data, methods and results, Thermochimica Acta, Vol. 355, pg. 125-143, 2000

Capehart, B.L., Encyclopedia of energy engineering and technology, CRC Press 2007

Channiwala, S.A., Parikh, P.P., A unified correlation for estimating HHV of solid, liquid, and gaseous fuels, Fuel, Vol. 81, pg. 1051-1063, 2002

Danilatos, G.D., Foundations of environmental scanning electron microscopy, Advances in Electronics and Electron Physics, Vol. 71, pg. 109–250, 1988

Dean, J.A., The Analytical Chemistry Handbook. New York: McGraw Hill, Inc., 1995

Demirbas, A., Importance of biomass energy sources for Turkey, Energy Policy, Vol. 36, pg. 834-842, 2008

Demirbaş, A., Combustion characteristics of different biomass fuels, *Progress in Energy and Combustion Science*, Vol. 30, pg. 219-230, 2004

Doğan, Ö.M., Uysal, B.Z., Non-isothermal pyrolysis kinetics of three Turkish oil shales, *Fuel*, Vol. 75, No:12, pg. 1424-1428, 1996

Duong, D., Lantos, G., Tillman, D., Kawecki, D., Coleman, A., Biomass cofiring and its effect on the combustion process, *The 35th International Technical Conference on Clean Coal & Fuel Systems – Clearwater, FL, USA, June 6-10, 2010*

Energy Information Administration (US), *International Energy Outlook*, Report No: DOE/EIA-0484, 2009

Ferreira, E.B., Lima, M.L., Zanotto, E.D., DSC method for determining the liquidus temperature of glass-forming systems, *Journal of the American Ceramic Society*, Vol. 93, pg. 3757-3763, 2010

Gil, M.V., Casal, D., Pevida, C., Pis, J.J., Rubiera, F., Thermal behaviour and kinetics of coal/biomass blends during co-combustion, *Bioresource Technology*, Vol. 101, pg. 5601-5608, 2010

Grotkjaer, T., Dam-Johansen, K., Jensen, A.D., Glarborg, P., An experimental study of biomass ignition, *Fuel*, Vol. 82, Iss. 7, pg. 825-833, 2003

Haines, P.J., *Principles of Thermal Analysis and Calorimetry*, The Royal Society of Chemistry, 2002

Hammad, M., Zurigat, Y., Khzai, S., Hammad, Z., Mobydeen, O., Fluidized bed combustion unit for oil shale, *Energy Conv. Manag.*, Vol. 39, pg. 269-272, 1998

Han, X.X., Jiang, X.M., Cui, Z.G., Thermal analysis studies on combustion mechanism of oil shale, *Journal of Thermal Analysis and Calorimetry*, Vol. 84-3, pg. 631-636, 2006

Han, X.X., Jiang, X.M., Cui, Z.G., Mathematical model of oil shale particle combustion, *Combustion Theory and Modelling*, Vol. 10, pg. 145-154, 2006

Hatakeyama, T., Quinn, F.X., *Thermal Analysis – Fundamentals and Applications to Polymer Science*, John Wiley & Sons 1999, 2nd edition

Haykiri-acma, H. and Yaman, S., Effect of co-combustion on the burnout of lignite/biomass blends: A Turkish case study, *Waste Management*, Vol. 28, Iss. 11, pg. 2077-2084, 2008

Haykiri-Acma, H., Combustion characteristics of different biomass materials, *Energy Conversion and Management*, Vol. 44, Iss. 1, pg. 155-162, 2003

Hohne, G., *Differential Scanning Calorimetry: an introduction for practitioners*, Springer-Verlag, 1996

Idris, S.S., Rahman, N.A., Ismail, K., Combustion characteristics of Malaysian oil palm biomass, sub-bituminous coal and their respective blends via thermogravimetric analysis (TGA), *Bioresource Technology*, Vol. 123, pg. 581-591, 2012

IEA (International Energy Agency), *Key World Energy Statistics Report*, 2012

Iscan, A.G., K k, M.V., Bađcı, A.S., Kinetic analysis of central anatolia oil shale by combustion cell experiments, *Journal of Thermal Analysis and Calorimetry*, Vol. 88, pg. 653-656, 2007

Ismail, A.F., Yusaf, T.F., Mahdi, F.M.A., Shamsuddin, A.H., Combustion process of rice husks for energy, *RERIC International Energy Journal*, Vol. 19, Iss. 2, pg. 63-75, 1997

Jaber, J.O., Probert, S.D., Non-isothermal thermogravimetry and decomposition kinetics of two Jordanian oil shales under different processing conditions, *Fuel Processing Technology*, Vol. 63, pg. 57-70, 2000

Jankovic, B., The kinetic modeling of the non-isothermal pyrolysis of Brazilian oil shale: Application of the Weibull probability mixture model, *Journal of Petroleum Science and Engineering*, Vol. 111, pg. 25-36, 2013

Jiang, X.M., Han, X.X., Cui, Z.G., Progress and recent utilization trends in combustion of Chinese oil shale, *Progress in Energy and Combustion Science*, Vol. 33, pg. 552-579, 2007

Johannes, I., Tiikma, L., Zaidentsal, A., Comparison of the thermobituminization kinetics of Baltic oil shale in open retorts and autoclaves, *Oil Shale*, Vol. 27, No: 1, pg. 17-25, 2010

Kaljuvee, T., Edro, E., Kuusik, R., Formation of volatile organic compounds at thermooxidation of solid fossil fuels, *Oil Shale*, Vol. 24, No.2, pg. 117-133, 2007

- Kaljuvee, T., Keelmann, M., Trikkel, A., Kuusik, R., Thermooxidative decomposition of oil shales, *Journal of Thermal Analysis and Calorimetry*, Vol. 105, pg. 395-403, 2011
- Karabakan, A., Yürüm, Y., Effect of the mineral matrix in the reactions of shales. Part 2. Oxidation reactions of Turkish Göynük and US Western Reference oil shales, *Fuel*, Vol. 79, pg. 785-792, 2000
- Karampinis, E., Vamvuka, D., Sfakiotakis, S., Grammelis, P., Itskos, G., Kakaras, E., Comparative study of combustion properties of five energy crops and greek lignite, *Energy & Fuels* 26 (2), 869-878, 2012
- Karayıldırım, T., Yanık, J., Yüksel, M., Sağlam, M., Thermogravimetric analysis of pretreated Göynük oil shale and Şırnak asphaltite, *Oil Shale*, Vol. 21, No:3, pg. 205-216, 2004
- Kask, Ü., Loosaar, J., Parve, T., Kask, L., Paist, A., Muiste, P., Padari, A., Astover, A., Potential of biomass in Narva Region regarding oil shale and biomass co-firing, *Oil Shale*, Vol. 26, No. 1S, pg. 181-192, 2011
- Kastanaki, E. and Vamvuka, D., A comparative reactivity and kinetic study on the combustion of coal–biomass char blends , *Fuel*, Vol. 85, pg. 1186-1193, 2006
- Keating, E. L., *Applied Combustion*, Marcel Dekker Inc., 1993
- Kerimov, K.M., Flash pyrolysis and kinetic parameters of decomposition of oil shales, *Russian Journal of Applied Chemistry*, Vol. 77, No. 4, pg. 154-158, 2004
- Khraisha, Y.H., Shabib, I.M., Thermal analysis of shale oil using thermogravimetry and differential scanning calorimetry, *Energy Conversion and Management*, Vol. 43, pg. 229-239, 2002
- Kök, M.V., Pamir, R., Karacan, Ö., Pener, M., Penguler, Y., Presented at 7th UNITAR International Centre for Heavy Hydrocarbons and Tar Sand, Beijing, CHINA, October 27-30, 1998
- Kök, M.V. and Pamir, M.R., ASTM kinetics of oil shales, *Journal of Thermal Analysis*, Vol. 53, pg. 567-575, 1998
- Kök, M.V. and Pamir, M.R., Comparative pyrolysis and combustion kinetics of oil shales, *Journal of Analytical and Applied Pyrolysis*, Vol. 55, pg. 185-194, 2000

Kök, M.V., Pokol, G., Keskin, C., Madarasz, J., Bagci, S., Combustion characteristics of lignite and oil shale samples by thermal analysis techniques, *Journal of Thermal Analysis and Calorimetry*, Vol. 76-1, pg. 247-254, 2004

Kök, M.V., Geological considerations for the economic evaluation of Turkish oil shale deposits and their combustion - pyrolysis behavior (review), "Recent Trends in Oil Shale", 7-9 Nov 2006, Amman, Jordan

Kök, M.V. and İşcan, A.G., Oil shale kinetics by differential methods, *Journal of Thermal Analysis and Calorimetry*, Vol. 88, pg. 657-661, 2007

Kök, M.V., Heating rate effect on the DSC kinetics of oil shales, *Journal of Thermal Analysis and Calorimetry*, Vol. 90-3, pg. 817-821, 2007

Kök, M.V., Şengüler, İ., Geological and thermal characterization of Eskişehir region oil shales, *Journal of Thermal Analysis and Calorimetry*, Article in Press, 2013

Lee, S., *Oil Shale Technology*. CRC Press., 1991

Lee, S., Speight J.G., Loyalka, S.K., *Handbook of Alternative Fuel Technologies*, CRC Press 2007

Leroy, V., Cancellieri, D., Leoni, E., Thermal degradation of ligno-cellulosic fuels: DSC and TGA studies, *Thermochimica Acta*, Vol. 451, pg. 131-138, 2006

Li, S., Yue, C., Study of different kinetic models for oil shale pyrolysis, *Fuel Processing Technology*, Vol. 85, pg. 51-61, 2003

Liang, X.H., Kozinski, J.A., Numerical modeling of combustion and pyrolysis of cellulosic biomass in thermogravimetric systems, *Fuel*, Vol. 79, pg. 1477-1486, 2000

Liu, H.P., Wang, X.D., Jia, C.X., Zhao, W.Z., Wang, Q., Co-combustion characteristics of oil shale semi-coke and corn stalk, *Advanced Materials Research*, Vol. 614-615, pg. 107-110, 2013

Mansaray, K.G., Ghaly, A.E., Determination of reaction kinetics of rice husks in air using thermogravimetric analysis, *Energy Sources*, Vol. 21:10, pg. 899-911, 1999

Marcio L. de Souza-Santos, *Solid Fuel Combustion and Gasification – Modeling, Simulation, and Equipment Operation*, Marcel Dekker Inc., 2004

- Martins, M.F., Salvador, S., Thovert, J.F., Debenest, G., Co-current combustion of oil shale – Part 1: Characterization of the solid and gaseous products, *Fuel*, Vol. 89, pg. 144-151, 2010
- Masuda, H., Higashitani, K., Yoshida, H., *Powder Technology Handbook*, Taylor & Francis, 2006
- Menczel, J.D., Prime, R.B., *Thermal Analysis of Polymers – Fundamentals and Applications*, John Wiley & Sons, 2009
- Meriste, T., Yörük, C.R., Trikkel, A., Kaljuvee, T., Kuusik, R., TG-FTIR analysis of oxidation kinetics of some solid fuels under oxy-fuel conditions, *Journal of Thermal Analysis and Calorimetry*, Article in Press, 2013
- Miller, B.G. and Tillman, D.A., *Combustion Engineering Issues for Solid Fuel Systems*, Elsevier 2008
- Miranda, T., Arranz, J.I., Montero, I., Roman, S., Rojas, C.V., Nogales, S., Characterization and combustion of olive pomace and forest residue pellets, *Fuel Processing Technology*, Vol. 103, pg. 91-96, 2012
- Miura, K., Maki, T., A simple method for estimating $f(E)$ and $k_0(E)$ in the distributed activation energy model, *Energy & Fuels*, Vol. 12, pg. 864-869, 1998
- Mohomed, K., *Thermogravimetric Analysis Theory, Operation, Calibration and Data Interpretation*, Presentation for TA Instruments, 2009
- Moon, C., Sung, Y., Ahn, S., Kim, T., Choi, G., Kim, D., Effect of blending ratio on combustion performance in blends of biomass and coals of different ranks, *Experimental Thermal and Fluid Science*, Vol. 47, pg. 232-240, 2013
- Munir, S., Daood, S.S., Nimmo, W., Cunliffe, A.M., Gibbs, B.M., Thermal analysis and devolatilization kinetics of cotton stalk, sugar cane bagasse and shea meal under nitrogen and air atmospheres, *Bioresource Technology*, Vol. 100, pg. 1413-1418, 2009
- Muthuraman, M., Namioka, T., Yoshikawa, K., A thermogravimetric analysis on effects of municipal solid waste blending on combustion characteristics of different rank coal, 34th International Technical Conference on Clean Coal & Fuel Systems, May 31 to June 4, 2009, Florida, USA

Oja, V., Elenurm, A., Rohtla, I., Tali, E., Tearo, E., Yanchilin, A., Comparison of oil shales from different deposits: oil shale pyrolysis and co-pyrolysis with ash, *Oil Shale*, Vol. 24, No: 2, pg. 101-108, 2007

Olivella, M.A., De Las Heras, F.X.C., Evaluation of linear kinetic methods from pyrolysis data of Spanish oil shales and coals, *Oil Shale*, Vol. 25, No: 2, pg. 227-245, 2008

Olukçu, N., Yanik, J., Sağlam, M., Yüksel, M., Liquefaction of beypazari oil shale by pyrolysis, *Journal of Analytical and Applied Pyrolysis*, Vol. 64, pg. 29-41, 2002

Otero, M., Sanchez, M.E., Gomez, X., Co-firing of coal and manure biomass: A TG-MS approach, *Bioresource Technology*, Vol. 102, pg. 8304-8309, 2011

Ots, A., Estonian Oil Shale As Power Fuel, *International Oil Shale Symposium – Estonia*, June 8-11, 2009

Petersan, H.I., Foopattanakamol, A., Ratanasthien, B., Petroleum potential, thermal maturity and the oil window of oil shales and coals in cenozoic rift basins, central and northern Thailand, *Journal of Petroleum Geology*, Vol. 29 (4), pg. 337-360, 2006

Petersan, H.I., Bojesen-Koefoed, J.A., Mathiesen, A., Variations in composition, petroleum potential and kinetics of ordovician –miocene type I and type I-II source rocks (oil shales): implications for hydrocarbon generation characteristics, *Journal of Petroleum Geology*, Vol. 33 (1), pg. 19-42, 2010

Phyllis, Database for biomass and waste, Energy Research Center of the Netherlands, 2013

Pungor, E., *A Practical Guide to Instrumental Analysis*. Florida: Boca Raton., 1995

Qing W, Baizhong S, Xiahua W, Jingru B, Jian S. Influence of retorting temperature on combustion characteristics and kinetic parameters of oil shale semicoke, *Oil Shale*. Vol. 23, pg. 328–339, 2006

Qing, W., Hao, X., Hongpeng, L., Chunxia, J., Jingru, B., Thermogravimetric analysis of the combustion characteristics of oil shale semi-coke/biomass blends, *Oil Shale*, Vol. 26, pg. 284-295, 2011

- Qing, W., Hongpeng, L., Jingru, B., Hong, Q., Wen, Y., Application of high-low bed CFB combustion technology to oil shale combustion, *Oil Shale*, Vol. 30, No:2, pg. 147-156, 2013
- Ramiah, M.V., Thermogravimetric and differential thermal analysis of cellulose, hemicellulose, and lignin, *Journal of Applied Polymer Science*, Vol. 14, pg. 1323-1337, 1970
- Reynolds, J.G., Burnham, A.K., Comparison of kinetic analysis of source rocks and kerogen concentrates, *Org. Geochem.*, Vol. 23 (1), pg. 11-19, 1995
- Sahu, S.G., Sarkar, P., Chakraborty, N., Adak, A.K., Thermogravimetric assessment of combustion characteristics of blends of a coal with different biomass chars, *Fuel Processing Technology*, Vol. 91, pg. 369-378, 2010
- Sami, M., Annamalai, K., Wooldridge, M., Co-firing of coal and biomass fuel blends, *Progress in Energy and Combustion Science*, Vol. 27, pg. 171-214, 2001
- Senneca, O., Chirone, R., Salatino, P., A thermogravimetric study of nonfossil solid fuels. 2. oxidative pyrolysis and char combustion, *Energy & Fuels*, Vol. 16, pg. 661-668, 2002
- Shukry, N., Ishak, F., Sefain, Z., DTA study of thermal degradation of bagasse and rice straw hemicelluloses, *Journal of Thermal Analysis*, Vol. 37, pg. 915-926, 1991
- Sjostrom, E., *Wood Chemistry: Fundamentals and Applications*, Academic Press, 1993
- Skreiberg, A., Skreiberg, Φ ., Sandquist, J., Sorum, L., TGA and macro-TGA characterisation of biomass fuels and fuel mixtures, *Fuel*, Vol. 90, pg. 2182-2197, 2011
- Skoog, D. A., Holler, F.J., and Nieman, T., *Principles of Instrumental Analysis*. New York, 1998
- Sluiter, A., R. Ruiz, C. Scarlata, J. Sluiter, and D. Templeton., Determination of extractives in biomass. Tech. Report NREL/TP-510-42619, 2005
- Sonibare, O.O., Ehinola, O.A., Egashira, R., Thermal and geochemical characterization of Lokpanta oil shales, Nigeria, *Energy Conv. Manag.*, Vol. 46, pg. 2335-2344, 2005
- Sütçü, H., Pişkin, S., Pyrolysis kinetics of oil shale from Ulukışla-Turkey, *Oil Shale*, Vol. 26, No:4, pg. 491-499, 2009

Syed, S., Qudaih, R., Talab, I., Janajrah, I., Kinetics of pyrolysis and combustion of oil shale sample from thermogravimetric data, *Fuel*, Vol. 90, pg. 1631-1637, 2011

Sener, M., Sengüler, I., Kök, M.V., Geological considerations for the economic evaluation of oil shale deposits in Turkey, *Fuel*, Vol. 74, No: 7, pg. 999-1004, 1995

Şengüler, İ., Oil shale: generation, usage and importance, *The bulletin of General Directorate of Mineral Research and Exploration of Turkey – Natural Resources and Economy*, No: 3, pg. 5-9, 2007

Şengüler, İ., MTA Report : " Shale oil production from oil shale", 2012

Tenorio, C., Moya, R., Thermogravimetric characteristics, its relation with extractives and chemical properties and combustion characteristics of ten fast-growth species in Costa Rica, *Thermochimica Acta*, Vol. 563, pg. 12-21, 2013

Tiwari, P., Deo, M., Compositional and kinetic analysis of oil shale pyrolysis using TGA–MS, *Fuel*, Vol. 94, pg. 333-341, 2012

Torrente, M.C., Galan, M.A., Kinetics of the thermal decomposition of oil shale from Puertollano (Spain), *Fuel*, Vol. 80, pg. 327-334, 2001

Turi, E.A., *Thermal Characterization of Polymeric Materials Volume 1*, Academic Press 1997

USDOE (U.S. Department of Energy) Report, *Oil Shale Report*, 2005

USGS (U.S. Geological Survey) Report – *Geology and Resources of Some World Oil Shale Deposits*, 2005

Vamvuka, D. and Sfakiotakis, S., Combustion behaviour of biomass fuels and their blends with lignite, *Thermochimica Acta*, Vol. 526, pg. 192-199, 2011

Van Loo, S. and Koppejan, J., *The Handbook of Biomass Combustion of Co-firing*, Earthscan 2008

Varol, M., Atımtay, A.T., Bay, B., Olgun, H., Investigation of co-combustion characteristics of low quality lignite coals and biomass with thermogravimetric analysis, *Thermochimica Acta*, Vol. 510, pg. 195-201, 2010

Vyazovkin, S., Model-free kinetics: staying free of multiplying entities without necessity, *Journal of Thermal Analysis and Calorimetry*, Vol. 83, pg. 45-51, 2006

Vyazovkin, S., Burnham, A.K., Criado, J.M., Perez-Maqueda, L.A., Popescu, C., Sbirrazzuoli, N., ICTAC kinetics committee recommendations for performing kinetic computations on thermal analysis data, *Thermochimica Acta*, Vol. 520, pg. 1-19, 2011

Wang, Q., Wang, X., Liu, H., Jia, C., Study of the combustion mechanism of oil shale semi-coke with rice straw based on gaussian multi-peak fitting and peak-to-peak methods, *Oil Shale*, Vol. 30, pg. 157-172, 2013

Wiley, *Characterization and analysis of polymers*, John Wileys & Sons, 2008

Willard, H.H., Merritt, L.L., Dean, J.A., Settle, F.A., *Instrumental Methods of Analysis*, Wadsworth - 1988, 7th edition

Williams, A., Pourkashanian, M., Jones, J.M., Combustion of pulverised coal and biomass, *Progress in Energy and Combustion Science*, Vol. 27, pg. 587-610, 2001

Williams, P.T., Ahmad, N., Influence of process conditions on the pyrolysis of Pakistani oil shales, *Fuel*, Vol. 78, pg. 653-662, 1999

Wolela, A., Fossil fuel energy resources of Ethiopia: Oil shale deposits, *Journal of African Earth Sciences*, Vol. 46, pg. 263-280, 2006

World Energy Council, *Survey of Energy Resources – Biomass for Electricity Generation*, 2007

Wunderlich, B., *Thermal Analysis*. New York: Academic Press, 1990

Yağmur, S. and Durusoy, T., Oil shale combustion kinetics from single thermogravimetric curve, *Energy Sources, Part A: Recovery, Utilization, and Environmental Effects*, Vol. 31, pg. 1227-1235, 2009

Yan, F., Song, Y., Properties estimation of main oil shale in China, *Energy Sources, Part A: Recovery, Utilization, and Environmental Effects*, Vol. 31, pg. 372-376, 2009

Yen, T.F., Chilingarian, G.V., *Oil Shale*, Elsevier Scientific Publication Company, 1976

Yi, Q., Qi, F., Cheng, G., Zhang, Y., Xiao, B., Hu, Z., Liu, S., Cai, H., Xu, S., Thermogravimetric analysis of co-combustion of biomass and biochar, *Journal of Thermal Analysis and Calorimetry*, Vol. 112, pg. 1475-1479, 2013

Yongjiang, X., Huaqing, X., Hongyan, W., Zhiping, L., Chaohe, F., Kinetics of isothermal and non-isothermal pyrolysis of oil shale, *Oil Shale*, Vol. 28, No:3, pg. 415-424, 2011

Yu, L.J., Wang, S., Jiang, X.M., Wang, N., Zhang, C.Q., Thermal analysis studies on combustion characteristics of seaweed, *Journal of Thermal Analysis and Calorimetry*, Vol. 93, pg. 611-617, 2008

Yüzbaşı, N.R. and Selçuk, N., Air and oxy-fuel combustion characteristics of biomass/lignite blends in TGA-FTIR, *Fuel Processing Technology*, Vol. 92, pg. 1101-1108, 2011

Zhang, D. and Wall, T.F., Ignition of coal particles: the influence of experimental technique, *Fuel*, Vol. 73, pg. 1114-1119, 1994

APPENDIX A

EQUIPMENT

A.1 Differential Scanning Calorimetry

Differential scanning calorimetry (DSC) is a thermoanalytical technique in which the difference between the amount of heat required to increase the temperature of a test sample and a reference are measured as a function of temperature [Wunderlich, 1990].

There are two basic types of differential scanning calorimeters which differ in the design and measuring principle:

- Heat flux DSC
- Power compensated DSC

In the power compensated DSC, the sample and reference units are heated independently using separate, identical furnaces. The temperature of the sample and reference are kept the same by changing the power input to the two furnaces. The energy required to perform this process is a measure of the enthalpy or heat capacity changes in the sample relative to the reference [Dean, 1995 and Pungor, 1995].

In a heat flux DSC, the sample and reference are placed in a low-resistance heat-flow path (a metal disc) and the assembly is enclosed in a single furnace. Enthalpy or heat capacity variations in the sample cause a change in its temperature with respect to the reference. The resulting heat flow is small compared with that in differential thermal analysis (DTA), because the sample and reference are in good thermal contact. The temperature difference is used to determine an enthalpy change in the sample [Bhadeshia, 2009].

A typical DSC experiment begins by weighing the sample and placing it into the empty sample pan. The instrument uses weight change information to calculate the heat of reactions. There are pan compositions including aluminum, copper, gold, and stainless steel for different applications and experimental conditions. Helium or nitrogen is the common purge gas. Air or oxygen are used to perform the oxidation tests. The purge gas removes the moisture of the sample and the gases formed during the reactions [Skoog et al, 1995].

The operation of the DSC system consists of several calibrations: baseline, heat flow, heat capacity, and temperature are the various components of the calibration process in DSC [Hohne, 1996].

Baseline calibration is performed without pans in place. The calibration computes the baseline slope and offset over the temperature range of interest. The computer system organizing the DSC stores these values and deducts baseline slope and offset from subsequent sample runs to minimize their effects. Heat flow calibration is performed after baseline calibration. Melting a known quantity of a material with a well-known heat of fusion forms the calibration procedure. Indium is the most often used standard. Indium is positioned in the sample pan and scanned against an empty reference pan. The area of the melting peak is related to the known enthalpy of fusion by a calibration factor known as the cell constant. This procedure also calibrates the temperature axis from the known melting temperature of indium. Temperature calibration should also be performed over a wider temperature range, by measuring the melting points of several well-known standards. Heat capacity calibration is performed by scanning a heat capacity standard, such as sapphire. This calibrates the system for C_p values and is used in separating the heat capacity component from the total heat flow.

DSC applications are performed in many applications for the characterizing of the materials. Quantitative applications include the calculation of heats and fusion and the extent of crystallization for crystalline materials. Glass transition temperatures and melting points are helpful for qualitative classification of materials, although thermal methods cannot be used by themselves for identification. Melting points are also very useful in determining the purity of various preparations. Hence, thermal methods are often used in quality control applications.

A typical DSC sensor assembly and sample holders can be seen in Figure A.1 and Figure A.2, respectively.

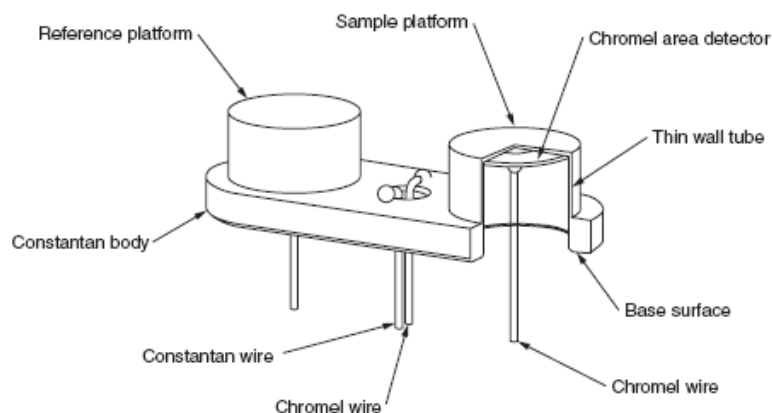


Figure A.1. DSC sensor assembly [Menczel and Prime, 2009]

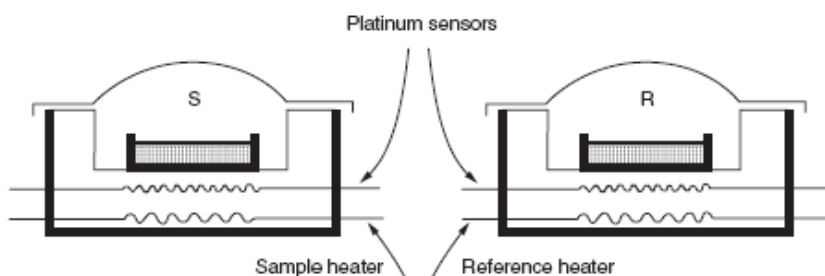


Figure A.2. Typical DSC power compensation sample holder with twin furnaces and sensors [Menczel and Prime, 2009]

A.2 Thermogravimetry

Thermogravimetry (TG) or thermogravimetric analysis (TGA) is a quantitative and qualitative measurement of any weight change associated with thermally-induced transitions [Williard et al, 1988]. For instance, TG can record the loss in weight as a function of temperature or time (under nonisothermal or isothermal conditions) for transitions that involve dehydration or decomposition. Thermogravimetric curves are characteristics of a given sample due to the unique sequence of physical transitions and chemical reactions that occur over specified temperature ranges. The rates of these thermally induced processes are often a function of the molecular structure. Weight changes result from physical and chemical bonds forming and breaking at increased temperatures. These processes may evolve volatile products or form reaction products that result in changes in weight of the

sample. TG data are useful in characterizing materials as well as in investigating the thermodynamics and kinetics of the reactions and transitions that result from the application of heat to these materials. It can provide information on the moisture, volatile, fixed carbon and ash content of the sample. From TGA curves, activation energies, reaction mechanisms, kinetics and thermodynamics of the chemical reactions are obtained. The TG can work from ambient temperature to 1500 °C in either inert or reactive atmospheres.

A thermogravimetric analyzer monitors mass flow into a sample or from a sample with increasing temperature. Samples are placed in a crucible that is located in a furnace on a quartz beam which is attached to an automatic recording balance. Figure A.3 shows the mechanism of a typical TGA instrument [Mohomed, 2009]. The horizontal quartz beam is kept in the null position by the current flowing through the transducer coil of an electromagnetic balance. A pair of photosensitive diodes works to determine the movement of the beam. Any change in the weight of the sample causes a deflection of the beam, which is sensed by one of the photodiodes. The beam is then brought to its original null position by a feedback current sent from the photodiodes to the coil of the balance. The current used in this process is proportional to the weight change of the sample.

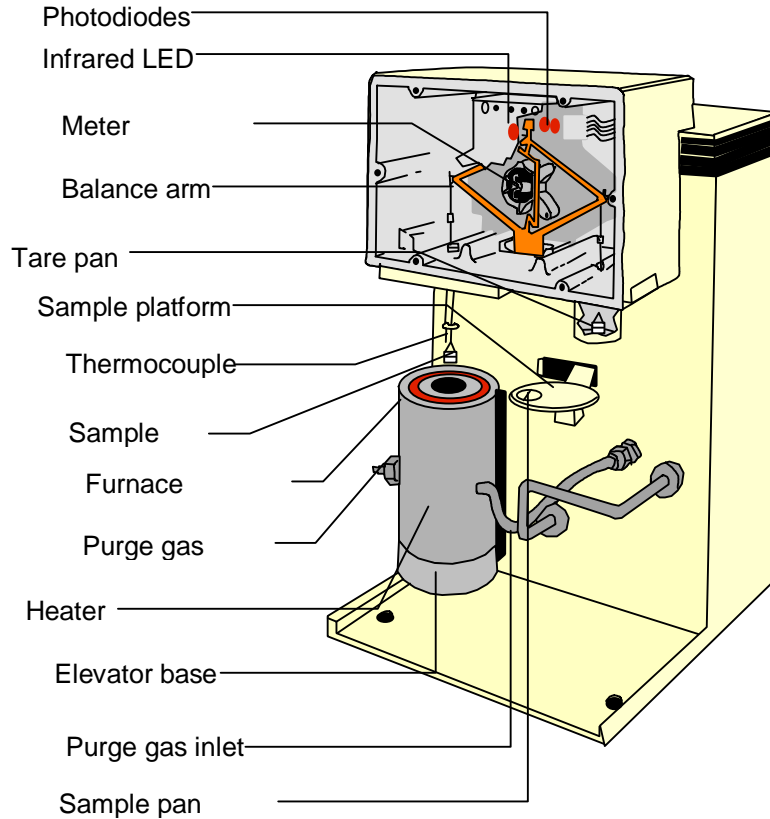


Figure A.3. Mechanism of a typical TGA [Mohomed, 2009]

Linear heating rates (HR) from 5 to 50 °C/min are typical in TG experiments. However, higher heating rates can be used depending on the objective of the experiment. Sample sizes range from 1 mg to 1 g. The computation of mass loss in a specific time interval ($\Delta w/\Delta t$) is important in kinetic interpretation of the reactions and processes. TGA output data are plotted as mass change vs. temperature using the analyzers.

A.3 Thermogravimetric Analyzer coupled to Mass Spectrometer

Mass Spectrometry (MS) is a high sensitive, non-specific technique used for studying unknown compounds [Hatakeyama and Quinn, 1999]. When bombarded by electrons, all substances ionize and fragment in a specific behavior. The mass spectrum, which records the mass and relative abundance of the ion fragments, gives information for each compound. MS is the most commonly used analysis technique for analyzing the gas that is evolved. The evolved gas components are identified provided that they stay in the

gaseous state at the temperature and pressure in the vicinity of the ion source. The whole mass spectrum, or some part of the spectrum, can be monitored continuously and the amount of sample can be of the order of nanograms. The greatest difficulty in connecting a mass spectrometer to a TGA instrument is the very wide pressure difference between the instruments. Coupling valves are available so that very small fraction of the purge gas enters the ion source, allowing the high vacuum of the mass spectrometer to be maintained. TGA-MS experiments were performed at The Pennsylvania State University.

A.4 Scanning Electron Microscopy

Since thermal analysis is a macroscopic technique, it is needed to get more detailed information about samples. Full understanding of a macroscopic observation requires the knowledge of the microscopic origin of the sample. Scanning electron microscopy is one of the microscopic techniques. It is a type of electron microscope that images the sample surface by scanning it with a high-energy beam of electrons in a raster scan model [Danilatos, 1988]. During scanning, the electrons interact with the atoms forming the structure of the sample to produce signals that include information about the morphology of the sample such as the particle structure, particle size, particle shape and several other properties as the surface composition and electrical conductivity [Turi, 1997].

A.5 Carbon-Hydrogen-Nitrogen (CHN) Analyzer

A CHN analyzer is a thermal analysis instrument, which can determine the elemental composition of a fuel. The instrument gives information about the concentration of carbon, hydrogen and nitrogen. Experiments were performed at The Pennsylvania State University – EMS Energy Institute.

APPENDIX B

DERIVATION OF DAEM EQUATION

Derivation of DAEM equation [Miura and Maki, 1998]:

$$1 - V/V^* = \int_0^{\infty} \exp\left(-\int_0^t \frac{k_o}{\beta} e^{-E/RT} dT\right) f(E) dE \quad (1)$$

Equation 1 was approximated by step function at $E=E_s$ for a selected temperature, T, where “a” is a constant heating rate.

$$\Phi(E, T) = \exp(-k_o \int_0^t e^{-E/RT} dt) \cong \exp\left(-\frac{k_o}{a} \int_0^T e^{-E/RT} dT\right) \quad (2)$$

Equation 1 was then simplified to equation 3.

$$V/V^* \cong 1 - \int_{E_a}^{\infty} f(E) dE = \int_0^{E_a} f(E) dE \quad (3)$$

The activation energy, E_s , was chosen to satisfy $\Phi(E_s, T) \approx 0.58$. The relationship of E_s to a, T, and k_o is given by

$$0.545aE_s / k_o RT^2 = e^{-E_a/RT} \quad (4)$$

with the following approximate equation for $\Phi(E, T)$:

$$\Phi(E, T) \cong \exp\left(-\frac{k_o RT^2}{aE} e^{-E/RT}\right) \quad (5)$$

This management approximates that only a reaction having E_s occurs at the specified T and a. The approximation is given mathematically by

$$dV/dt \cong d(\Delta V)/dt = k_o e^{-E/RT} (\Delta V^* - \Delta V) \quad (6)$$

Equation 6 can be integrated for a constant heating rate “a” as

$$1 - \Delta V / \Delta V^* = \exp\left(-k_o \int_0^t e^{-E/RT} dt\right) \cong \exp\left(-\frac{k_o RT^2}{aE} e^{-E/RT}\right) \quad (7)$$

Equations 6 and 7 are rewritten

$$\ln\left\{\frac{d(V/V^*)}{dt}\right\} = \ln\left\{k_o \frac{\Delta V^*}{V^*} \left(1 - \frac{\Delta V}{\Delta V^*}\right)\right\} - \frac{E}{RT} \quad (8)$$

and

$$\ln\left(\frac{a}{T^2}\right) = \ln\left(\frac{k_o R}{E}\right) - \ln\left\{-\ln\left(1 - \frac{\Delta V}{\Delta V^*}\right)\right\} - \frac{E}{RT} \quad (9)$$

Evaluating more closely at equation 9, it can be written like $1 - \Delta V/\Delta V^* = \Phi(E,T) \approx 0.58$. This is the approximation used to derive equation 4. Equation 9 then can be simplified to

$$\ln\left(\frac{a}{T^2}\right) = \ln\left(\frac{k_o R}{E}\right) + 0.6075 - \frac{E}{RT} \quad (10)$$

The term 0.6075 in equation 10 can be set equal to zero for simplicity and then activation energy can be calculated using $\ln(a/T^2)$ vs $1/T$.

APPENDIX C

DSC&TGA CURVES OF SAMPLES

C.1 DSC Curves

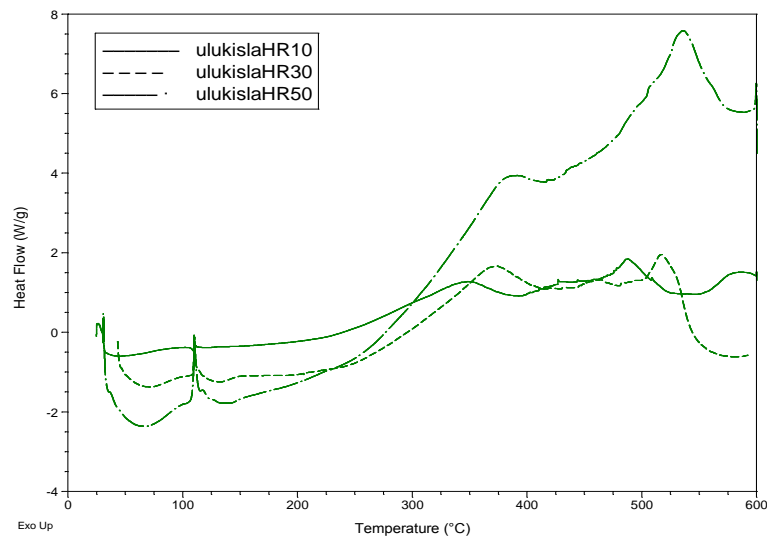


Figure C.1. DSC curve of Ulukışla oil shale at different HR

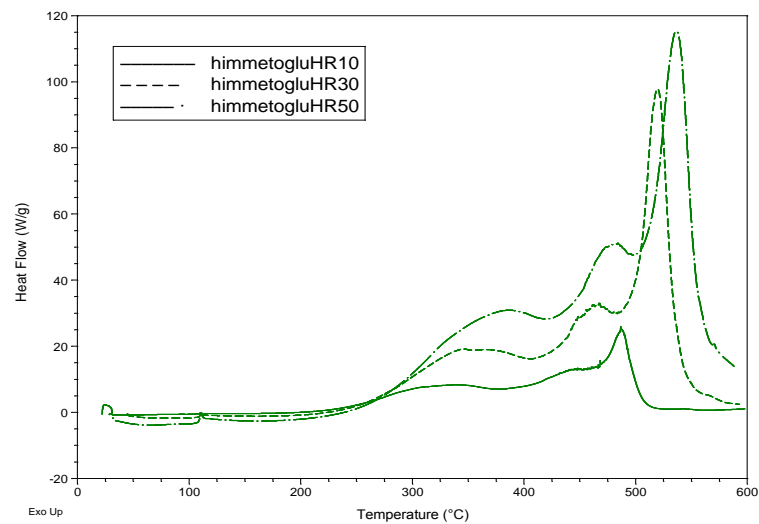


Figure C.2. DSC curve of Himmetoğlu oil shale at different HR

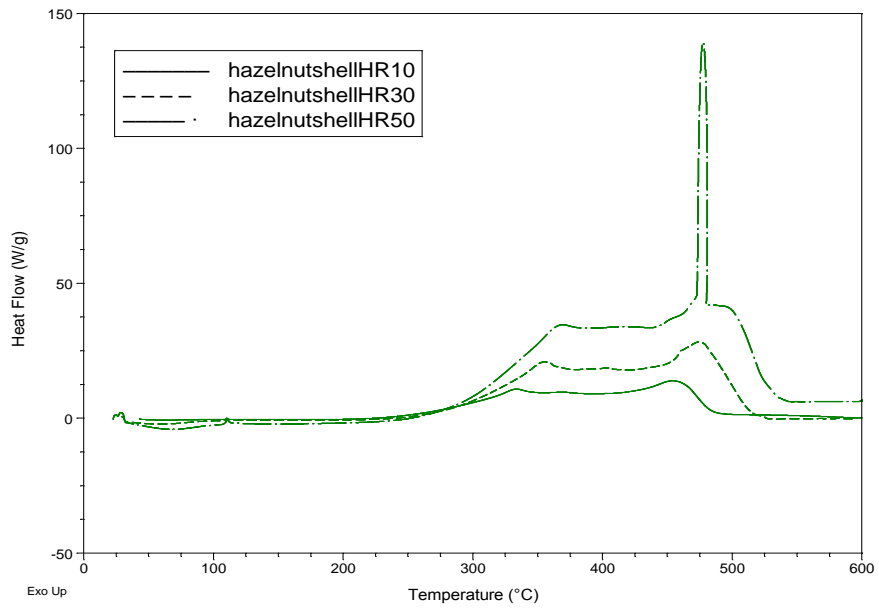


Figure C.3. DSC curve of hazelnut shell at different HR

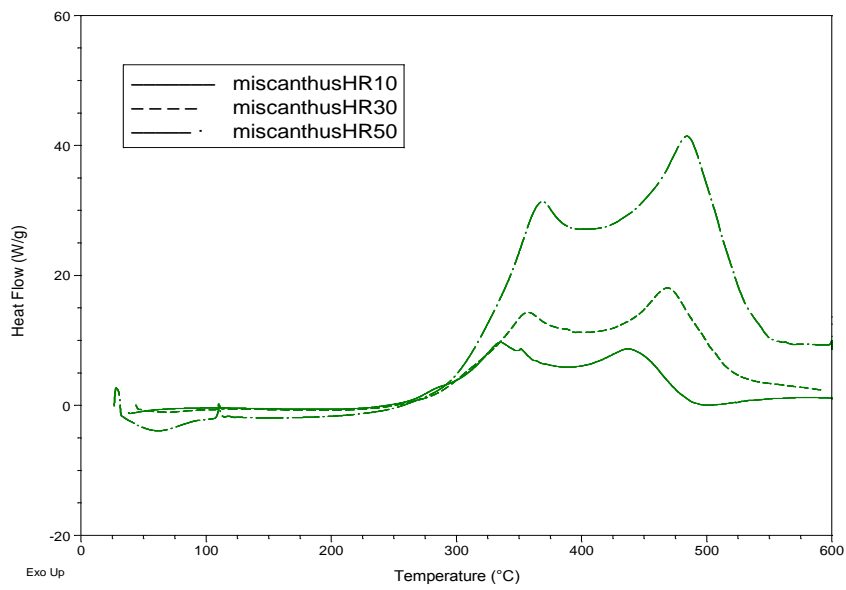


Figure C.4. DSC curve of miscanthus at different HR

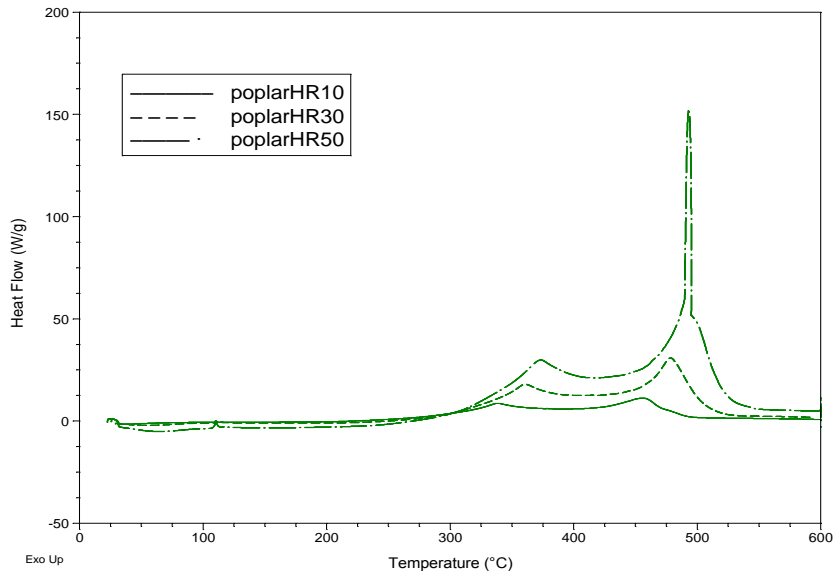


Figure C.5. DSC curve of poplar at different HR

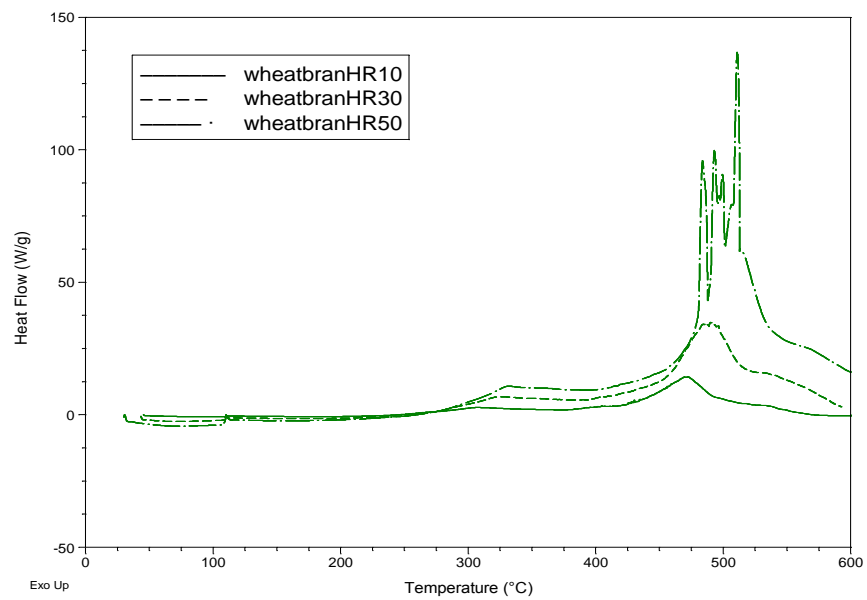


Figure C.6. DSC curve of wheat bran at different HR

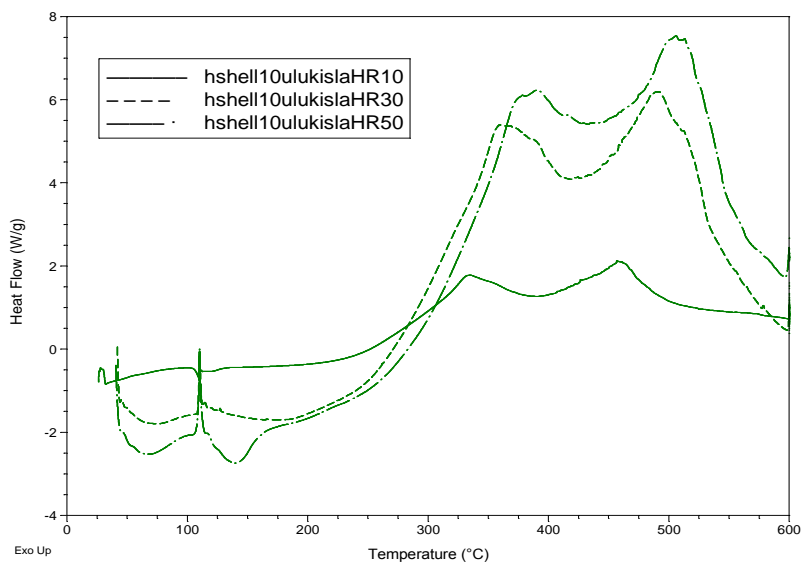


Figure C.7. DSC curve of hazelnut shell – oil shale blend (10-90) at different HR

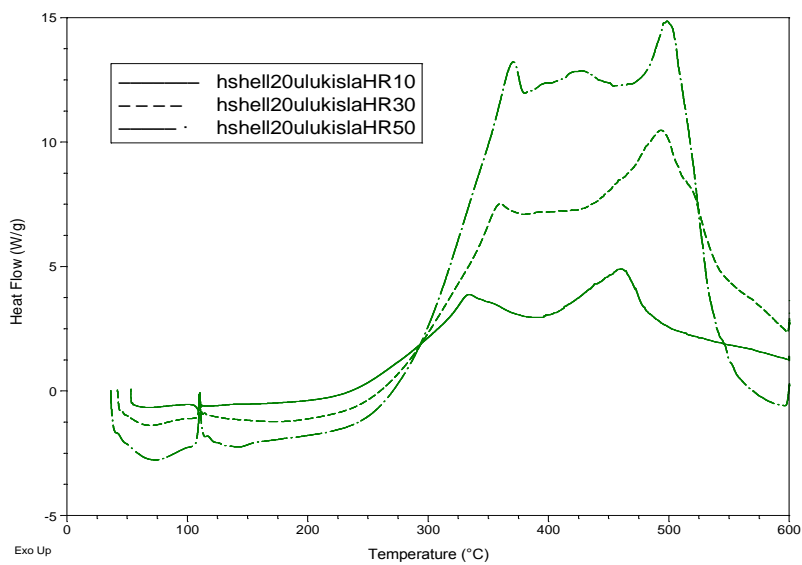


Figure C.8. DSC curve of hazelnut shell – oil shale blend (20-80) at different HR

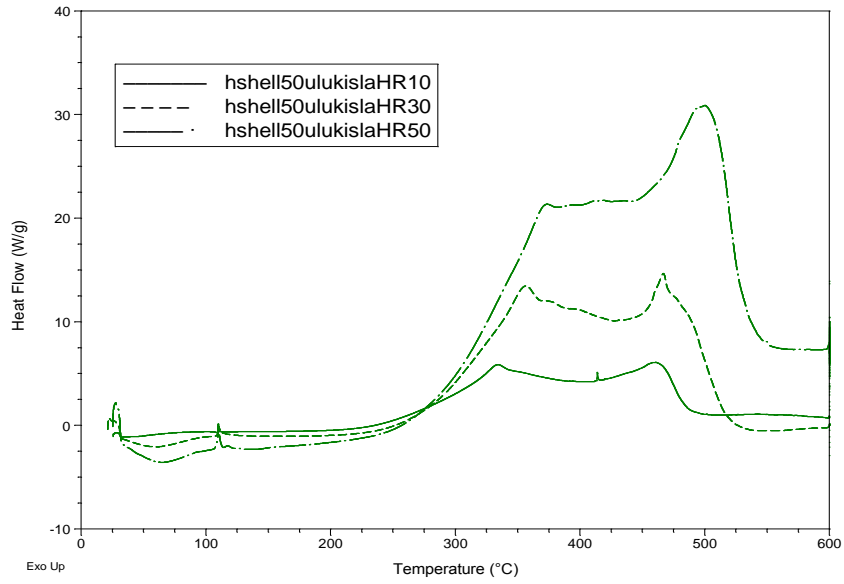


Figure C.9. DSC curve of hazelnut shell – oil shale blend (50-50) at different HR

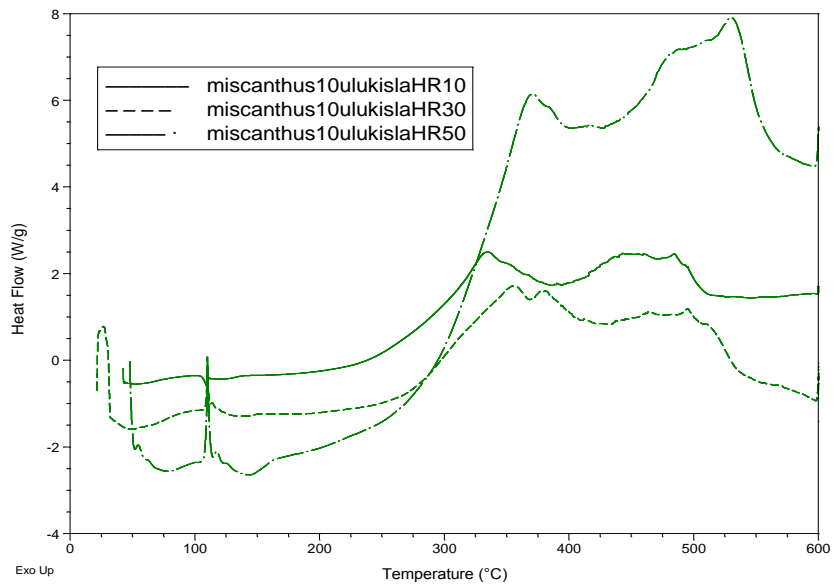


Figure C.10. DSC curve of miscanthus – oil shale blend (90-10) at different HR

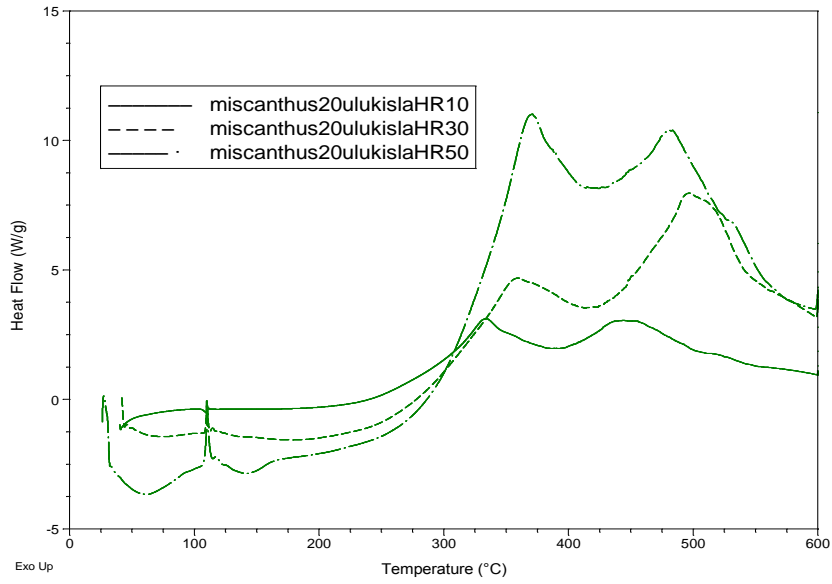


Figure C.11. DSC curve of miscanthus – oil shale blend (80-20) at different HR

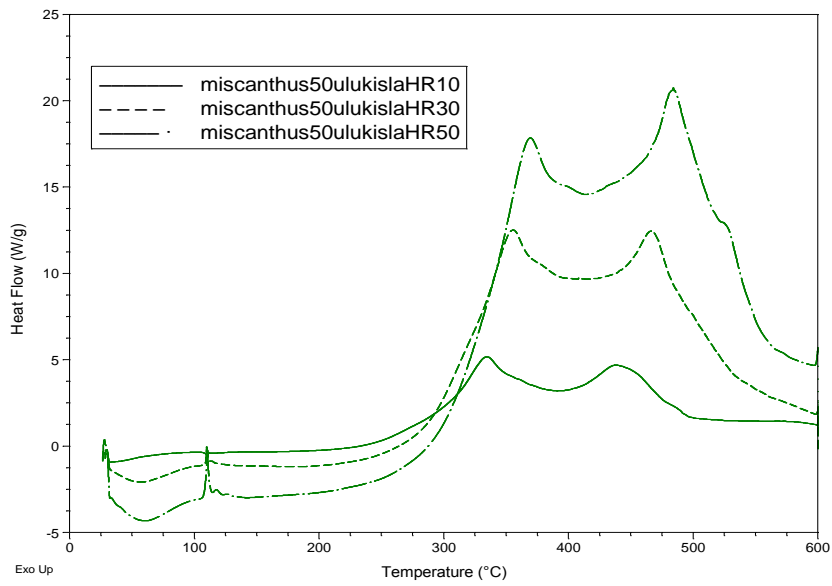


Figure C.12. DSC curve of miscanthus – oil shale blend (50-50) at different HR

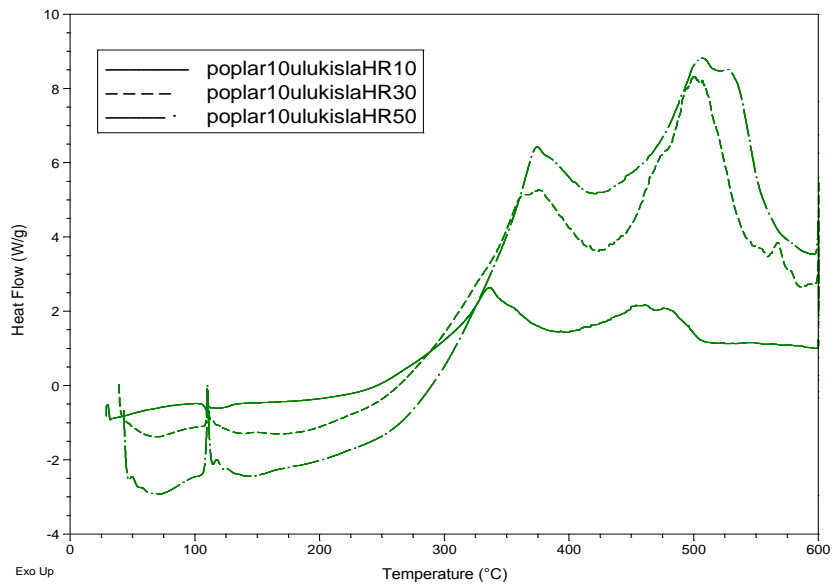


Figure C.13. DSC curve of poplar – oil shale blend (10-90) at different HR

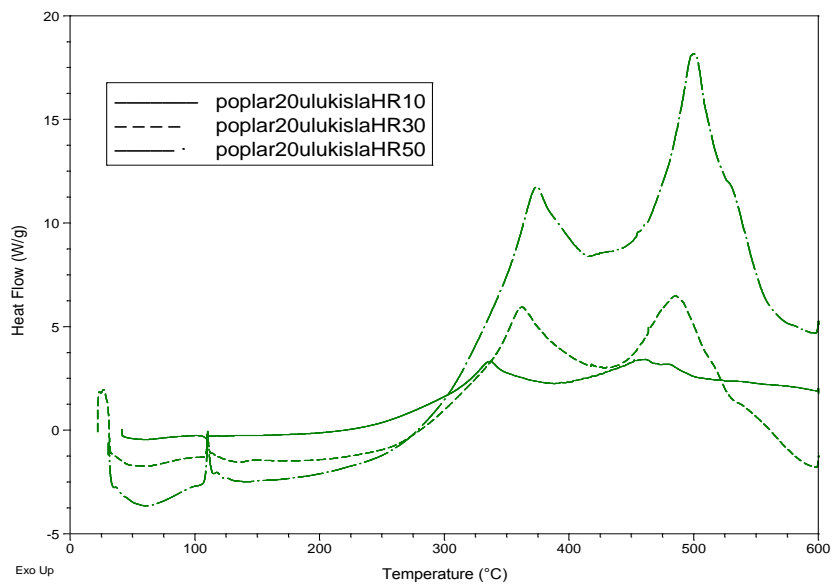


Figure C.14. DSC curve of poplar – oil shale blend (20-80) at different HR

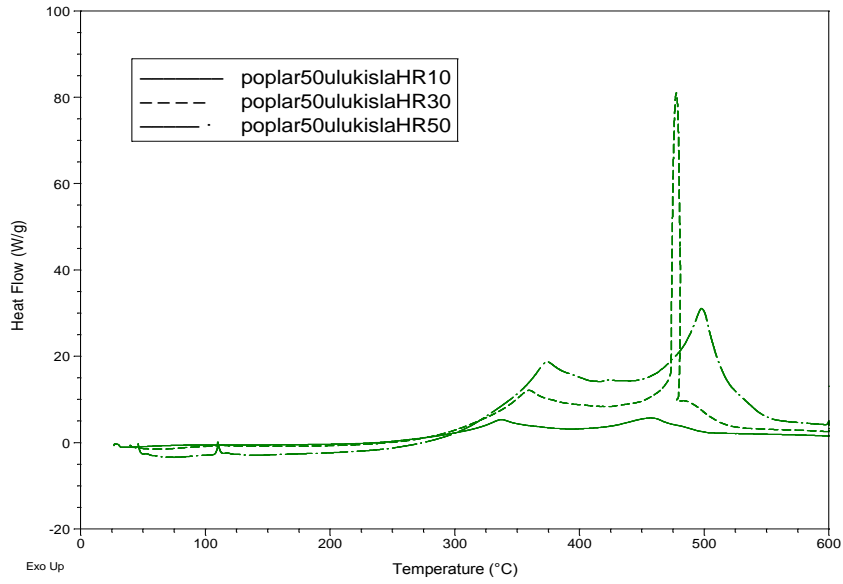


Figure C.15. DSC curve of poplar – oil shale blend (50-50) at different HR

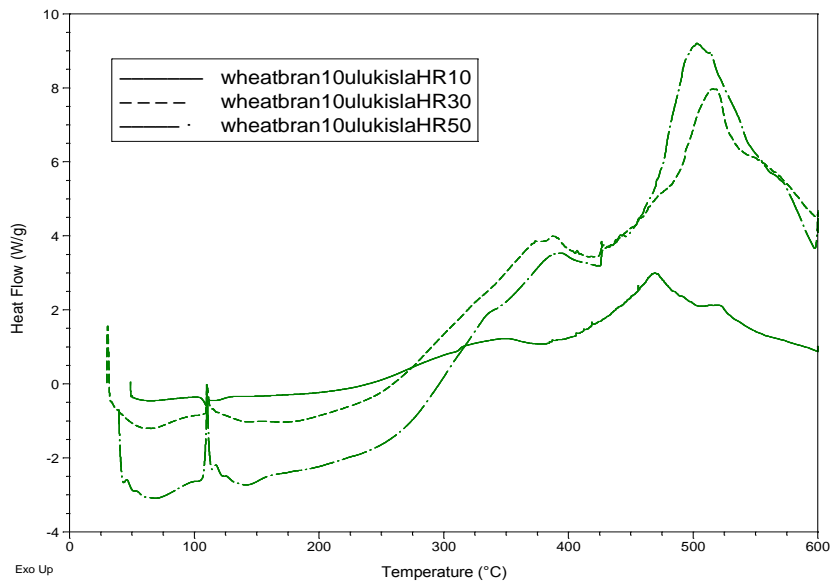


Figure C.16. DSC curve of wheat bran – oil shale blend (10-90) at different HR

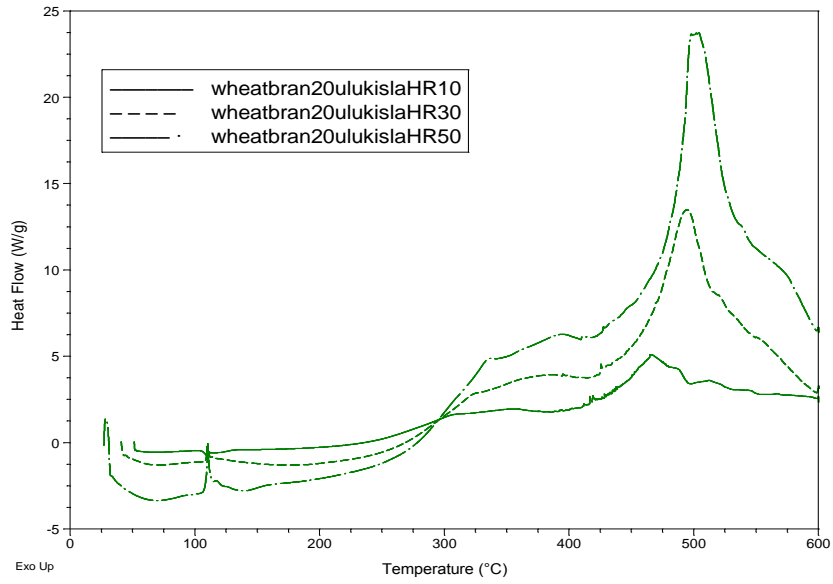


Figure C.17. DSC curve of wheat bran – oil shale blend (20-80) at different HR

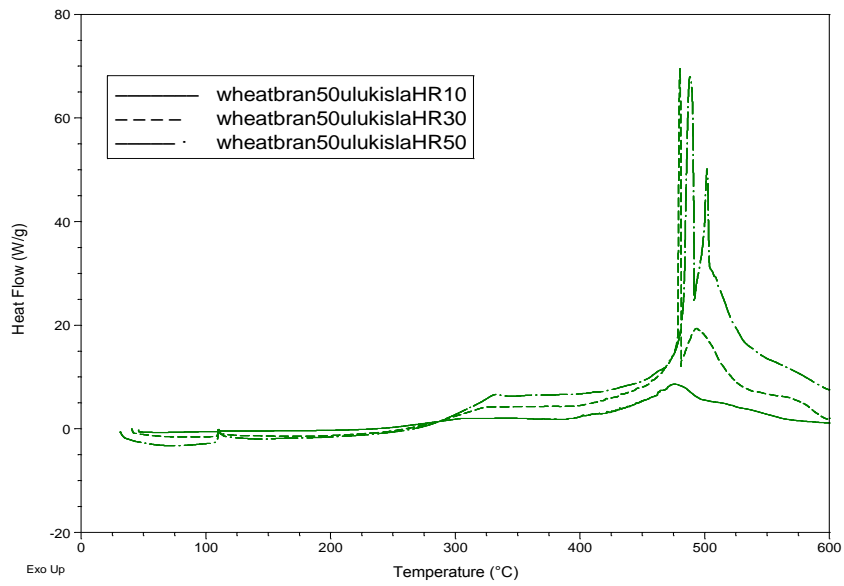


Figure C.18. DSC curve of wheat bran – oil shale blend (50-50) at different HR

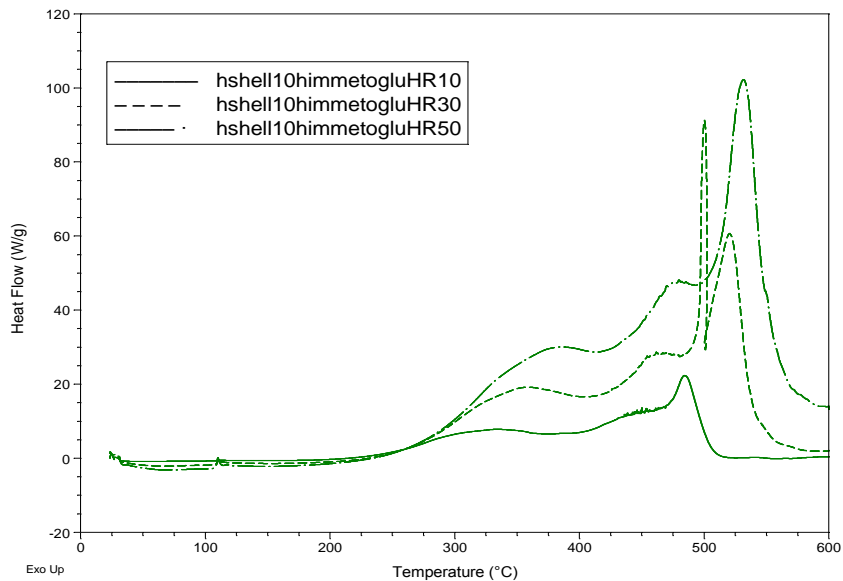


Figure C.19. DSC curve of hazelnut shell – oil shale blend (10-90) at different HR

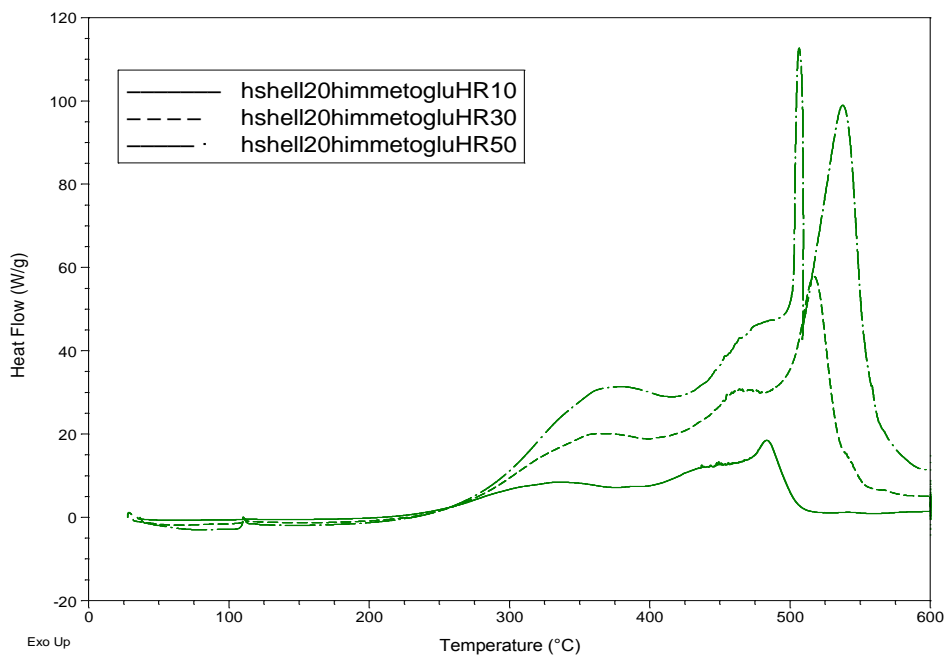


Figure C.20. DSC curve of hazelnut shell – oil shale blend (20-80) at different HR

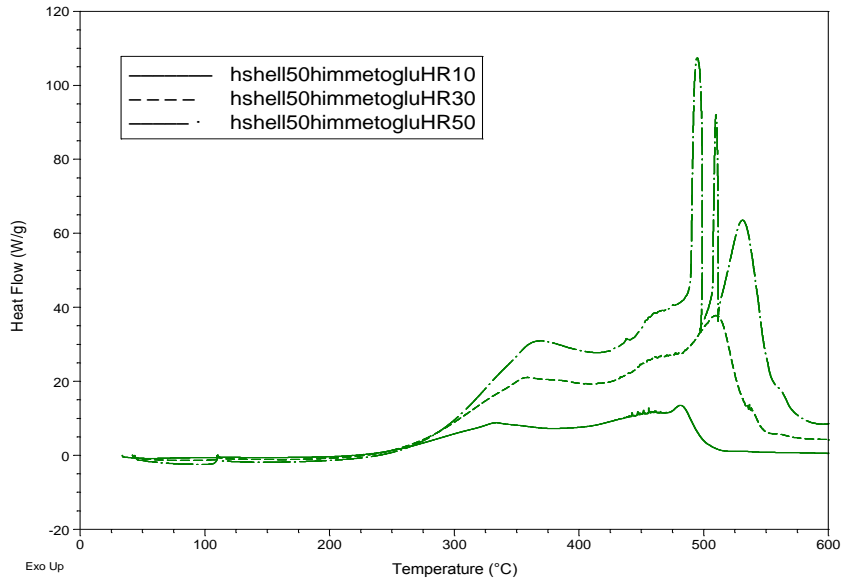


Figure C.21. DSC curve of hazelnut shell – oil shale blend (50-50) at different HR

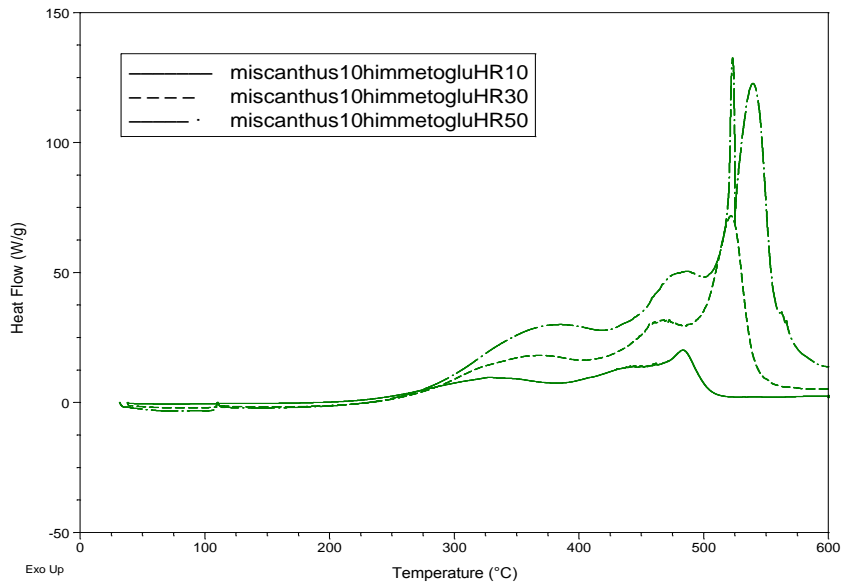


Figure C.22. DSC curve of miscanthus – oil shale blend (90-10) at different HR

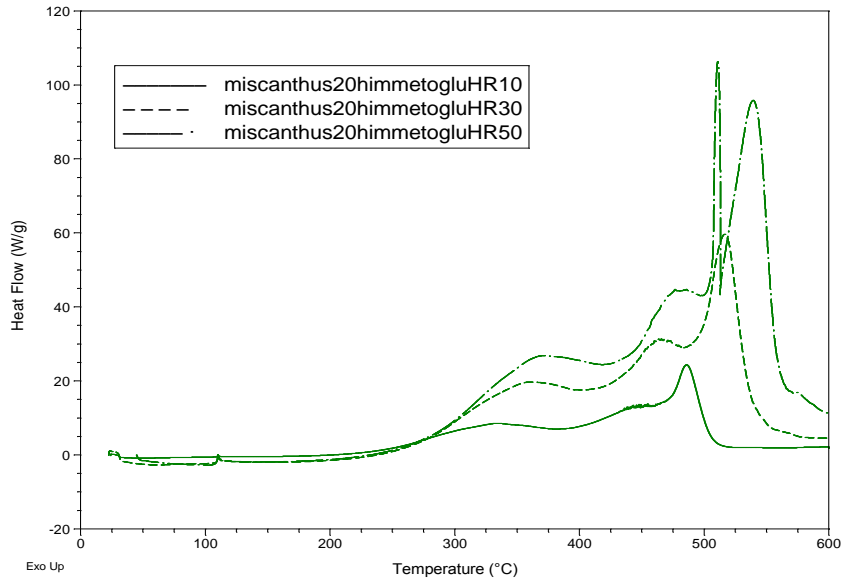


Figure C.23. DSC curve of miscanthus – oil shale blend (80-20) at different HR

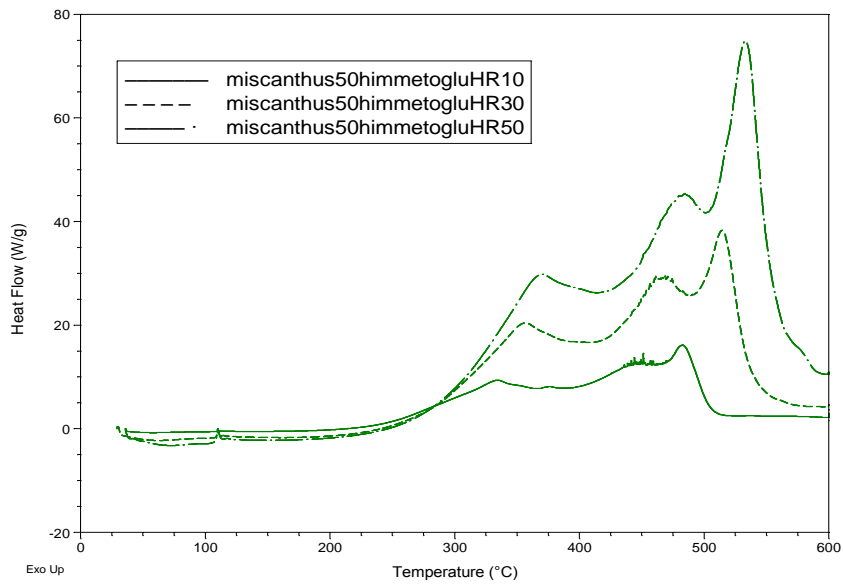


Figure C.24. DSC curve of miscanthus – oil shale blend (50-50) at different HR

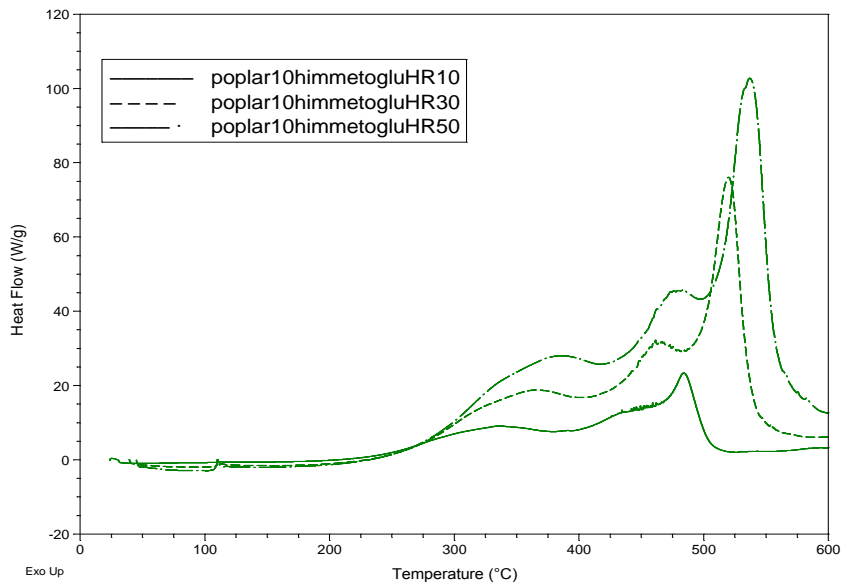


Figure C.25. DSC curve of poplar – oil shale blend (10-90) at different HR

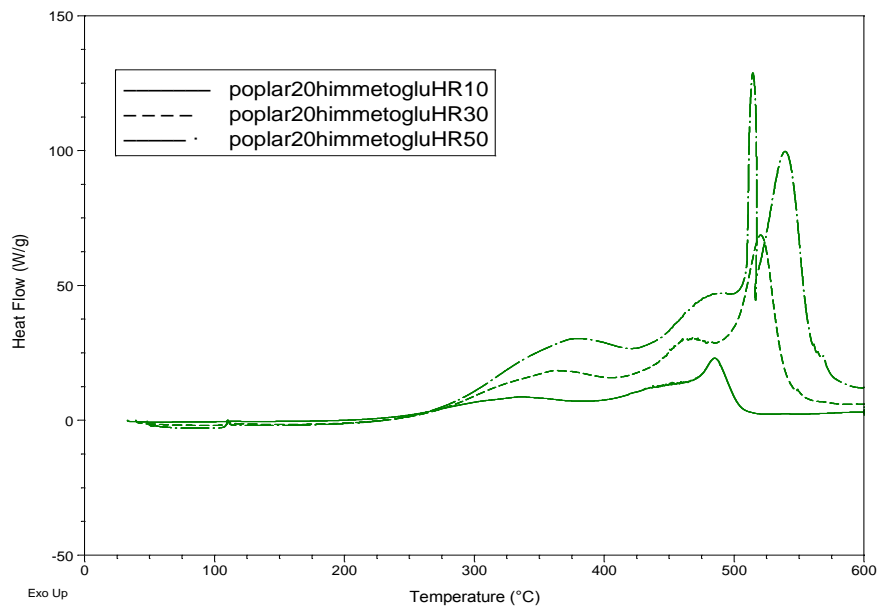


Figure C.26. DSC curve of poplar – oil shale blend (20-80) at different HR

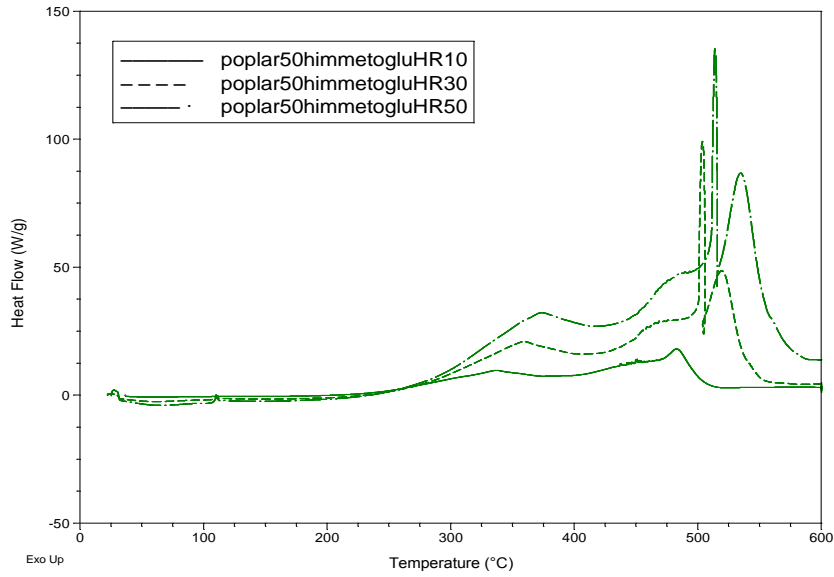


Figure C.27. DSC curve of poplar – oil shale blend (50-50) at different HR

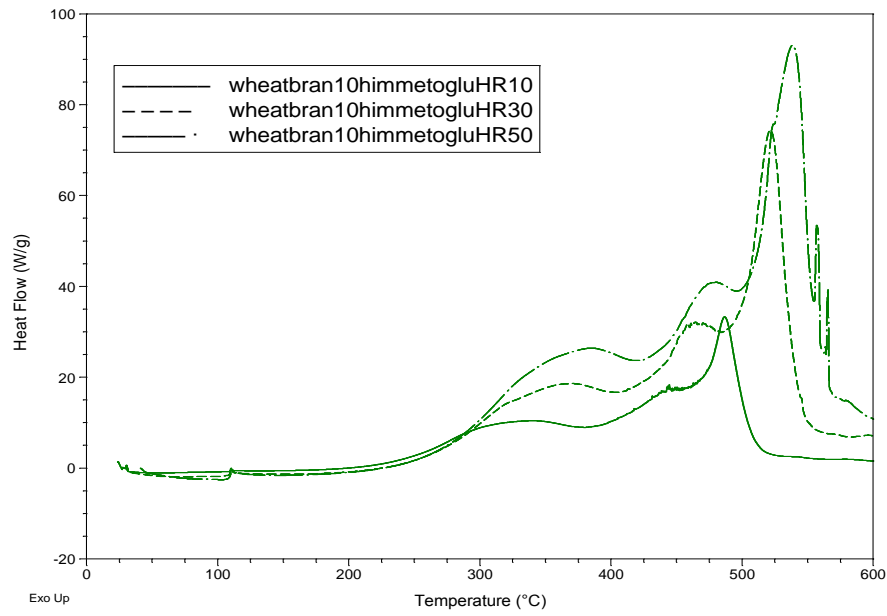


Figure C.28. DSC curve of wheat bran – oil shale blend (10-90) at different HR

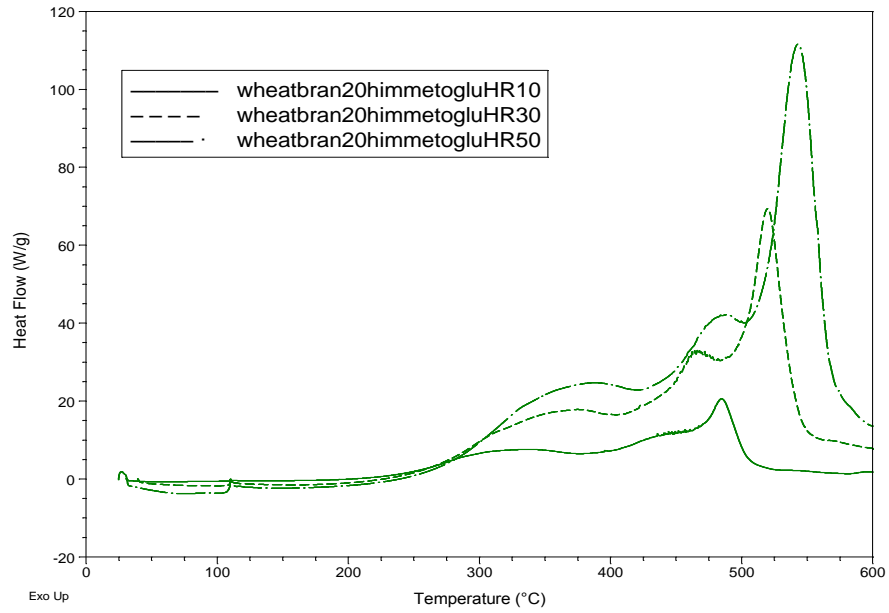


Figure C.29. DSC curve of wheat bran – oil shale blend (20-80) at different HR

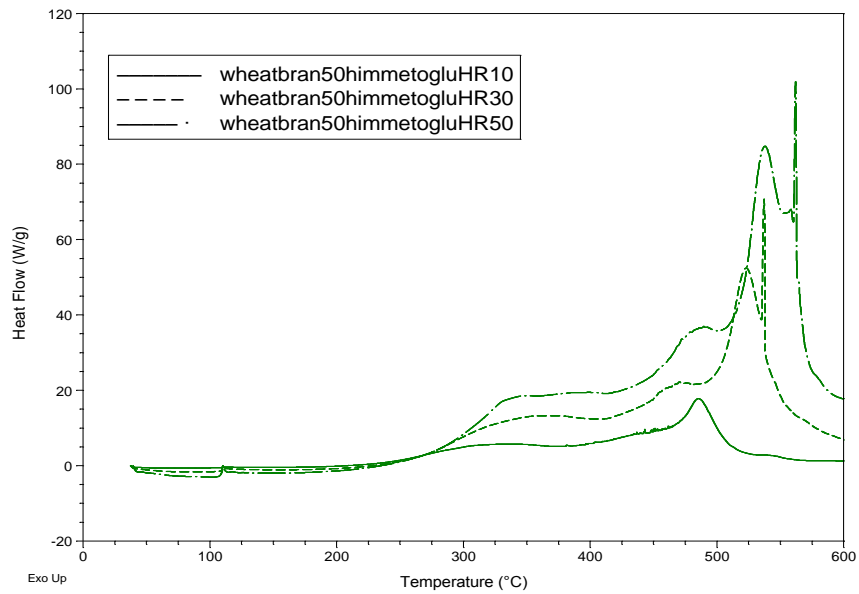


Figure C.30. DSC curve of wheat bran – oil shale blend (50-50) at different HR

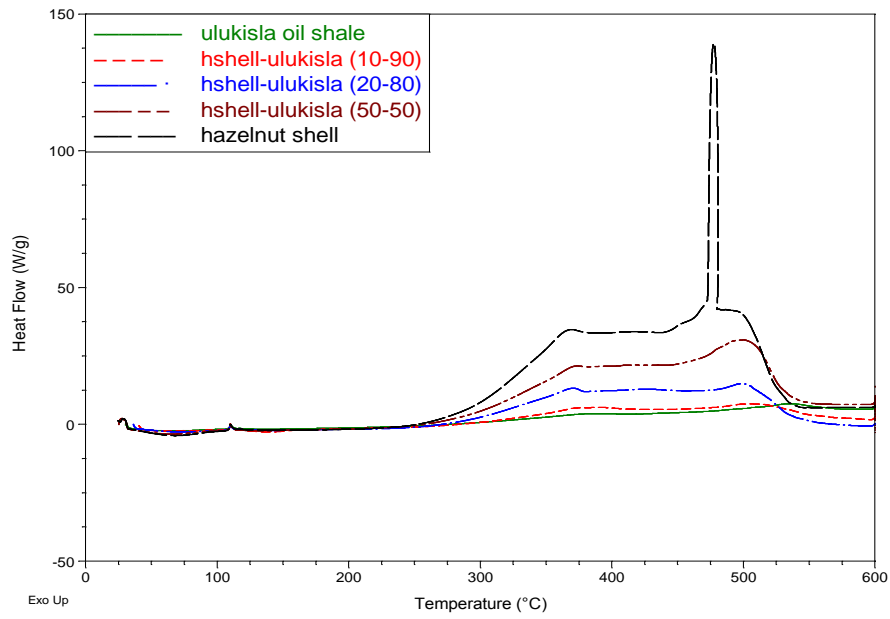


Figure C.31. Comparison of DSC curves for hazelnut shell- Ulukışla at 50 °C/min

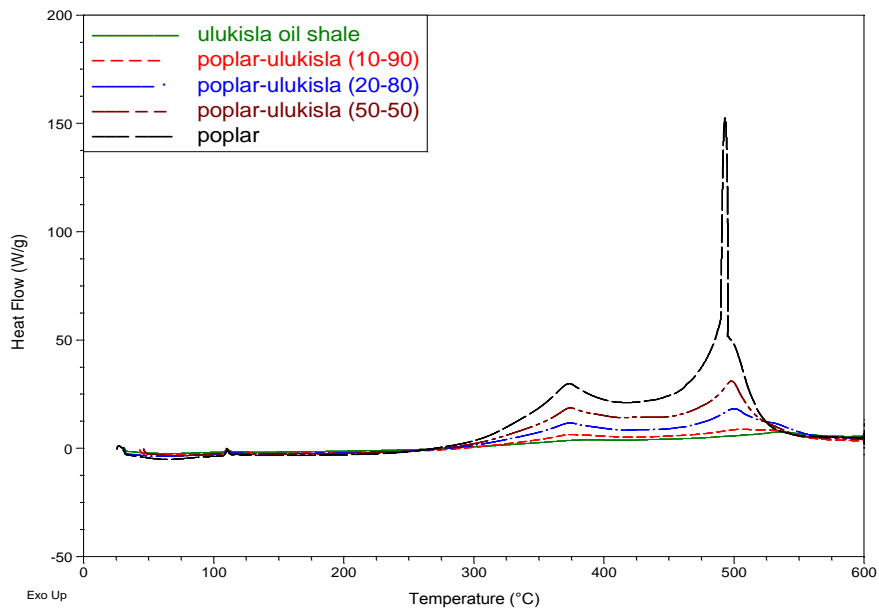


Figure C.32. Comparison of DSC curves for poplar-Ulukışla at 50 °C/min

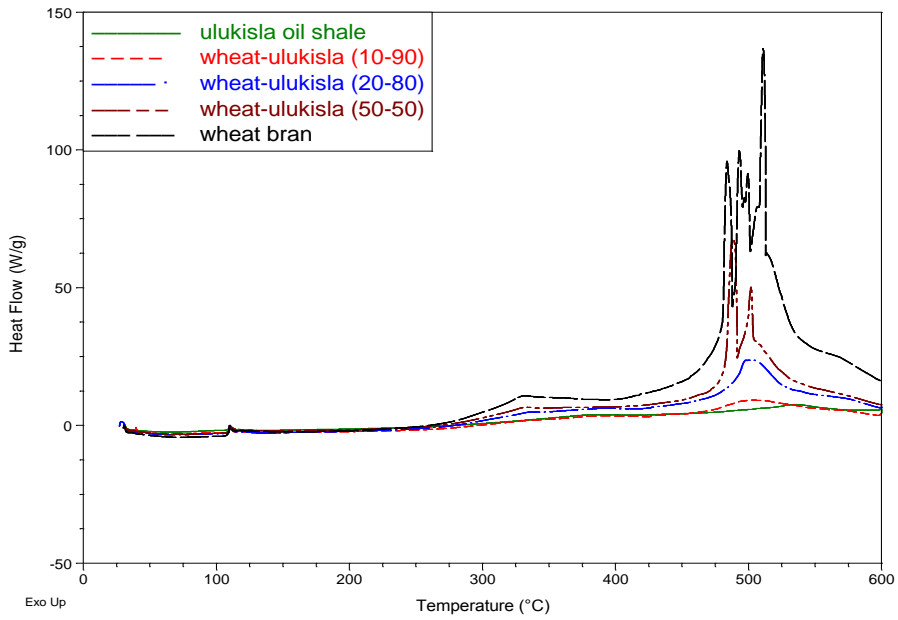


Figure C.33. Comparison of DSC curves for wheat bran-Ulukışla at 50 °C/min

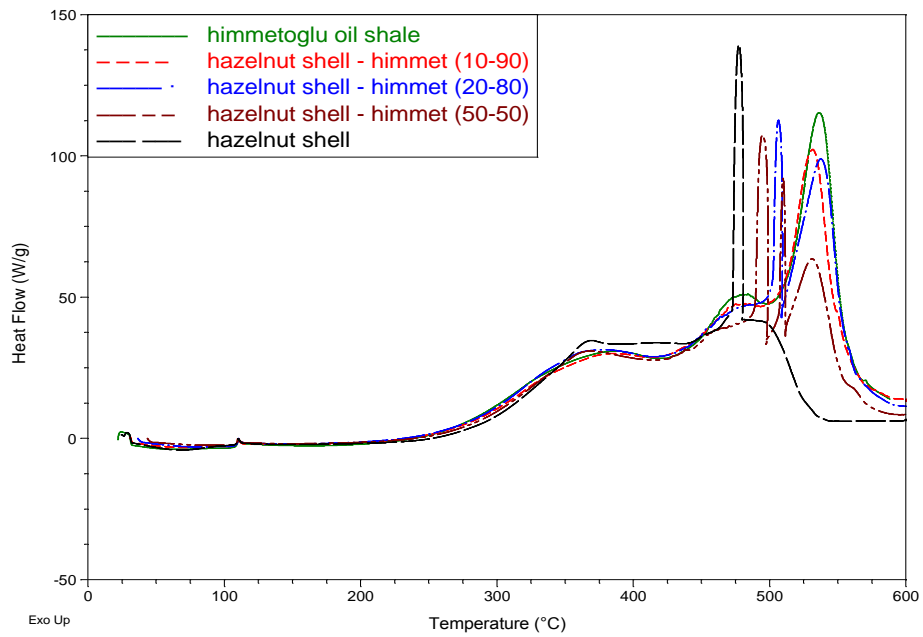


Figure C.34. Comparison of DSC curves for hazelnut shell-Himmetoğlu at 50 °C/min

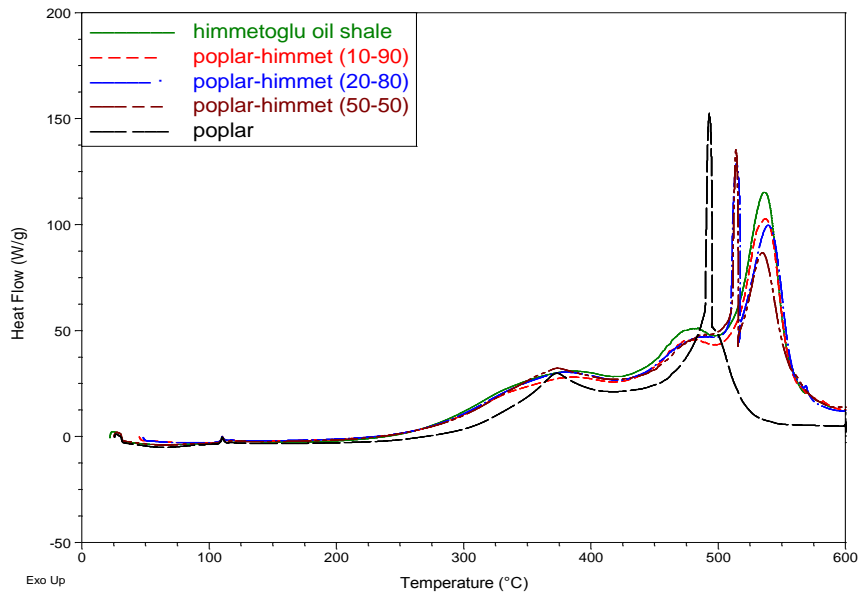


Figure C.35. Comparison of DSC curves for poplar- Himmetoğlu at 50 °C/min

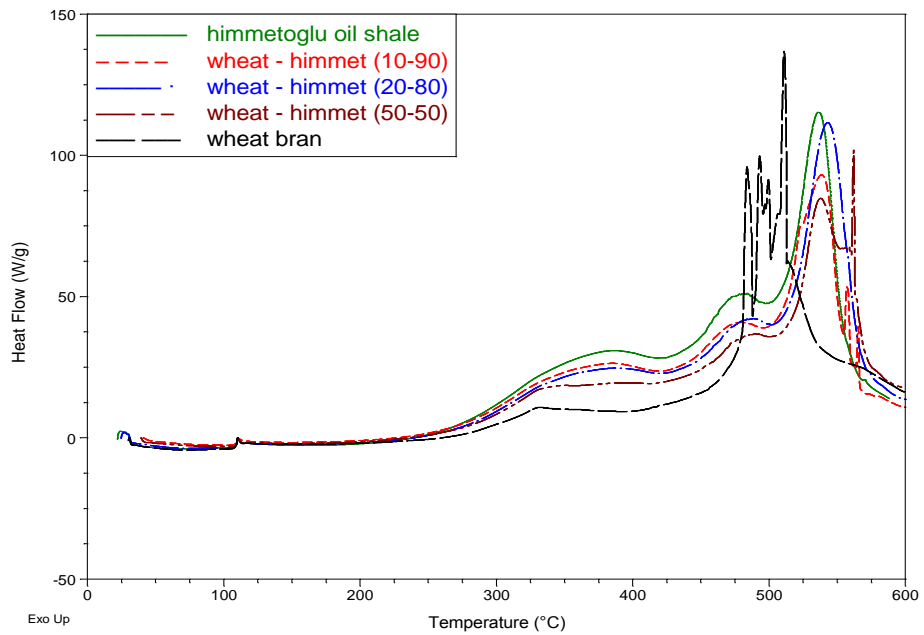


Figure C.36. Comparison of DSC curves for wheat bran- Himmetoğlu at 50 °C/min

C.2 TGA Curves

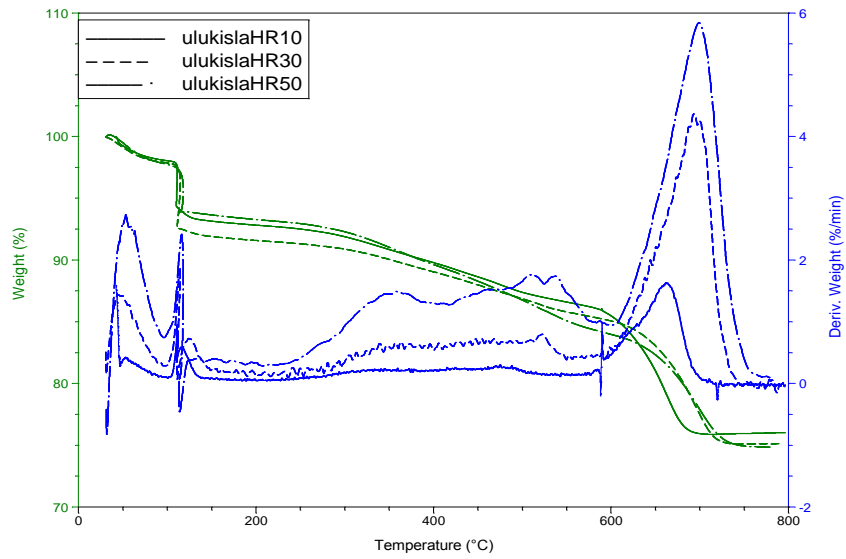


Figure C.37. TGA curve of Ulukışla oil shale at different HR

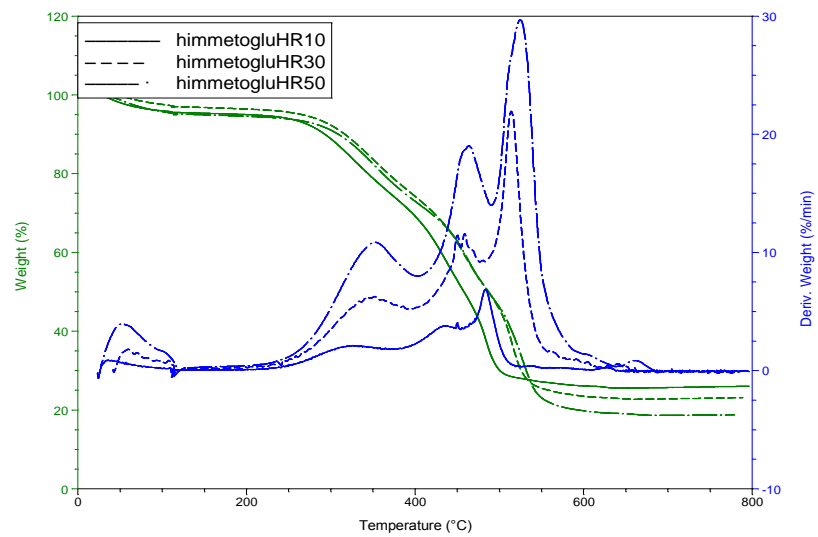


Figure C.38. TGA curve of Himmetoğlu oil shale at different HR

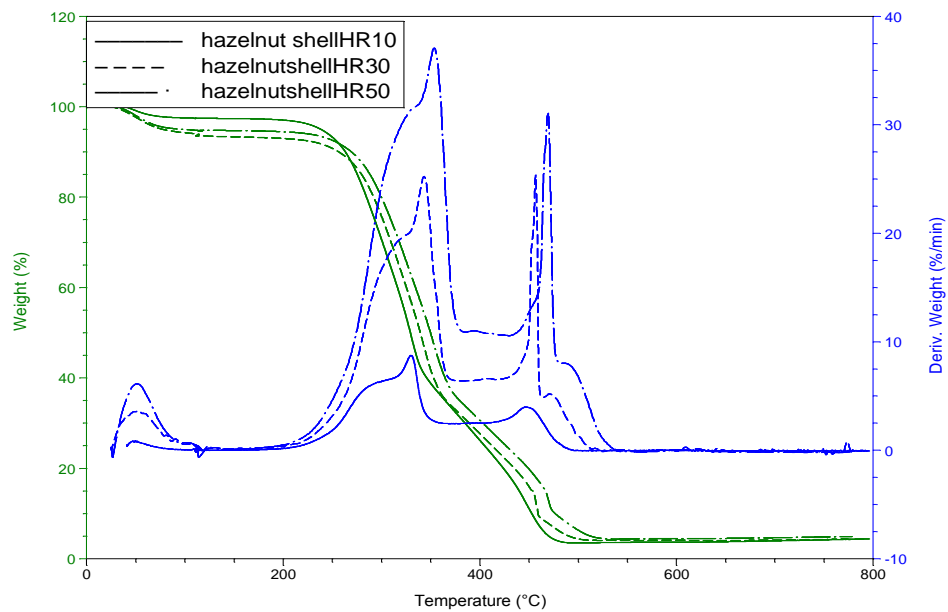


Figure C.39. TGA curve of hazelnut shell at different HR

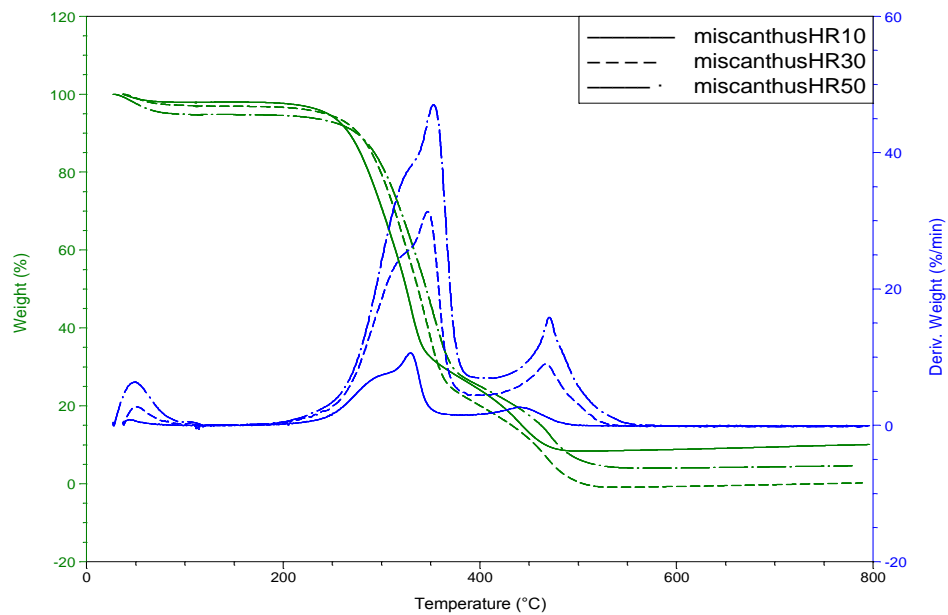


Figure C.40. TGA curve of miscanthus at different HR

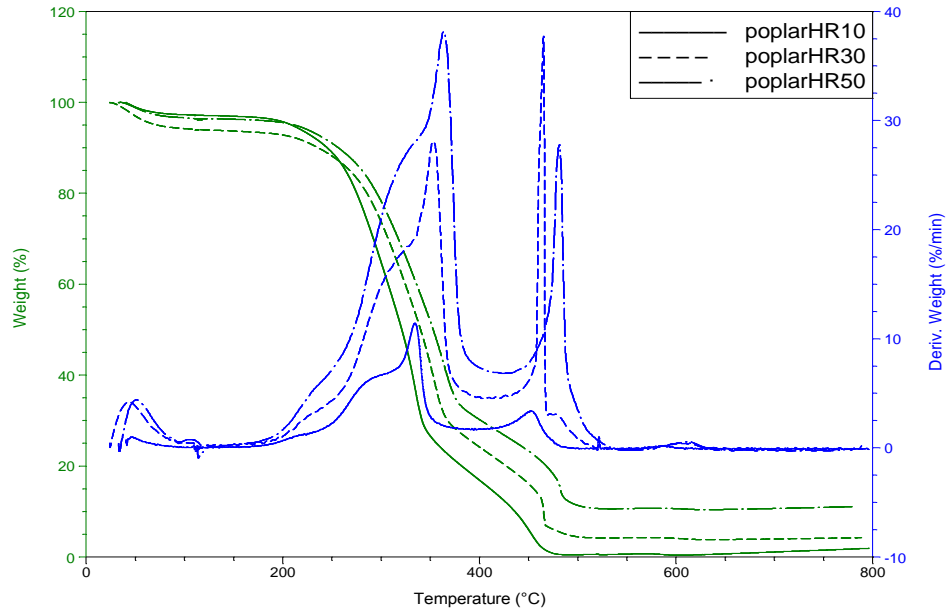


Figure C.41. TGA curve of poplar at different HR

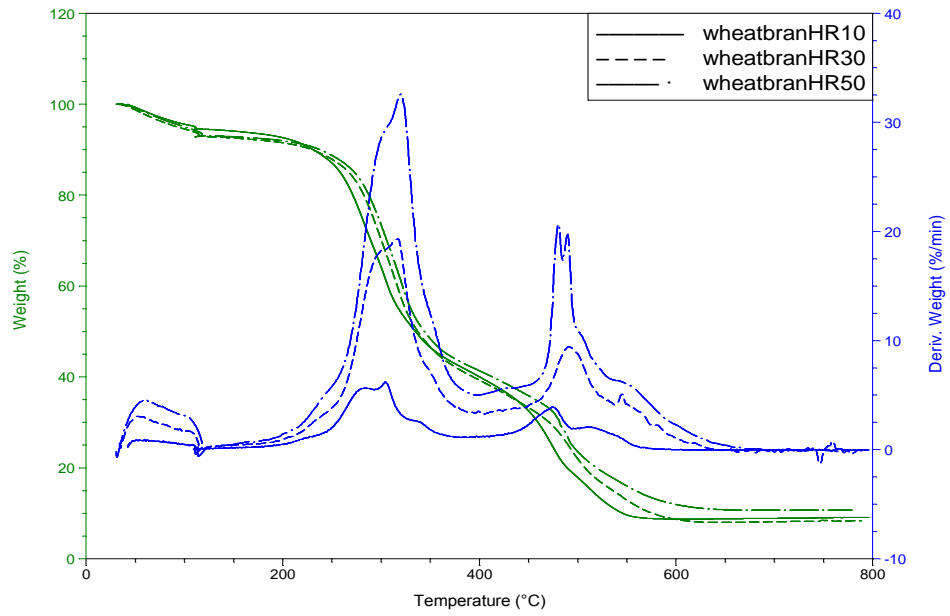


Figure C.42. TGA curve of wheat bran at different HR

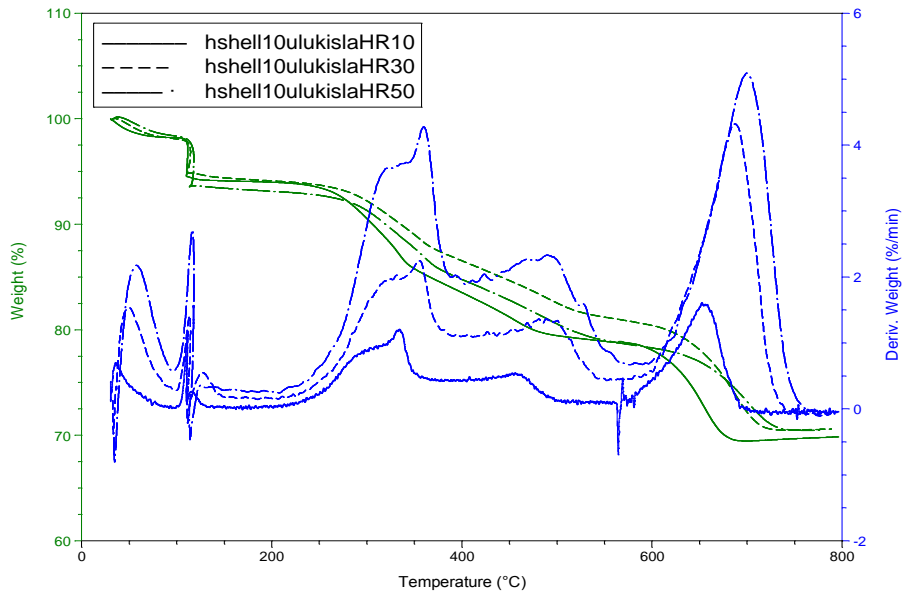


Figure C.43. TGA curve of hazelnut shell – oil shale blend (10-90) at different HR

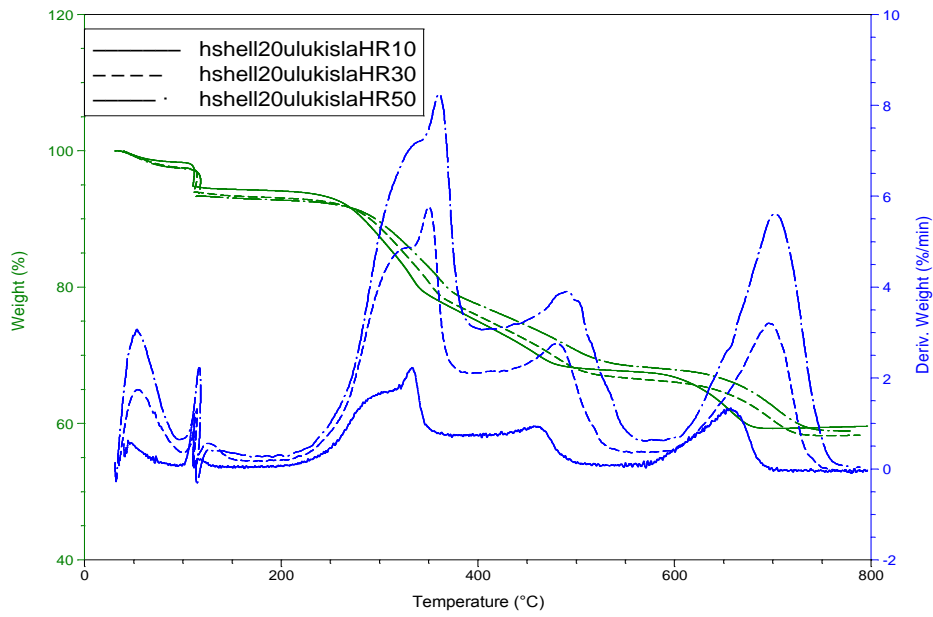


Figure C.44. TGA curve of hazelnut shell – oil shale blend (20-80) at different HR

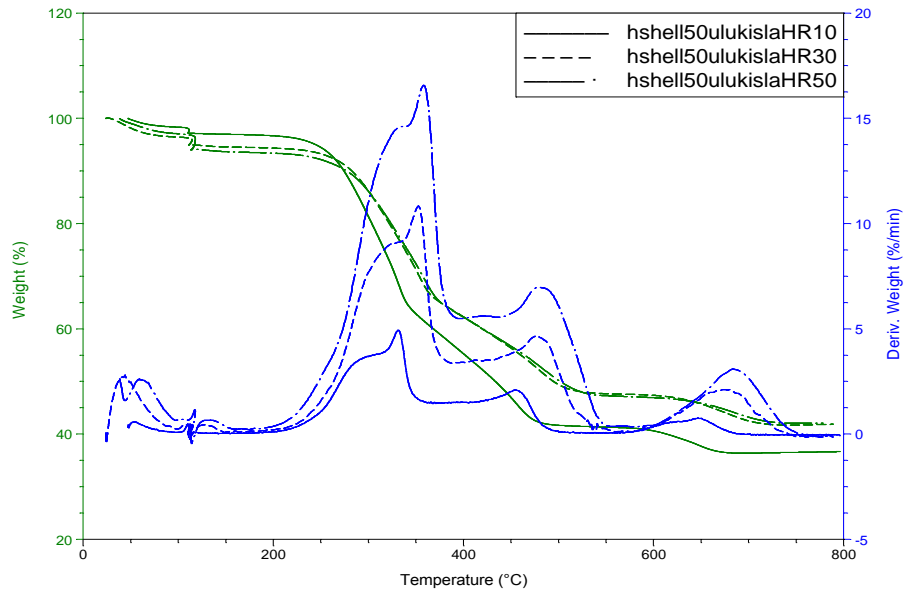


Figure C.45. TGA curve of hazelnut shell – oil shale blend (50-50) at different HR

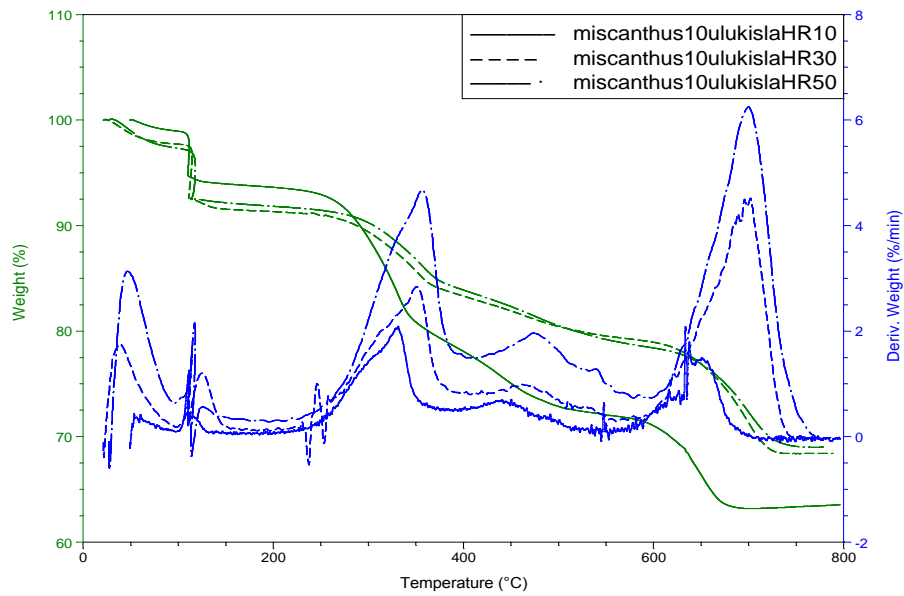


Figure C.46. TGA curve of miscanthus – oil shale blend (10-90) at different HR

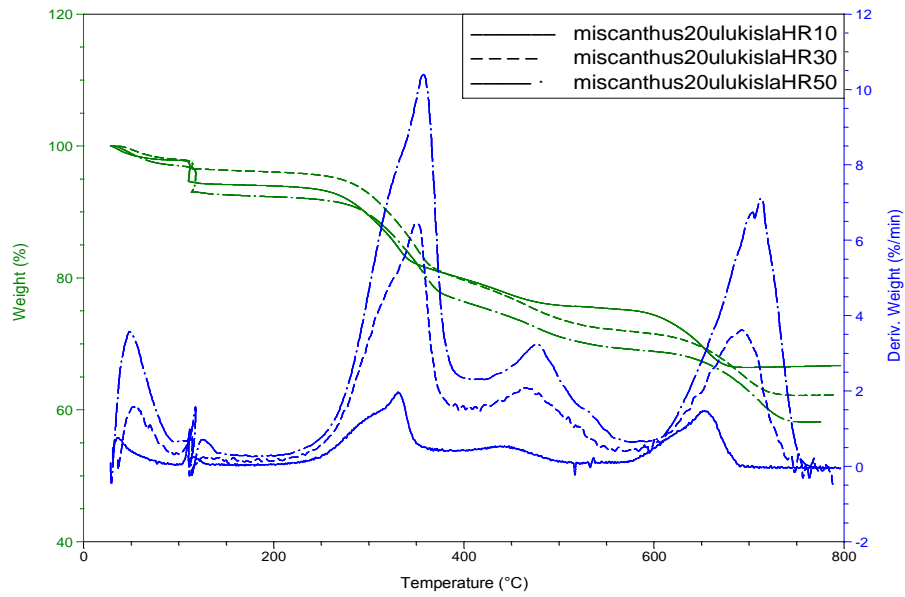


Figure C.47. TGA curve of miscanthus – oil shale blend (20-80) at different HR

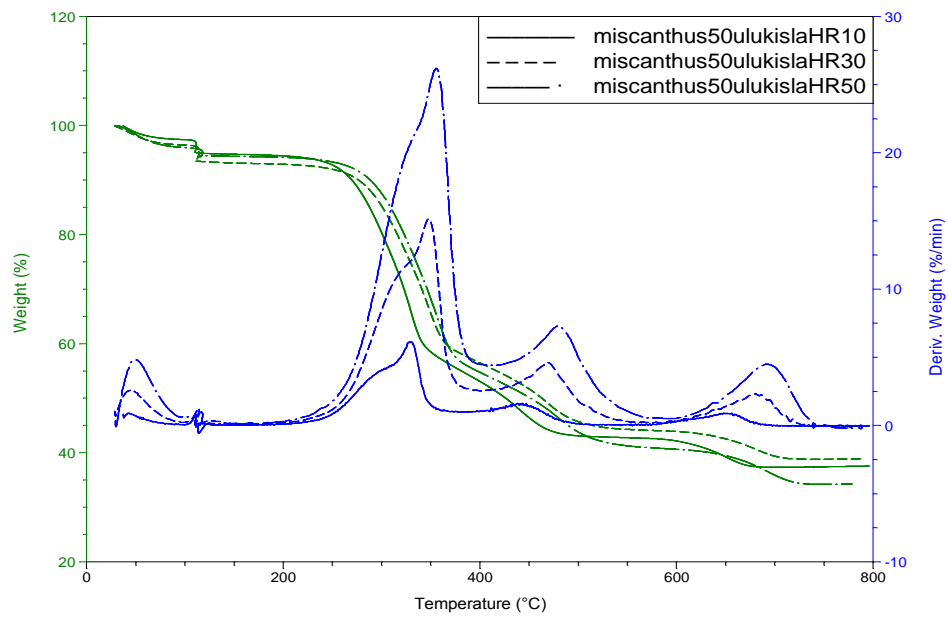


Figure C.48. TGA curve of miscanthus – oil shale blend (50-50) at different HR

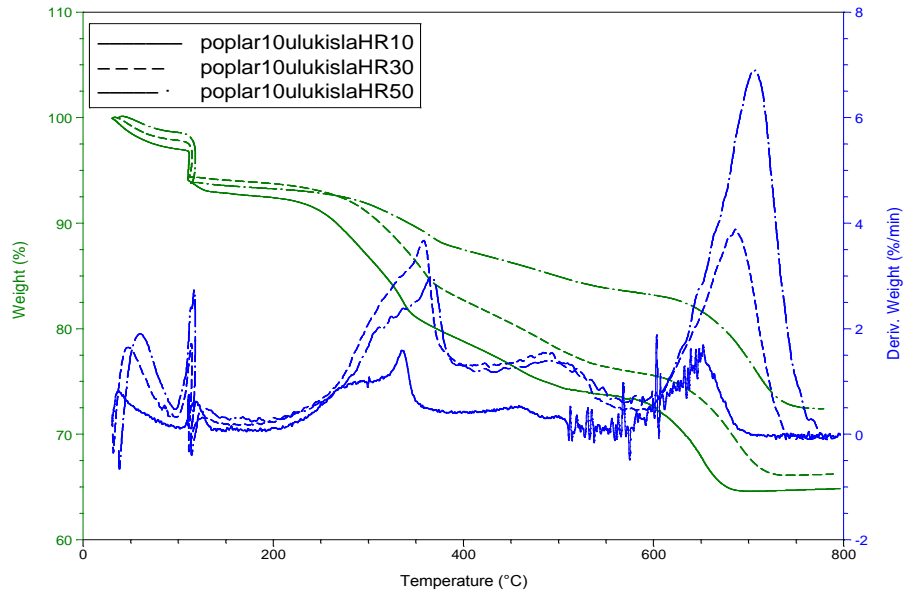


Figure C.49. TGA curve of poplar - oil shale blend (10-90) at different HR

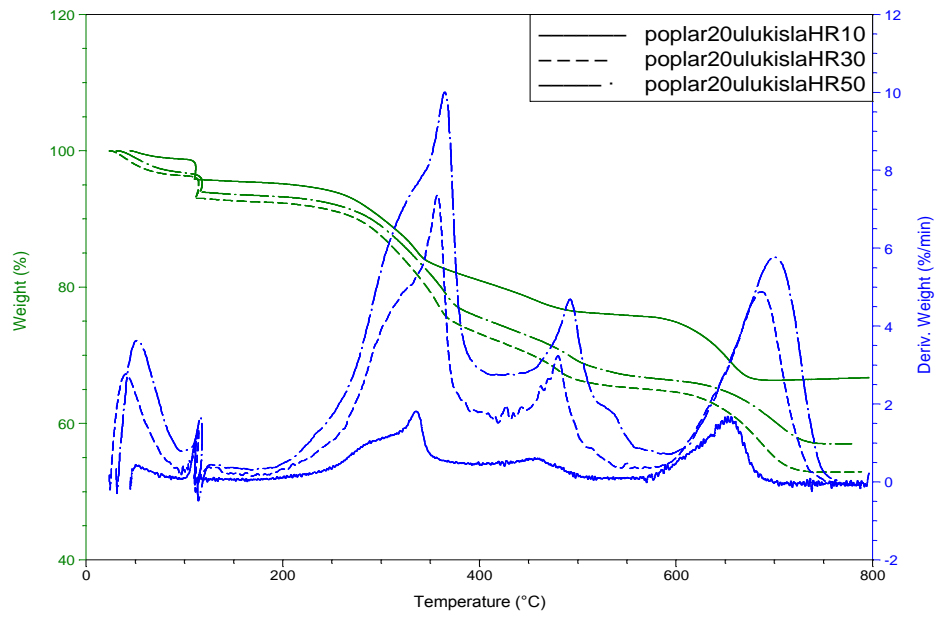


Figure C.50. TGA curve of poplar – oil shale blend (20-80) at different HR

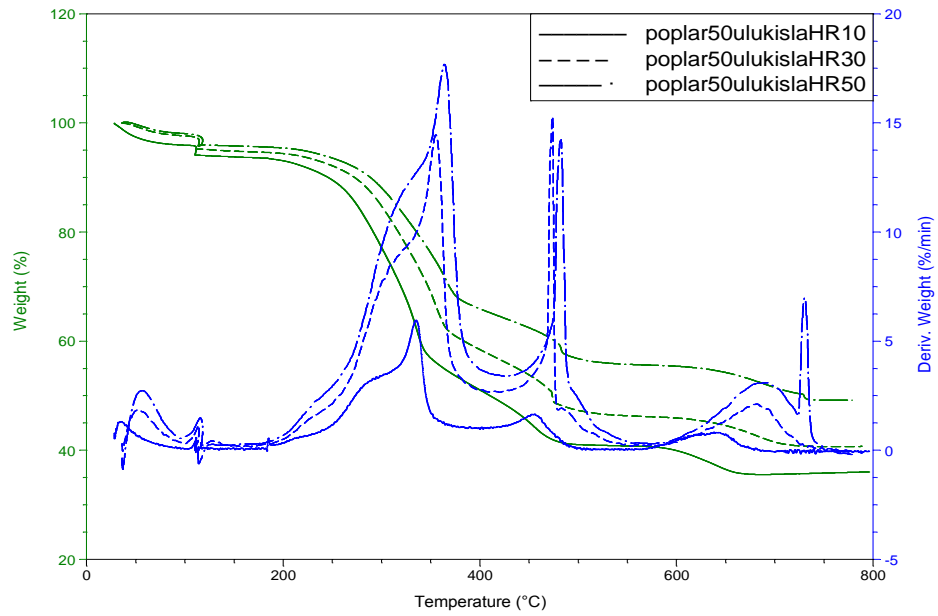


Figure C.51. TGA curve of poplar – oil shale blend (50-50) at different HR

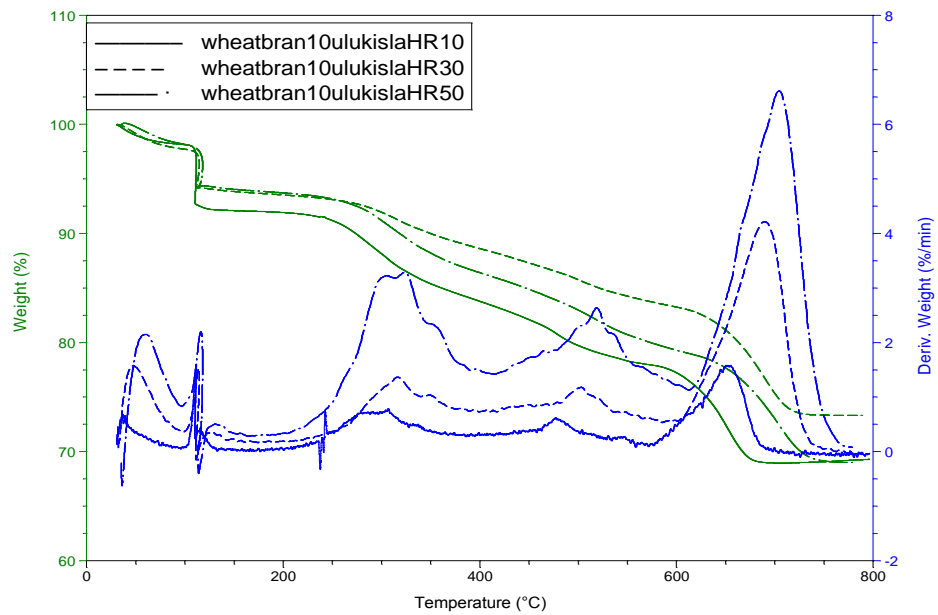


Figure C.52. TGA curve of wheat bran – oil shale blend (10-90) at different HR

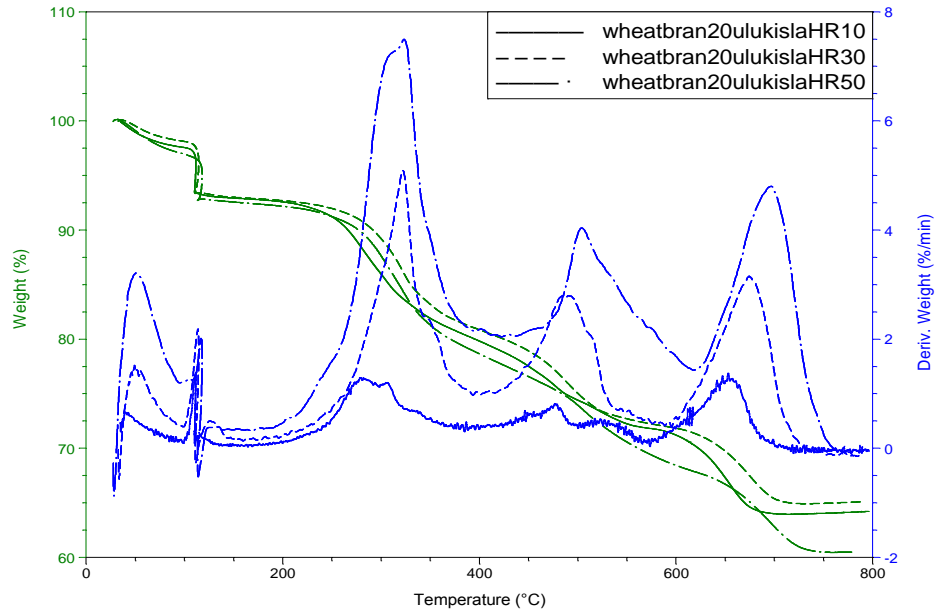


Figure C.53. TGA curve of wheat bran – oil shale blend (20-80) at different HR

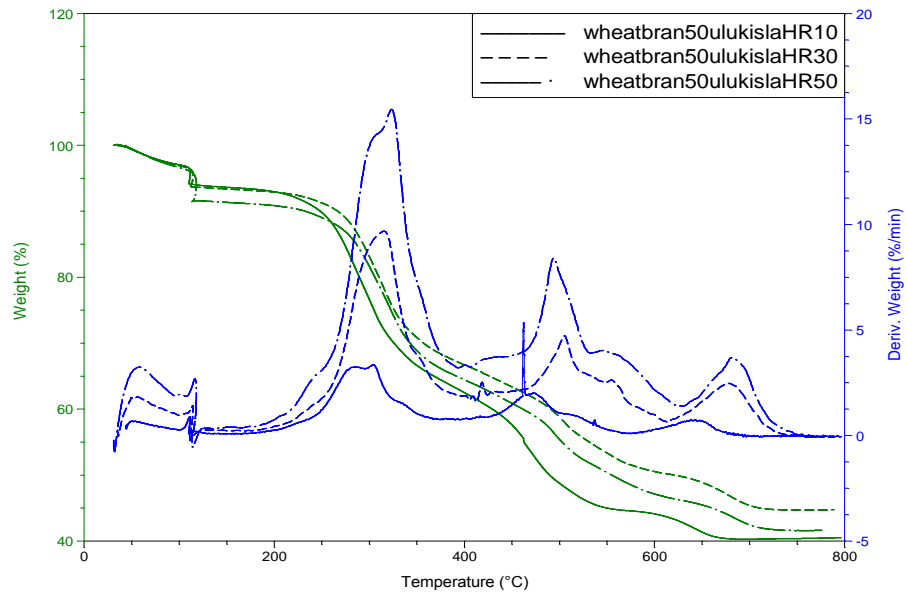


Figure C.54. TGA curve of wheat bran – oil shale blend (50-50) at different HR

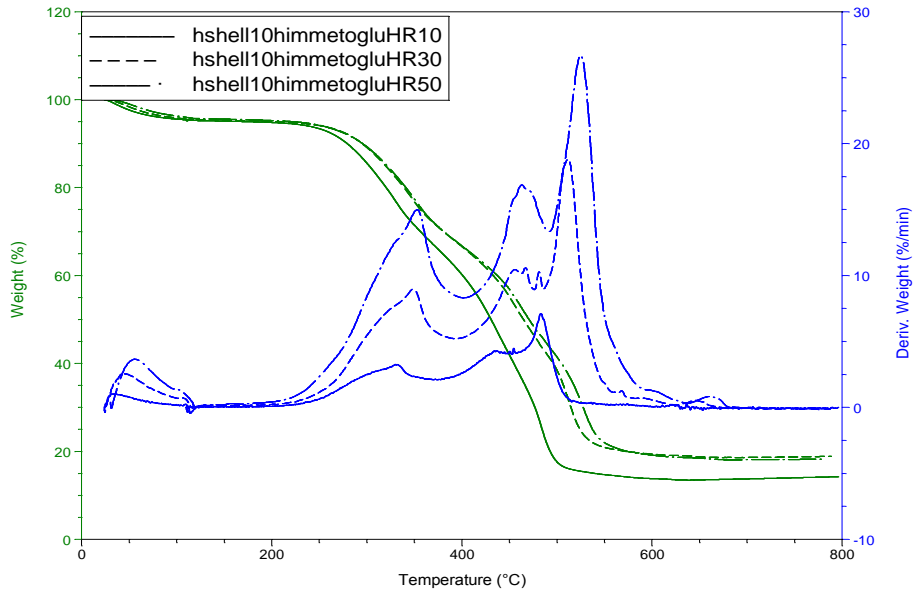


Figure C.55. TGA curve of hazelnut shell – oil shale blend (10-90) at different HR

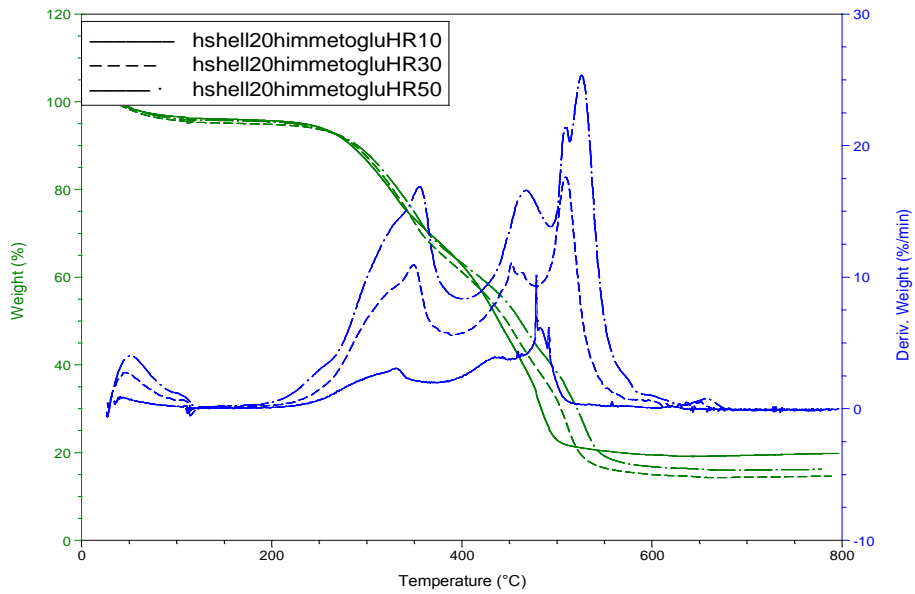


Figure C.56. TGA curve of hazelnut shell – oil shale blend (20-80) at different HR

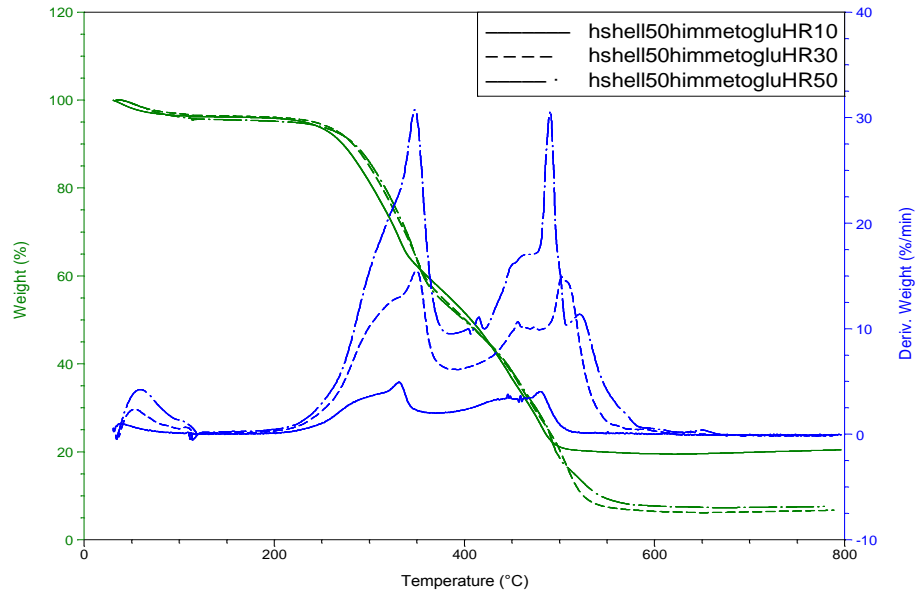


Figure C.57. TGA curve of hazelnut shell – oil shale blend (50-50) at different HR

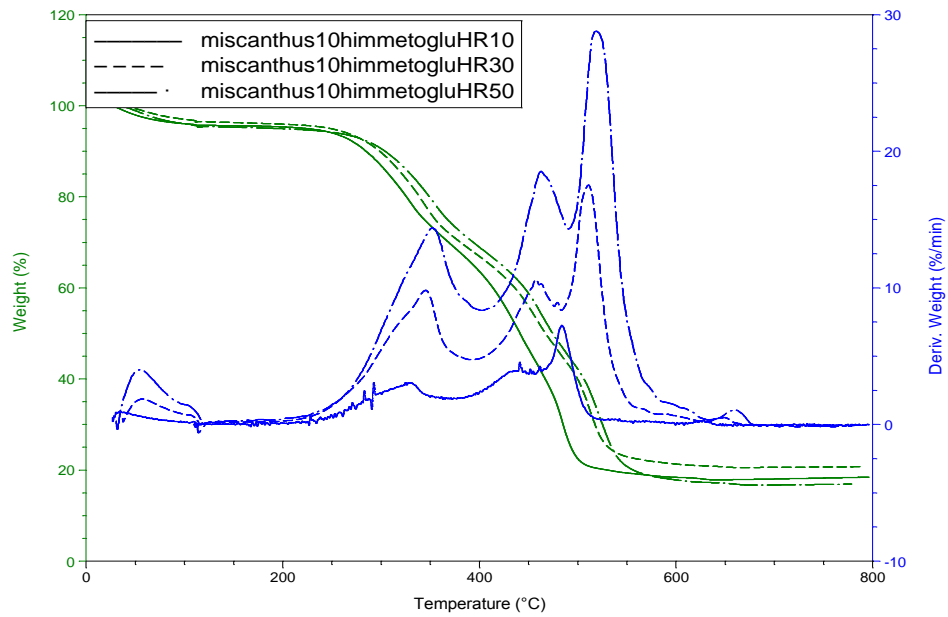


Figure C.58. TGA curve of miscanthus – oil shale blend (10-90) at different HR

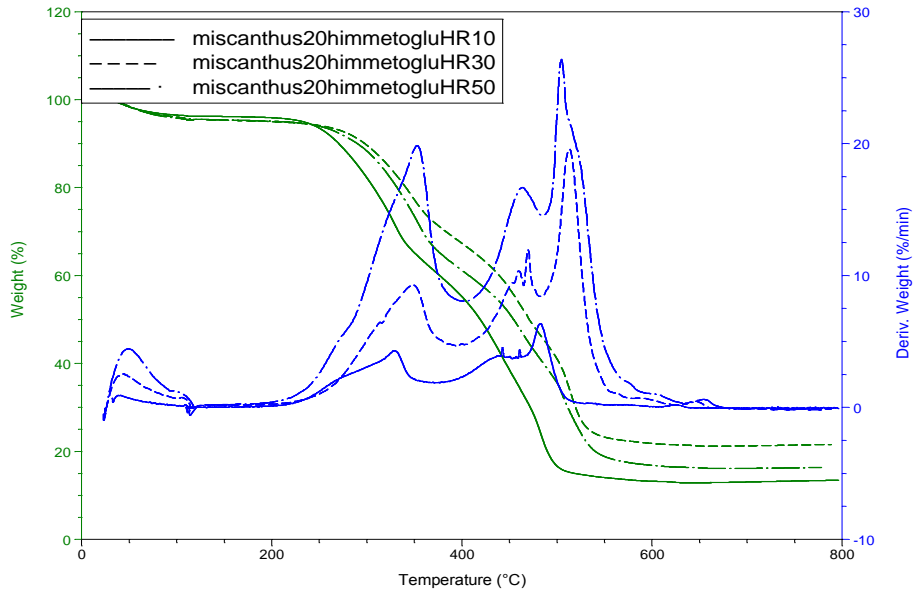


Figure C.59. TGA curve of miscanthus – oil shale blend (20-80) at different HR

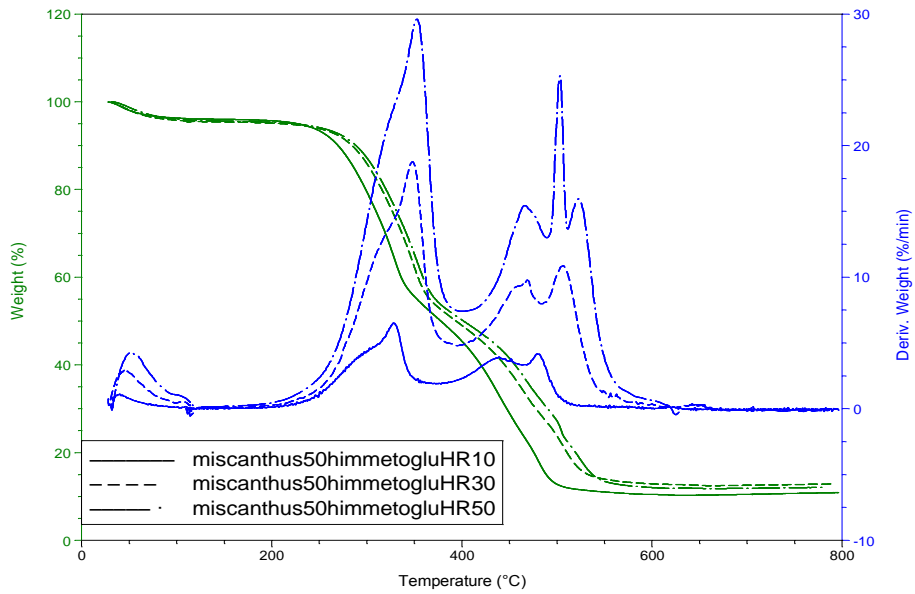


Figure C.60. TGA curve of miscanthus – oil shale blend (50-50) at different HR

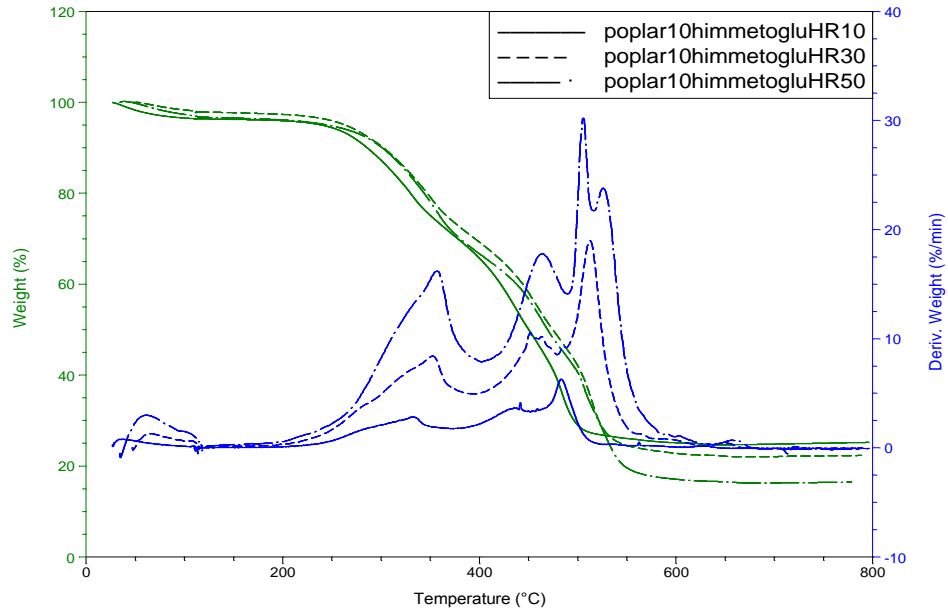


Figure C.61. TGA curve of poplar - oil shale blend (10-90) at different HR

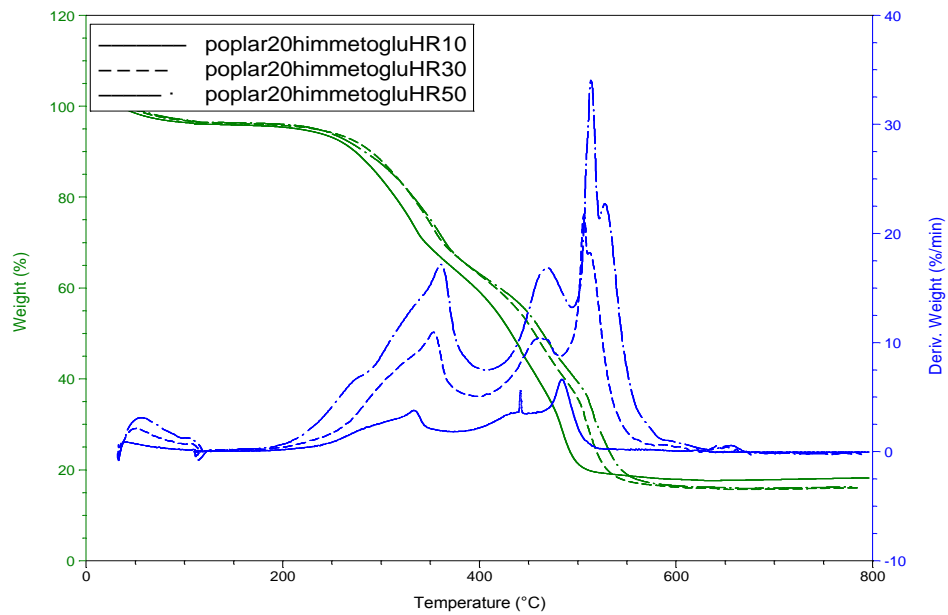


Figure C.62. TGA curve of poplar – oil shale blend (20-80) at different HR

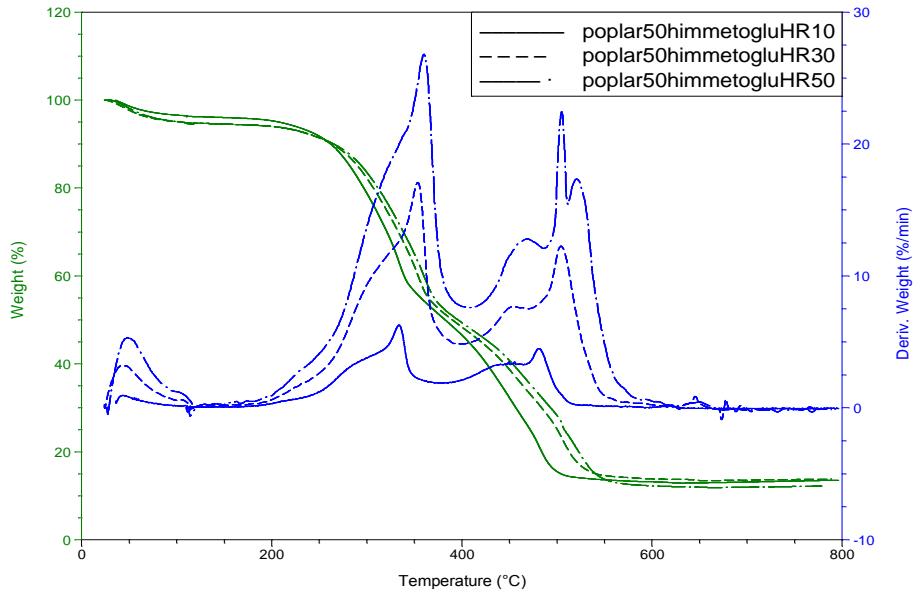


Figure C.63. TGA curve of poplar – oil shale blend (50-50) at different HR

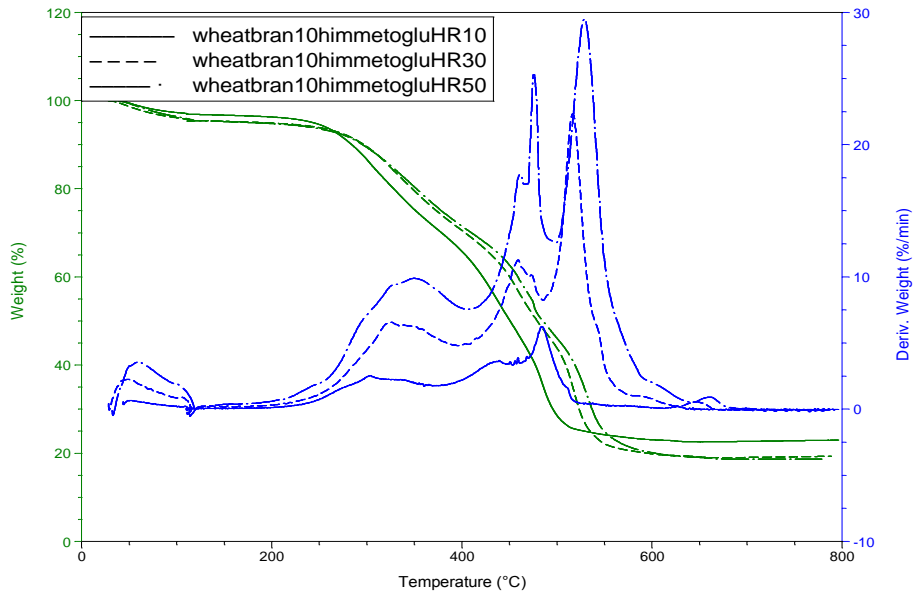


Figure C.64. TGA curve of wheat bran – oil shale blend (10-90) at different HR

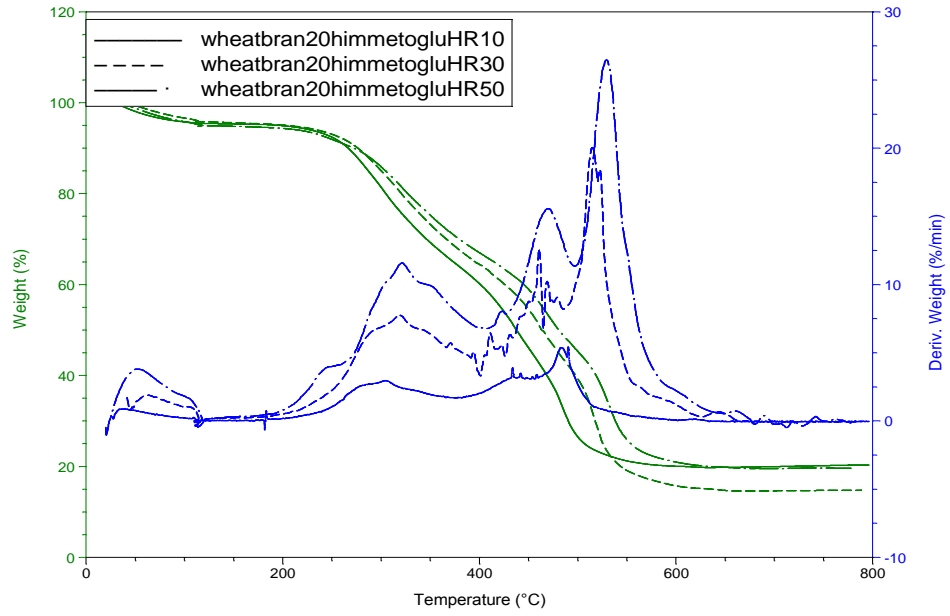


Figure C.65. TGA curve of wheat bran – oil shale blend (20-80) at different HR

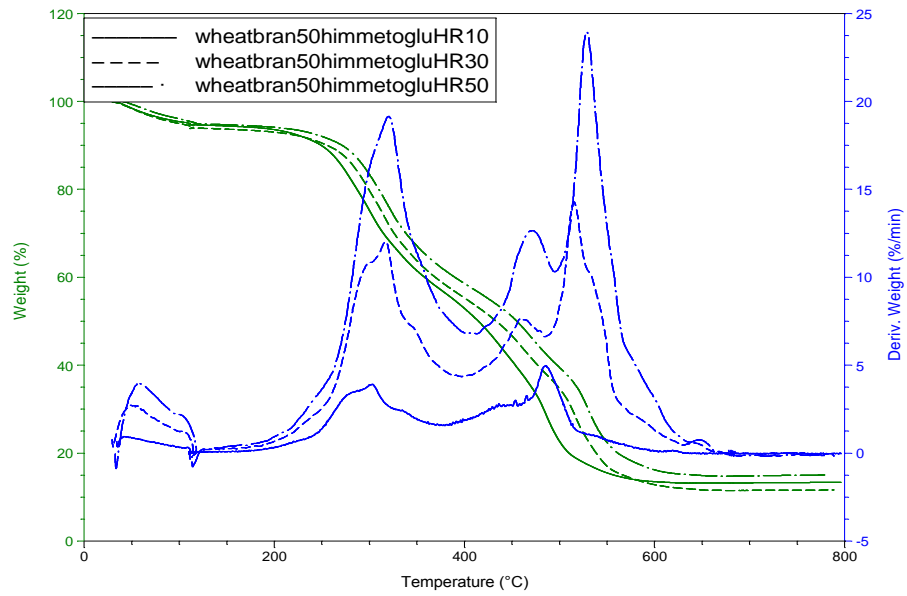


Figure C.66. TGA curve of wheat bran – oil shale blend (50-50) at different HR

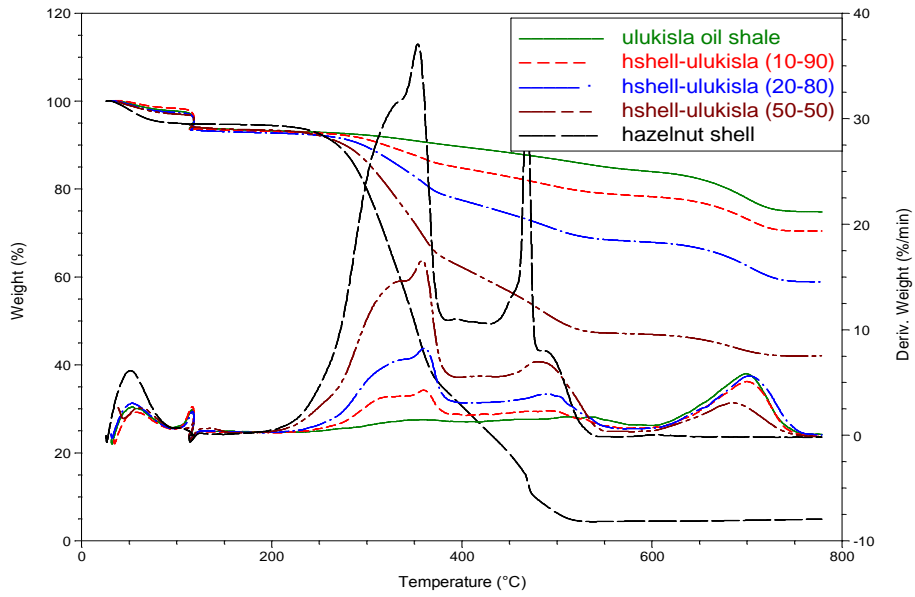


Figure C.67. Comparison of TGA curves for hazelnut shell-Ulukışla at 50 °C/min

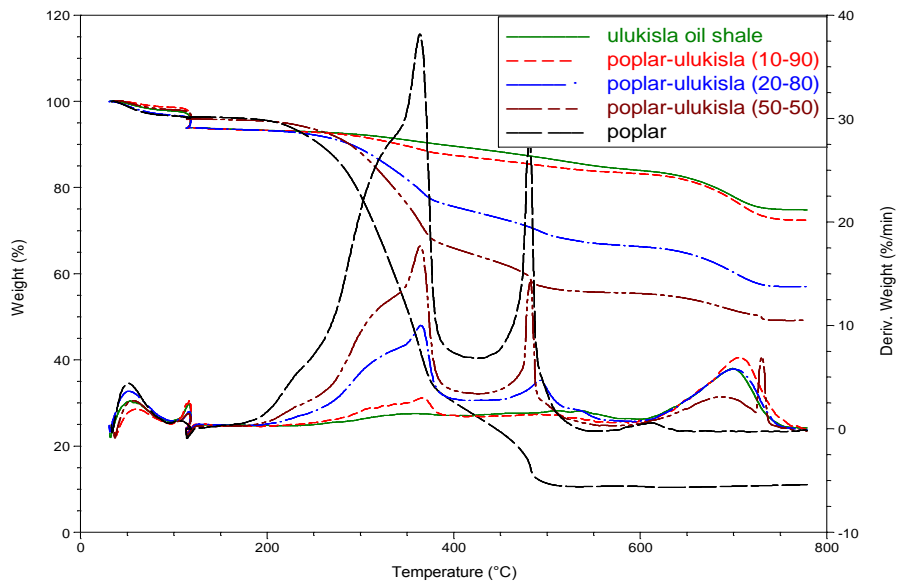


Figure C.68. Comparison of TGA curves for poplar-Ulukışla at 50 °C/min

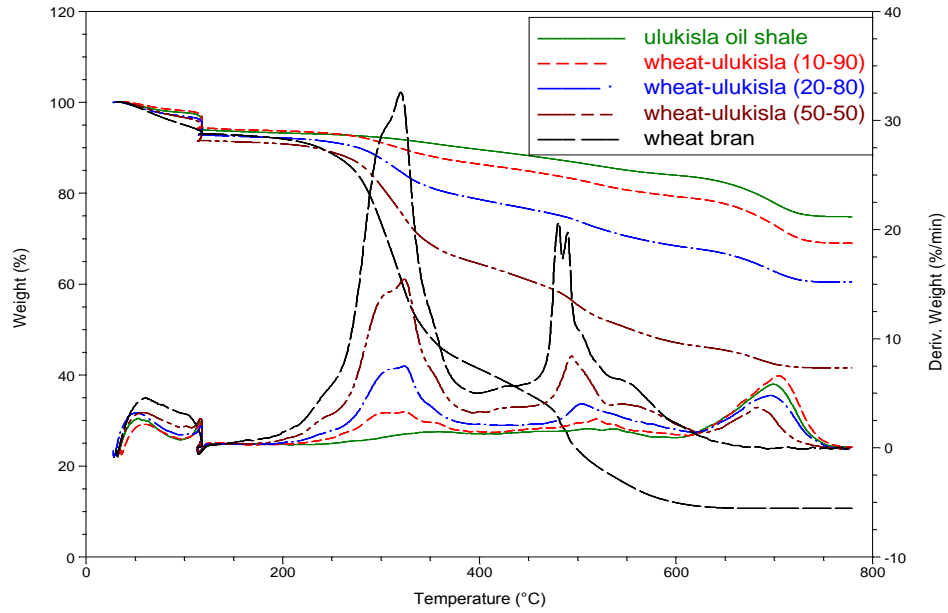


Figure C.69. Comparison of TGA curves for wheat bran-Ulukışla at 50 °C/min

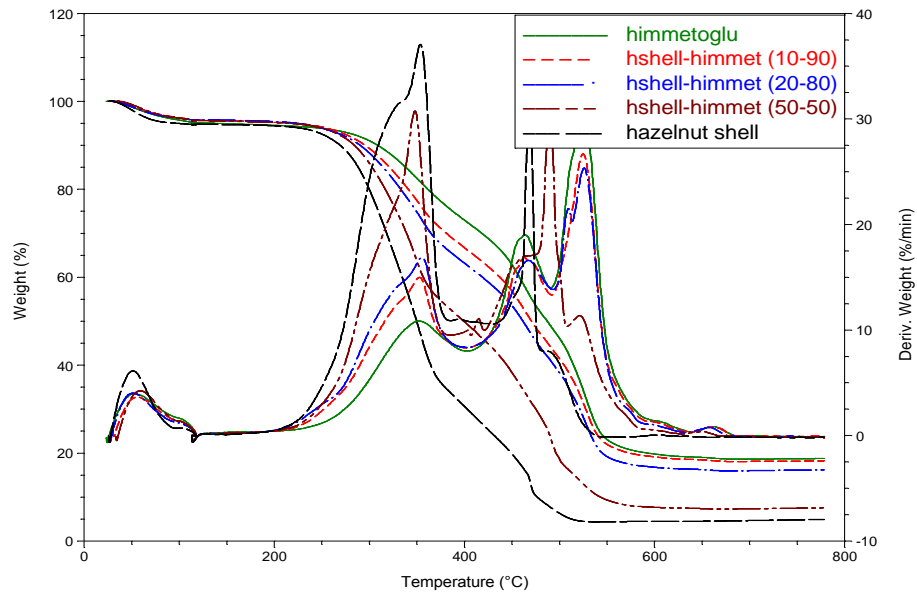


Figure C.70. Comparison of TGA curves for hazelnut shell-Himmetoğlu at 50 °C/min

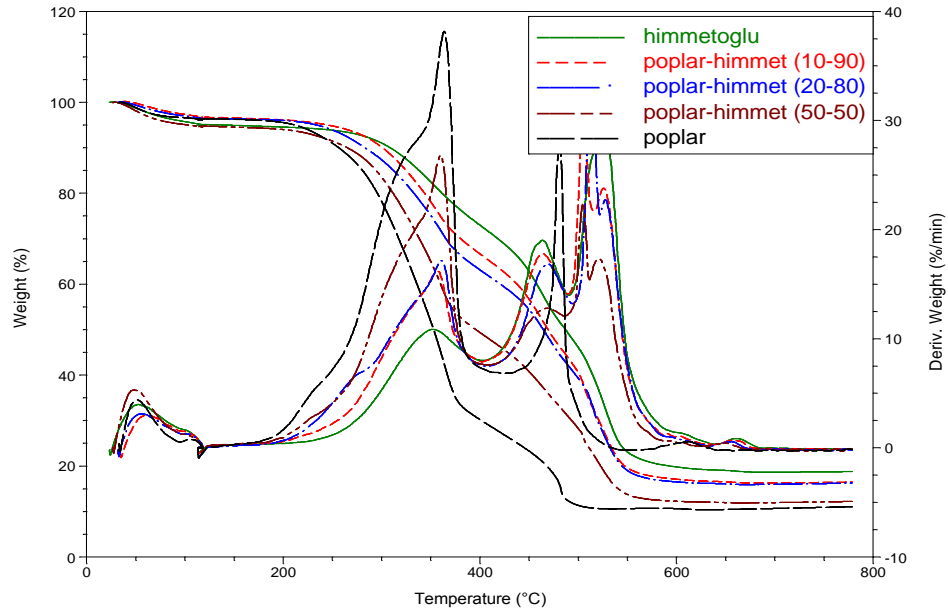


Figure C.71. Comparison of TGA curves for poplar-Himmetoğlu at 50 °C/min

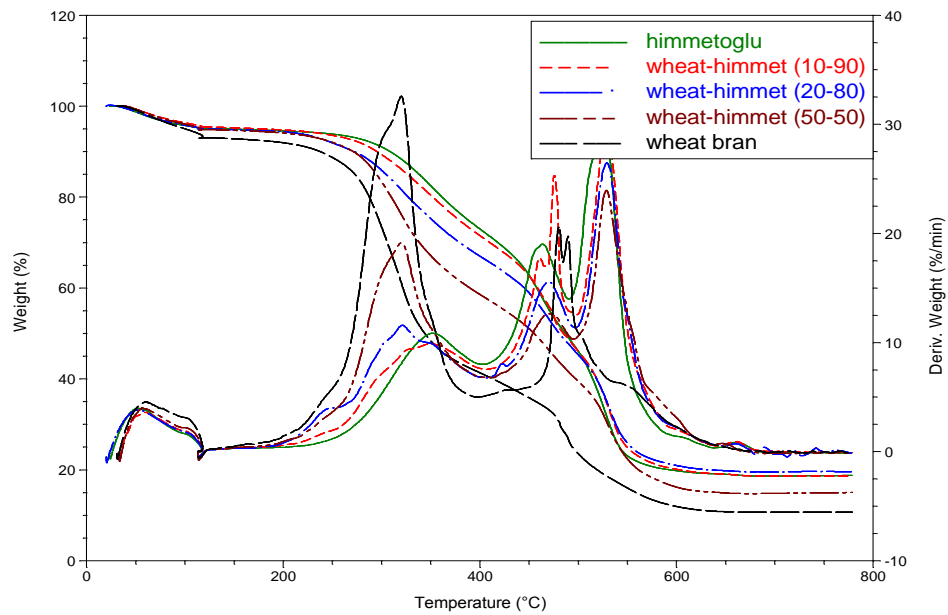


Figure C.72. Comparison of TGA curves for wheat bran-Himmetoğlu at 50 °C/min

APPENDIX D

REPEATABILITY TESTS

A statistical method, analysis of variance (ANOVA), was used to perform repeatability tests on the experimental data in Minitab Software. Measurements were made for DSC and TGA output data of some parent and blended fuels for more than 3500 observation data. The repeated runs for DSC and TGA curves can be seen between Figures D.1-D.6. Heat flow values were used to perform statistical analysis for the DSC results with respect to temperatures; weight loss contents from the reaction regions were used for the TGA results. It was observed that the results were in the range of confidence of interval ($P < 0.05$) indicating that the results are very consistent as seen in Table D.1.

Table D.1. Repeatability Test Results

Test	Statistical Parameters			
	S	$R^2, \%$	$R^2_{adj}, \%$	P
DSC	0.159	98.86	98.85	0.000
TGA	0.256	99.99	99.99	0.000

P : Confidence of interval

R^2 : Coefficient of determination

R^2_{adj} : Coefficient of determination - adjusted

S : Standart deviation

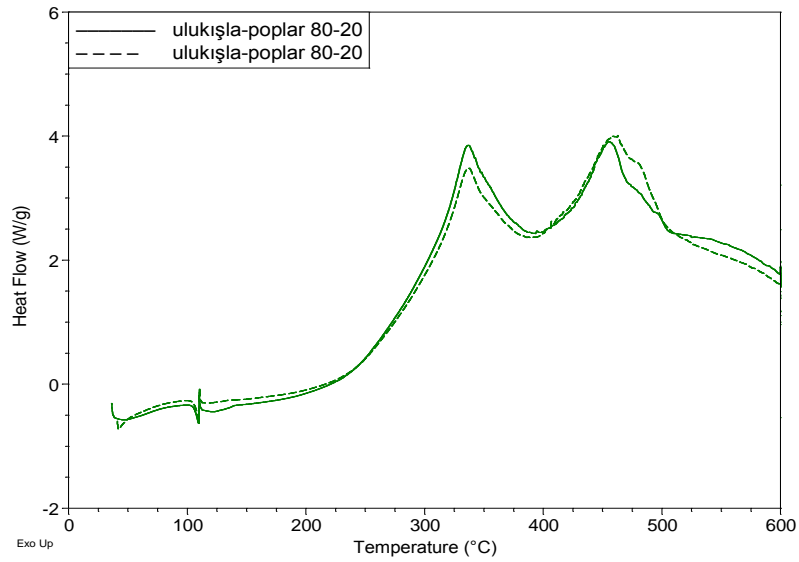


Figure D.1. Repeatability Test for DSC Curve at HR 10 (ulukışla-poplar 80%-20% blend)

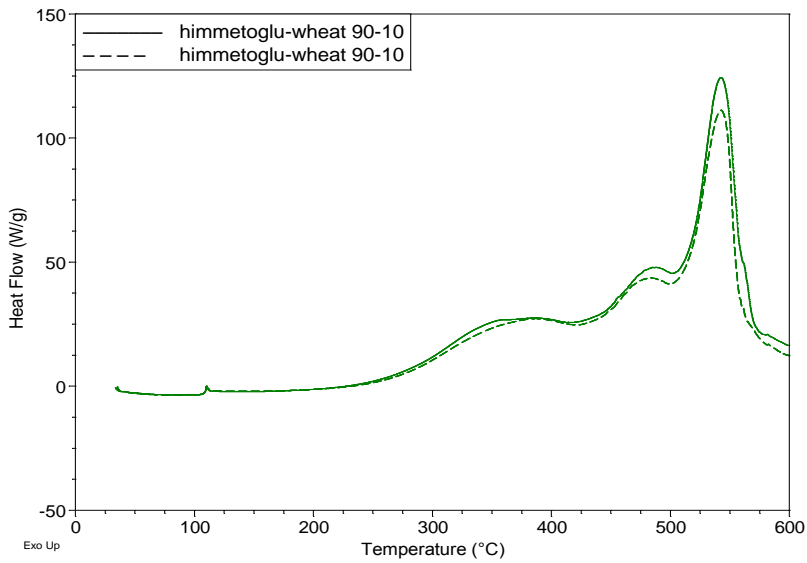


Figure D.2. Repeatability Test for DSC Curve at HR 50 (himmetoğlu-wheat 90%-10% blend)

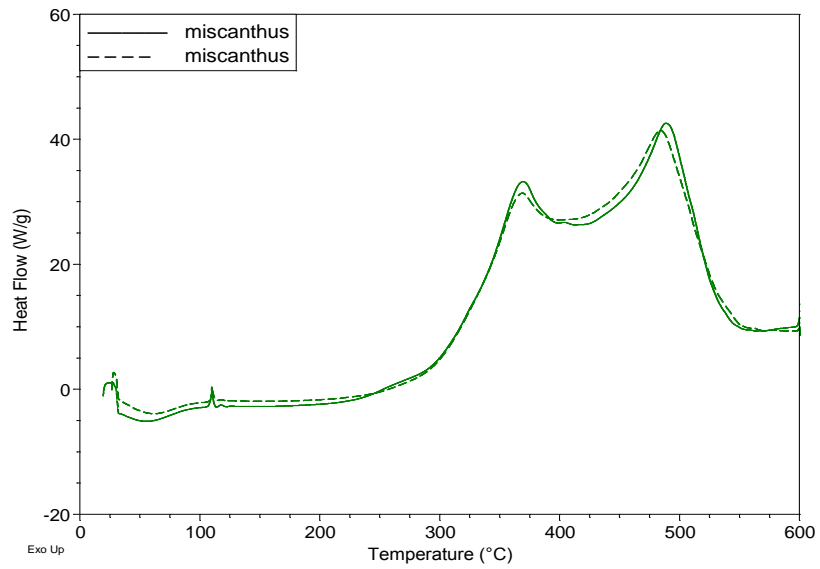


Figure D.3. Repeatability Test for DSC Curve at HR 50 (miscanthus)

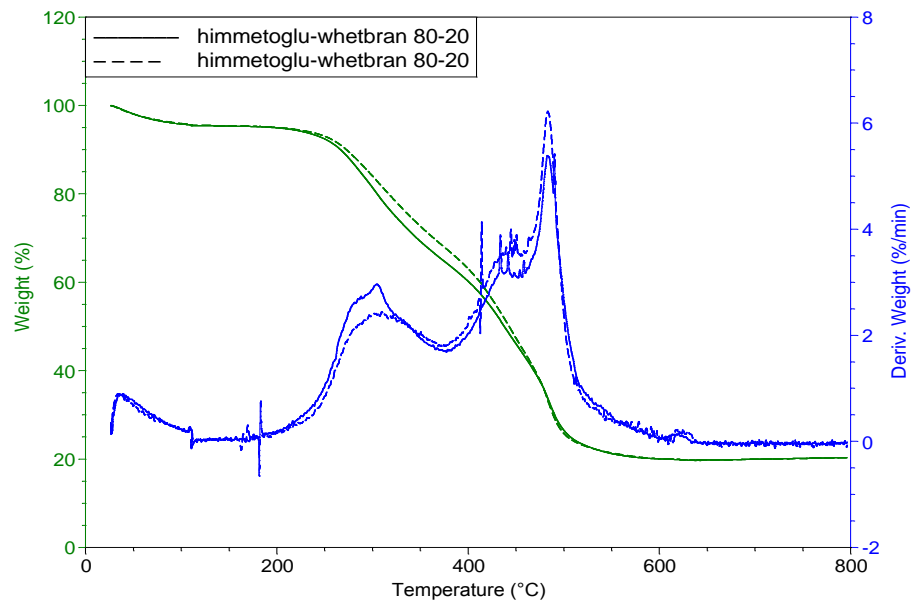


Figure D.4. Repeatability Test for TGA Curve at HR 10 (himmetoğlu-wheatbran 80%-20% blend)

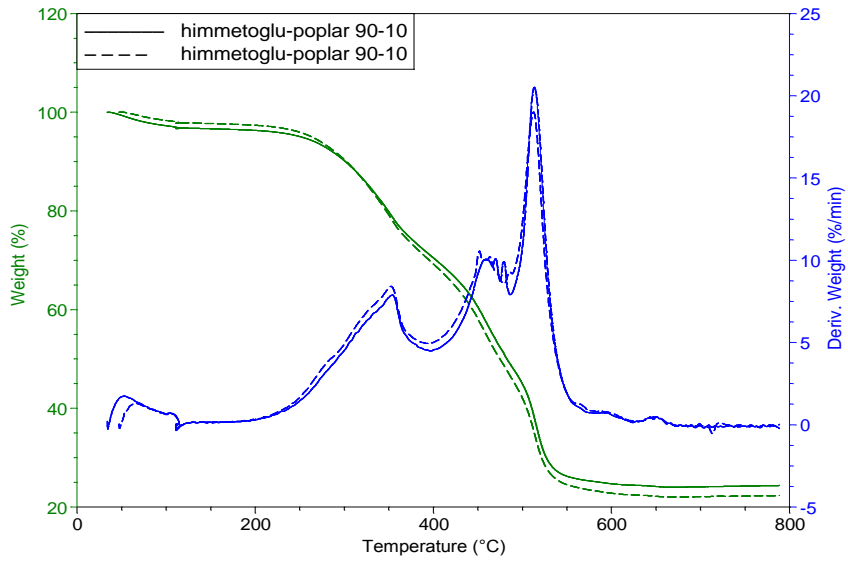


Figure D.5. Repeatability Test for TGA Curve at HR 30 (himmetoğlu-poplar 90%-10% blend)

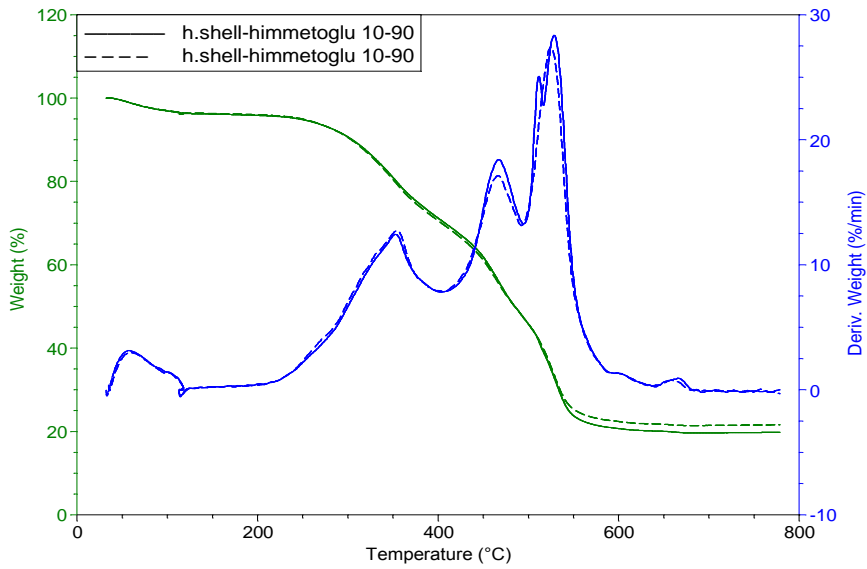


Figure D.6. Repeatability Test for TGA Curve at HR 50 (himmetoğlu-h. shell- 90%-10% blend)

APPENDIX E

OTHER RESULTS

Table E.1 Results of other Turkish oil samples in the literature

Authors	Oil Shale	Origin	P.A, wt. %	U.A, wt.%, HHV, cal./g, E _a ^{comb.} , kJ/mol
COMBUSTION				
Kök and Pamir (2000) Kök (2006) Şengüler (2012)	Beypazarı	Turkey	Moisture: 2.4, Ash: 65.2	C: 8.4, H: 1.6, O,N: 4.55, S: 0.21 HHV: 860 E _a : 81.1-111.6 (Arr.-Ct.&Rd.)
	Çan		Moisture: 12.4 Ash: 80.5	C: 10.1, H: 1.95, O,N: 10.06, S: 0.98 E _a : 59.2-56.1
	Demirci		Moisture: 10.2, Ash: 70.3	C: 9.8, H: 2.2, O,N: 9.6, S: 1.10 E _a :51.9-67.3
	Hatıldağ		Moisture: 1.6, Ash: 66.2,	C: 5.63, H: 1.3, O,N: 3.89, S: 1.25 HHV:385 E _a :101.6-88.7
	Himmetoğlu		Moisture: 12.9, Ash: 60.5,	C: 13.6, H: 1.5, O,N: 10.48, S: .99 HHV: 3085 E _a :82.4-127.6
	Mengen		Moisture: 9.5, Ash: 68.4	C: 10.05, H: 1.9, O,N: 8.8, S: 0.85 HHV: 1000 E _a :78.2-67.6
	Sarıcakaya		Moisture: 1.67 Ash: 65.8	C: 14.24, H: 1.78, O,N: 17.46, S: 0.58 E _a :83.5-57.4
	Seyitömer		Moisture: 2.8, Ash: 70.9	C: 8.58, H: 1.4, O,N: 4.39, S: 0.19 HHV:1000 E _a : 93.6-73.8
Yağmur and Durusoy (2009)	Göynük	Turkey	Ash: 74.9	Org. C: 47.9, H: 6, N: 1.2, S: 4 HHV:265 E _a :6.6-13.5 (Arr.-Ct.&Rd.)
Karabakan and Yürüm (2000)	Göynük	Turkey	Moisture: 8.4	Org. C: 62.2, H: 7.4, N: 1.5, S: 8.4, O: 20.9 E _a :47.3-59.8 Arrhenius
Kök and Şengüler (2013)	Eskişehir	Turkey	Ash: 60-75	TOC: 1.07-6.70 E _a : 210.6-278.2 (Kissenger)
PYROLYSIS				
Karayıldırım et al (2004)	Göynük	Turkey	Moisture: 11.3, Ash: 18, F.C: 16.7, V.M: 54	Org. C: 46.3, H: 4.8, N: 1.3, S: 2.2 E _a :56.9 (pyrolysis) Runge-Kutta
Sütçü and Pişkin (2009)	Ulukışla	Turkey	Ash: 29.45 V.M: 45.73, F.C: 24.82	C:57.8, H: 4.2, N:1, S: 5.6 HHV: 5330 (dry-ash free) E _a : 92-198 (pyrolysis) Coats-Redfern
Olukçu et al (2000) Doğan and Uysal (1996)	Beypazarı	Turkey	Moisture: 1.43 Ash: 61.9 F.C.:13.54 V.M.:23.13	C: 20.33, H: 2.09, N: 0.41, O:15.28 S: 3.38, HHV:860 E _a : 22.5-32.1 (pyrolysis) Coats-Red.
Doğan and Uysal (1996)	Beypazarı	Turkey	Moisture: 5, Ash: 70.8, F.C: 6, V.M: 23.2	C:12.8, H: 1.05, N:0.48, S: 1.9, O:13.1 HHV: 720 E _a :22.5-32.1 (pyrolysis) Coats-Redfern
	Seyitömer		Moisture: 10.2, Ash: 67.7, F.C: 1.8, V.M: 30.5	C:19.4, H: 2.32, N:0.79, S: 2.5, O: 7.29 HHV: 1315 E _a :12.5-19.2 (pyrolysis) Coats-Redfern
	Himmetoğlu		Moisture: 8.4, Ash: 27.4, F.C: 30.7, V.M: 41.9	C:53.7, H: 6.13, N:1.73, S: 3.9, O: 7.14 HHV: 2700 E _a :19-40.6 (pyrolysis) Coats-Redfern

Table E.2 Results of other oil shale samples in the literature

Authors	Oil Shale	Origin	P.A, wt. %	U.A, wt. %, HHV, cal/g, E _a ^{comb} , kJ/mol
Barkie et al (2003)	Tarfaya	Morocco	Ash: 49.65, Org. matter: 16.25	HHV: 1219 E _a =103 <i>Kissenger</i>
	Timahdit		Ash: 64.29, Org. matter: 12.84	HHV:1100 E _a = 118 <i>Kissenger</i>
Martins et al (2010)	Timahdit	Morocco	Ash: 63.7, V.M.:26.9 F.C.:6.9, Moisture:2.5	C: 15.9, H: 1.5, N: 0.24, O: 10.5 S: 1.5
Aboulkas et al (2007)	Tarfaya	Morocco	Moisture: 5.15, Ash: 52.83, VM: 40.09	C: 17.6, H: 1.78, N: 0.7, S: 0.37 E _a :100-109 (<i>Flynn-Ozawa-Wall, Kissenger, Friedman</i>)
Kaljuvee et al (2007) Kaljuvee et al (2011)	Various	Morocco	Ash: 66.4	C: 16.3, H: 1.65, N: 0.5, S: 1.97, HHV: 1170 E _a :130.4 (<i>Friedman</i>)
		Israel	Ash: 60.3	C: 17.1, H: 1.46, N: 0.39, S: 2.6, HHV: 1170 E _a :161.4 (<i>Friedman</i>)
		Jordan	Ash: 61.9	C: 22.2, H: 2.24, N: 0.42, S: 3.52, HHV: 1936 E _a : 160.9 (<i>Friedman</i>)
Jaber and Probert (2000)	El-lajjun	Jordan	Ash: 62.8	C: 19.6, H:2.1 N: 0.3, S: 1.5 E _a : 151-177 (<i>Coats-Red.</i>)
	Sultani		Ash: 61	C: 22.3, H:2.6 N: 0.4, S: 3.5 E _a : 149-203 (<i>Coats-Red.</i>)
Al-Makhadmeh et al (2013)	El-lajjun	Jordan	Moisture: 0.78, Ash: 54.99	C: 54.3, H: 5.3, N: 0.9, O: 30.44, S: 9 (water-ash free)
Hammad et al (1998)	El-lajjun	Jordan	Ash: 54.68 Moisture: 4.39	C: 14.88, H:1.64 N: 0.38, O: 1.87
Amer et al (2014)	El-Lajjun	Jordan	Ash: 75.8	C: 17.4, H: 2.1, N: 0.4, S: 2.4, O:2.6
	Sultani		Ash: 72.8	C: 17.8, H: 2.5, N: 0.5, S: 2.7, O:2.5
	Attrat		Ash: 82.8	C: 11.2, H: 1.8, N: 0.4, S: 2.5, O:1.3
	Ma'an		Ash: 77.8	C: 13.4, H: 2.1, N: 0.5, S: 3.1, O:3
	Yarmouk		Ash: 87.1	C: 9.7, H: 1.2, N: 0.3, S: 1.4, O:0.3
Alali (2006)	Jurf Ed Darawish	Jordan	Moisture: 2.8, Org. Mat.: 18	HHV: 860
	Wadi Maghar		Moisture: 3.8, Org. Mat.: 20.8	HHV: 1000
	El-Lajjun		Moisture: 2.4, Org. Mat.: 22.1	HHV: 1000
	Sultani		Moisture: 2.6, Org. Mat.: 21.5	HHV: 1575
	Attarat		Moisture: 1.7, Org. Mat.: 23.2	HHV: 1720
Abu-Qudais et al (2005)	Attarat	Jordan	Moisture: 3.25, Org. Mat: 29 Ash: 53.2	S: 2.6, HHV: 1195 E _a =11.46-17.79 kJ/mol (pyrolysis) <i>Coats-Redfern</i>
Syed et al (2011)	El-lajjun	Jordan	Moisture: 1, Ash: 68, F.C.:3.2, V.M.:28.8	C: 12.9, H: 1, N: 0.3, S: 1.5 E _a = 64.5 (pyrolysis) <i>Arrhenius</i>
Al-Ayed (2006)	El-lajjun	Jordan	Moisture: 1.21	S:2.29, HHV: 1315 E _a =99-141.4 kJ/mol (pyrolysis) <i>Coats-Redfern</i>
Khraisha and Shabib (2002)	El-lajjun	Jordan	Moisture: 1.1, Ash: 54.5, F.C.:0.42, V.M.:43.9	E _a =20.61-29.55 kJ/mol (pyrolysis) <i>Coats-Redfern</i>
	Sultani		Moisture: 0.84, Ash: 54.75, F.C.:0, V.M.:44.4	
Meriste et al (2013)	Two different	Estonia	Ash: 49.3, Moisture:0.7	C: 30.4, H: 3, N: 0.1, S: 1.63 HHV: 2835 E _a : 80-100 <i>Friedman</i>
			Ash: 45.6, Moisture:0.7	C: 35, H: 3.6, N: 0.1, S: 1.87 HHV: 3260 E _a : 80-100 <i>Friedman</i>

Table E.2.con't. Results of other oil shale samples in the literature

Authors	Oil Shale	Origin	P.A, wt. %	U.A, wt. %, HHV, cal./g, $E_a^{comb.}$, kJ/mol
Oja et al (2007)	Kukersite	Estonia	Ash: 51.09, O.M: 26.89,	S:1.55
	Dictyonema	Estonia	Ash: 81.42, O.M: 18.06,	S: 2.94
	El-lajjun	Jordan	Ash: 63.10, O.M: 21.96,	S:3.70
	Saveljev	Russia	Ash: 61.41, O.M: 27.79,	S:3.86
Johannes et al (2010)	Baltic	Estonia-Russia	-	$E_a=183-280$ kJ/mol (pyrolysis) <i>Arrhenius</i>
Altun et al (2006)	Glen Davis	Australia	-	Organic Carbon: 40, N: 0.5, S: 0.6
	Tremembe	Brazil	-	Organic Carbon: 16.5,N: 1.1,S:0.7 Organic Carbon: 81, N: 0.8, S: 1.7
	Irati	Brazil	-	
	Autun	France	-	Organic Carbon: 22, N: 0.9, S: 0.6
	Crenevay	France	-	Organic Carbon: 10, N: 1, S: 3.5
	Ermelo	S. Africa	-	Organic Carbon: 52, N: 0, S: 0.6
	Puertollano	Spain	-	Organic Carbon: 26, N: 0.7, S: 0.4
	Kvarntorp	Sweden	-	Organic Carbon: 19, N: 0.7, S: 1.7
	Scotland	USA	-	Organic Carbon: 12, N: 0.8, S: 0.4
	Alaska	USA	-	Organic Carbon: 55, N: 0, S: 0
Yen (1976)	Colorado	USA	-	Organic Carbon: 16, N: 2.1, S: 0.8
	Green River	USA	Ash: 65.7	C: 12.4, H: 1.20, N: 0.41, S: 0.63
	Sunbury	USA	Ash: 83.43	C: 11.42, H: 1.20, N: 0.41, S: 3.55
	New Glasgow	Canada	Ash: 84	Org. C: 7.92, N: 0.54, S: 0.70
Reynolds and Burnham (1995)	Dunnet	Scotland	Ash: 77.8	Org. C: 12.3, N: 0.46, S: 0.73
Green River	USA	TOC: 9.9	C: 16, H: 1.4, N: 0.3, S: 0.3 E_a : 228 <i>(Friedman)</i>	
Tiwari and Deo (2012)	Green River	USA	Ash: 80	C: 17.45, H: 1.6, N: 0.53, S: 0.18 E_a :95-245 kJ/mol (pyrolysis) <i>Kissenger</i>
Avid et al (2004)	Khoot	Mongolia	Moisture: 5.2 Ash: 59.8 V.M.:31.8	C: 21.1, H: 2.7, N: 0.6, O:10.3 S: 0.3
Sonibare et al (2005)	Lokpanta	Nigeria	Moisture:2, Ash: 82, V.M:12	$E_a=74$ (pyrolysis) <i>Arrhenius</i>
Wolela (2006)	Lalo-Sapo	Ethiopia	Moisture: 12.1 Ash: 78.5 F.C.:1 V.M.:8.7	HHV= 910
Williams and Ahmad (1999)	Malgeen	Pakistan	Moisture: 1 Ash: 67.7 F.C.:3.2 V.M.:29	C: 32.2, H:2.9 N: 0.34 HHV: 1360
Kerimov (2004)	Dzhangichai	Azerbaijan	Moisture: 2.8 Ash:45	C: 21.93, H:2.56 N: 0.92, S:3.24 E_a : 13.95-29.86(pyrolysis) <i>Coats-Red.</i>
Torrento and Galan (2001)	Puertollano	Spain	Ash: 62.8	Org. C: 26 $E_a=102-171$ (pyrolysis) <i>Arrhenius, Integral, Differential</i>
Olivella and De Las Heras (2008)	Ribesalbes	Spain	-	C:10.7, H:2.38,N:0.66,S:0.33 $E_a=98.2-282.4$ (pyrolysis) <i>Integral, Differential</i>
Petersan et al (2010) Petersan et al (2006)	Mae Sot	Thailand	Moisture: 3.4, Ash: 53.6, TOC: 29.56	C: 69.11, H: 9.28, N: 1.88, S: 2.48, O:17.25(ash-free) E_a : 218 <i>(Friedman)</i>
	Li		Moisture: 2.3, Ash: 63.6, TOC: 15.90	C: 47.88, H: 6.48, N: 1.05, S: 30.02, O:14.57 (ash-free) E_a : 230 <i>(Friedman)</i>
Jankovic (2013)	Geopark Paleoroute	Brazil	Ash: 65	Org.C: 69.7, H: 6.7, N: 2.3, O: 12.22, S: 9.1 $E_a=148-198$ (pyrolysis) <i>Kissenger, Friedman</i>

Table E.2.con't. Results of other oil shale samples in the literature

Authors	Oil Shale	Origin	P.A, wt.%	U.A, wt.%, HHV, cal./g, $E_a^{comb.}$, kJ/mol
Yan and Song (2009)	Fushun	China	Org. Cont: 21.3 Moisture:4.9	C: 13.77, H: 2.29, N: 0.51, S: 0.59
	Maoming		Org. Cont: 26 Moisture:17.2	C: 14.82, H: 2.51, N: 0.52, S: 1.06
	Huadian		Org. Cont: 20.3 Moisture:12.3	C: 13.83, H: 2.03, N: 0.32, S: 0.53
	Huangxian		Org. Cont: 39 Moisture:13.4	C: 30.71, H: 3.23, N: 0.41, S: 0.99
Liu et al (2013)	Wangqing (semicoke)	China	Moisture: 0.11, Ash: 89.64, F.C.:1.1, V.M.:9.2	C: 4.01, H: 0.31, N: 0.35, O: 5.49, S: 0.09, $E_a=100-120$ (Flynn-Ozawa-Wall)
Qing et al (2013)	Huadian (semicoke)	China	Moisture: 0.89, Ash: 82.62, F.C.:6.1, V.M.:10.44	C: 11.29, H: 0.35, N: 0.11, O: 4.21, S: 0.53, $E_a=99.73$ (Arrhenius)
Han et al (2006) Jiang et al (2007)	Huadian	China	Moisture: 2.9, Ash: 51.61, V.M: 41.96, F.C: 3.6	C: 31.63, H: 4.37, O: 7.76, N: 0.73, S: 1 HHV: 2000 E_a : 78.2-152.2 (Freeman-Carroll)
Yongjiang et al (2011)	Huadian	China	Ash: 64.17, V.M.: 29.48	C: 23.69, H: 3.93, N: 0.66, S: 0.83 $E_a = 127.6$ (pyrolysis) Coats-Redfern
Qing et al (2013)	Maoming	China	Ash: 61.83	C: 13.38, H: 2.23, N: 0.46, O: 5.1 S: 0.61 HHV:1290
Li and Yue (2003)	Fushun	China	Ash: 77.36 Volatiles: 17.10	$E_a= 154.8$ $E_a= 139.1$ Friedman (pyrolysis)
	Maoming		Ash: 71.94 Volatiles: 22.80	

CURRICULUM VITAE

Personal Information

Name : Emre Özgür
Citizenship : Turkish
E-mail address : emreozgur@gmail.com
Personal web site : www.emreozgur.com

Background

A – Educational

2007 – 2014, Phd “*Co-firing of Oil Shale and Biomass Fuels*”: Middle East Technical University - Petroleum & Natural Gas Engineering, Ankara – TURKEY (2009-2010 in Pennsylvania State University as an exchange student)

2004 – 2006, MS “*Analytical and Numerical Investigation of CO₂ Sequestration Into Deep Saline Aquifers*”: Middle East Technical University - Petroleum & Natural Gas Engineering, Ankara – TURKEY

1999 – 2004, BS: Middle East Technical University - Petroleum & Natural Gas Engineering, Ankara – TURKEY

1996 – 1999, High School: Özel Yüce Fen Lisesi / Ankara – TURKEY

B - Professional

2004 – 2013 : Research and Teaching Assistant in Middle East Technical University - Petroleum & Natural Gas Engineering Department

2007 – 2009 : Researcher in the joint research project of TÜBİTAK (The Scientific and Technological Research Council of Turkey) and CNR (National Research Council of Italy), “Analysis and Characterization of Solid and Biomass Fuels by Thermal Analysis Techniques” – Project Code: 107T888

March, 2009 – March, 2010 : Research Scholar (Exchange Visitor) in Energy Institute - Pennsylvania State University, USA

Training Mission:

Kızılcahamam Geothermal Field Trip, 2004 November (1 day)

PERENCO Diyarbakır Region Summer Practice (Workover and Production), 2004 June (3 weeks)

TPAO Adıyaman Region Summer Practice (Drilling, Workover, and Production), 2003 June (3 weeks)

Language: English (good), German (fair), Russian (elementary)

Computer Literacy: MS Windows/Office, Visual Modflow, CMG/GEM, C Programming

Interests: Chess, Science and Technology, Swimming, International Relations and Politics

Attended Seminars: 8 February 2007 (Offshore Petroleum Technology, Chamber of Petroleum Engineers), 18-19-20 April 2007 (Geothermal Energy Course, Chamber of Petroleum Engineers), 8-9 November 2007 (Casing and Tubing Design, VAM), 24 January 2008 (Advanced Materials Characterization by Thermal Analysis, TA Instruments)

Publications & Conference Papers:

- KÖK, M.V., ÖZGÜR, E, “Thermal Analysis and Kinetics of Biomass Samples”, Fuel Processing Technology, Vol: 106, pg. 739-743, 2013
- ÖZGÜR, E., MILLER, B.G., MILLER, S.F., KÖK, M.V., “Thermal Analysis of Co-firing of Oil Shale and Biomass Fuels”, Oil Shale, Vol: 29, No: 2, pg. 190-201, 2012
- ÖZGÜR, E., KÖK, M.V., MILLER, B.G., MILLER, S.F., “Thermal Analysis of Oil Shale and Biomass Fuels”, presented at the 18th International Petroleum and Natural Gas Congress and Exhibition of Turkey, Sheraton Hotel, Ankara-TURKEY, May 11-13, 2011
- ÖZGÜR, E., MILLER, B.G., MILLER, S.F., KÖK, M.V., “Co-Combustion Performance of Oil Shale and Biomass Fuels”, presented at the 27th Annual International Pittsburgh Coal Conference, Hilton Hotel, İstanbul-TURKEY, October 11-14, 2010

- ÖZGÜR, E., KÖK, M.V., TARTARELLI, R., BIAGINI, E., SIMONI, M., “Analysis and Characterization of Solid Fuels by Thermal Analysis Techniques”, presented at the 32th AICAT Congress on Calorimetry, Thermal Analysis and Applied Thermodynamics, University of Trieste, ITALY, May 26-28, 2010
- ÖZGÜR, E. and GÜMRAH, F., “Analytical and Numerical Modeling of CO₂ Sequestration in Deep Saline Aquifers”, Energy Sources Part A – Recovery, Utilization and Environmental Effects, Vol : 32 Issue : 7 pg. 674-687, 2010
- ÖZGÜR, E. and GÜMRAH, F., “Diffusive and Convective Mechanisms during CO₂ Sequestration in Aquifers”, Energy Sources Part A – Recovery, Utilization and Environmental Effects, Vol : 31 Issue : 8 pg. 698-709, 2009
- AKBAŞ, C.Y. and ÖZGÜR, E., “Biodiesel : An alternative fuel in EU and TURKEY”, Energy Sources Part B – Economics, Planning and Policy, Vol : 3 Issue : 3 pg. 243-250, 2008
- ÖZGÜR, E. and GÜMRAH, F. “Modeling of CO₂ Sequestration in Deep Saline Aquifers”, presented at the 16th International Petroleum and Natural Gas Congress and Exhibition of Turkey, Ankara – Turkey, May 29-31, 2007